

Investigation of mechanisms underlying L1 syndrome in mouse model and in vitro

Dissertation

Zur Erlangung des Grades

Doktor der Naturwissenschaften

(Dr. rer. nat.)

Am Fachbereich Biologie

Der Johannes Gutenberg-Universität Mainz

Dominik Appel

Geboren am 11.06.1990 in Kaiserslautern

Mainz, 2022

Dekan: Prof. Dr. Eckhard Thines

1. Berichterstatter: [REDACTED]

2. Berichterstatter: [REDACTED]

Zweitbetreuerin: [REDACTED]

Tag der mündlichen Prüfung:

17.01.2023

Table of Contents

1. Introduction	1
1.1 Nervous system	1
1.2 Development of the cortex	2
1.3 Human embryonic stem cells in research and clinic.....	3
1.4 Neural cell adhesion molecule L1/L1CAM.....	5
1.5 L1 syndrome	7
1.6 Investigation of L1CAM in animal models	10
1.7 Genomic sequencing and Gene ontology analysis	10
1.8 Key points of this work	12
2. Material and Methods	13
2.1 Materials.....	13
2.2 Methods	20
2.2.1 Animal husbandry and assessment of L1CAM-mutant mice.....	20
2.2.2 Generation of L1CAM mutant mouse lines	20
2.2.3 Genotyping of transgenic mice.....	21
2.2.4 Motor function and behavior tests	23
2.2.5 Mouse killing, brain dissection and storage	27
2.2.6 Cryosectioning	28
2.2.7 Nissl/cresyl violet staining	28
2.2.8 Luxol fast blue/Nissl staining.....	29
2.2.9 Immunohistochemical labeling	29
2.2.10 RNA extraction from brain tissue and cDNA synthesis	30
2.2.11 qPCR gene expression analysis	31
2.2.12 Preparation of human cerebral organoids.....	31
2.2.13 β -Catenin nuclear translocation assay and subcellular fractionation	31
2.2.14 Protein extraction.....	32

2.2.15 Lowry DC protein assay	32
2.2.16 SDS-PAGE and Western Blot	33
2.2.17 NEBNext Ultra™ II RNA Library Prep for Illumina and NGS	33
2.2.18 Statistics.....	34
2.3 Acknowledgements	34
3. Results.....	35
3.1 Low numbers of hemizygous mutant males in litters	35
3.2. Neurological alterations in L1D201N mutant mice	36
3.3 Neurological deficits in L1KO mutant male mice	37
3.4 Altered travel paths in mutant male mice	39
3.5 L1D201N male mice show enlarged ventricles	40
3.6 L1KO mutant mice do not show enlarged ventricles	42
3.7 Thinned corpus callosum in L1D201N and L1KO mutant mice	43
3.8 Principal component analysis of transcriptomes from adult L1KO mutant mice	45
3.9 L1KO males display more down-regulated than up-regulated DEG.....	47
3.10 Panther GO analysis showed changes in “cellular processes”, “binding” and “WNT signaling”	48
3.10.1 DEG between L1KO and WT males associated with “cellular processes”	48
3.10.2 DEG between L1KO and WT males associated with “binding”	50
3.10.3 DEG between L1KO and WT associated with “WNT signaling”	51
3.11 Altered expression of TJP genes and genes involved in oligodendrogenesis	52
3.12 L1CAM-deficiency increases lethality at late embryonic or neonatal stages	54
3.13 E16 L1KO males show enlarged ventricles and altered expression patterns in the cortex and CP	55
3.14 No L1CAM expression in L1KO E16 cortex	56
3.15 Thinned SOX2 layer in L1KO mutant dorsal cortex.....	57
3.16 Less KI67 ⁺ cells in the L1KO choroid plexus.....	59
3.17 No major changes of mRNA expression of selected genes in E16 L1KOs	61
3.18 Almost no expression of L1CAM in L1KO hESCs	63

3.19 Growth of cerebral organoids peaked after 28DIV	64
3.20 <i>PAX6</i> and <i>VGLUT2</i> expression altered in L1KO cerebral organoids	66
3.21 Principal component analysis of transcriptomes from human cerebral organoids.....	68
3.22 Imbalanced ratio of up- and downregulated genes in L1KO organoids.....	69
3.23 Panther GO analysis revealed changes in “binding processes” and “WNT signaling” in L1KO organoids	70
3.23.1 DEG between L1KO and wildtype associated with “cellular processes”	71
3.23.2 DEG between L1KO and wildtype organoids associated with "binding".....	72
3.23.3 DEG between L1KO and wildtype organoids associated with “WNT signaling”.....	73
3.24 GOrilla/REVIGO analysis revealed DEG between L1KO and wildtype organoids are associated with proliferation, adhesion and development.....	75
3.25 IPA revealed DEG between L1KO and wildtype organoids are associated with axonal guidance, WNT signaling and hESC pluripotency	76
3.26 Increased WNT signaling in L1KO organoids.....	77
3.27 Similarities between L1KO adult mouse brains and L1KO cerebral organoids	78
3.28 L1OE diminishes induction of WNT signaling by LiCl.....	79
4. Discussion	81
4.1 L1CAM mutant males show features of human L1 syndrome	81
4.2 Elevated WNT signaling in L1KO mutant males.....	84
4.3 Embryonic L1KO mice show L1CAM related pathologies	88
4.4 L1KO organoids share similar dysregulations as L1KO mice.....	90
4.5 L1-OE alleviates nuclear translocation of β -Catenin-GFP	93
5. Abstract.....	96
6. Zusammenfassung	97
7. References	99
8. Appendix.....	117
8.1 List of figures	117
8.2 List of tables	119

8.3 Publications.....	120
8.4. Acknowledgements	121
8.5 Statutory declaration	122

Abbreviations

2	square
%	percent
(q)PCR	(quantitative) polymerase chain reaction
°	degrees
°C	degrees celsius
A	ampere
abs.	absolute
BBB	blood-brain barrier
bFGF	basic fibroblast growth factor
bp	base pairs
BSA	bovine serum albumin
CAM	cell adhesion molecule
cDNA	complementary DNA
CHL1	cell adhesion molecule L1-like
CNS	central nervous system
CoP	cortical plate
CRASH	Corpus callosum agenesis, Retardation, Adducted thumbs, Spastic paraplegia and Hydrocephalus
CSF	cerebrospinal fluid
DAPI	4',6-Diamidin-2-phenylindol
dest.	distilled
DIV	days <i>in vitro</i>
DMEM	Dulbeccos Modified Eagle Medium
DNA	deoxyribonucleic acid
e.g.	example given
E16	embryonic day 16
EDTA	ethylenediaminetetraacetic acid
ER	endoplasmic reticulum
FCS	fetal calf serum
g	gram
g	centrifugal force
GAPDH	glyceraldehyde 3-phosphate dehydrogenase

gDNA	genomic DNA
GFAP	glial fibrillary acidic protein
GFP	green fluorescent protein
GnRH	gonadotropin-releasing hormone
GO	gene ontology
HCl	hydrochloric acid
HEK	human embryonic kidney
hESC	human embryonic stem cells
HSAS	hydrocephalus with stenosis of the aqueduct of sylvius
Hz	hertz
i.e.	lat. id est / that is
IHC	immunohistochemistry
IZ	intermediate zone
L1 -/x	L1CAM hemizygous male mouse
L1 -/y	L1CAM hemizygous male mouse
L1KO	L1CAM knockout
L1WT	L1CAM wildtype
LiCl	lithiumchloride
MAP3K	mitogen-activated protein kinase kinase kinase
max	maximum
MEM	minimum essential medium
min	minute
mm	millimeter
mRNA	messenger RNA
NDS	neurological deficit score
NFκB	nuclear factor 'kappa-light-chain-enhancer' of activated B-cells
ng	nanogram
NGS	Next Generation Sequencing
nm	nanometer
NMDA	N-Methyl-D-aspartic acid
NPC	Neural Progenitor Cell
NSC	Neural Stem cell
OFT	Open Field Test

PBS	phosphate-buffered saline
PCA	principal component analysis
PFA	paraformaldehyde
PNS	peripheral nervous system
pts	points
RFP	red fluorescent protein
RGD	Arginine, Glycine, and Aspartate-tripeptide
RIN	RNA integrity number
RIPA	radioimmuno precipitation assay
RNA	ribonucleic acid
RR	RotaRod-test
RT	room temperature
SCF	subcellular fractionation
SDS	sodium dodecyl sulfate
SDS-PAGE	SDS-polyacrylamide gel electrophoresis
SEM	standard error of the mean
Sema3A	semaphorin3A
SVZ	subventricular zone
TBS	tris-buffered saline
TBST	tris-buffered saline + Tween
TE	tris-EDTA
TEMED	tetramethylethylenediamine
ULA	ultra-low attachment
V	Volt
WNT	Wingless and Int-1
μl	microlitre
μm	micrometer

1. Introduction

1.1 Nervous system

The vertebrate nervous system consists of the peripheral nervous system (PNS) and the central nervous system (CNS). The CNS comprises the brain and the spinal cord, while the PNS involves the cranial and all the spinal nerves that connect the CNS with muscles and organs. The brain itself can be divided into 5 main compartments (from anterior to posterior): the telencephalon (or cerebrum), diencephalon, mesencephalon, metencephalon and myelencephalon. The telencephalon includes the cerebral cortex as well as several important subcortical structures like the hippocampus, amygdala and striatum [1]. The largest structure of white matter in the human telencephalon is the corpus callosum. This commissure made of axon fibers serves as a connection between both brain hemispheres to ensure their communication [2]. In general, axon fibers are essential for signal transmission, either from the CNS to efferent targets like muscles or *vice versa* from the body surface to the CNS. For example, the pyramidal tract is composed of large axon bundles which refer to the upper motor neurons located in the primary motor cortex and project to the spinal cord and brainstem and to control movements in the limbs and the torso [3]. The second brain compartment is called diencephalon and incorporates regions like the pituitary gland, several thalamic structures and the third ventricle [4]. The mesencephalon combines structures like tectum, tegmentum, some cranial nerve nuclei and the aqueduct of sylvius. The aqueduct of sylvius connects the third to the fourth ventricle and malformations are associated with some types of hydrocephalus [5,6]. The metencephalon comprises e.g. the pons, the fourth ventricle and the cerebellum [7]. The most caudal compartment is the myelencephalon (or medulla oblongata). The medulla is a connection between the pons and the spinal cord and controls autonomic functions like the regulation of respiration and the cardiovascular system [8].

1.2 Development of the cortex

In mice, the final formation of the neural tube can be defined as the onset of corticogenesis in the brain at around embryonic day 10 (Fig. 1). The interior of the neural tube is layered by a monolayer of radial glia which have the potential of asymmetrical and symmetrical cell division giving them stem cell-like properties [9]. Symmetrical cell division of radial glia gives rise to another pair of radial glia while asymmetrical division gives rise to one radial glia and one neuroepithelial cell. Neuroepithelial cells are the primary neural progenitors that are the origin of all other progenitors in the CNS and also differentiate to neurons [10]. The generation of neural progenitors and immature neurons is mostly restricted to the ventricular layer. Postmitotic neurons exit the ventricular zone to the apical site to form the preplate which then subdivides into the marginal zone, the cortical plate and the inner subplate. As more and more neurons are generated by asymmetric division of radial glia and migrate out of the ventricular zone six cortical layers emerge [11]. Each layer displays specific protein expression patterns that can be used as markers for investigations. For example, expression of the transcription factors (TF) Pax6 and Sox2 is restricted to the ventricular zone, making them useful markers for it, although Pax6 is only expressed at earlier stages of differentiation [12]. Further, Tbr2, another TF, can be used as a marker for intermediate progenitors located in the subventricular zone [13].

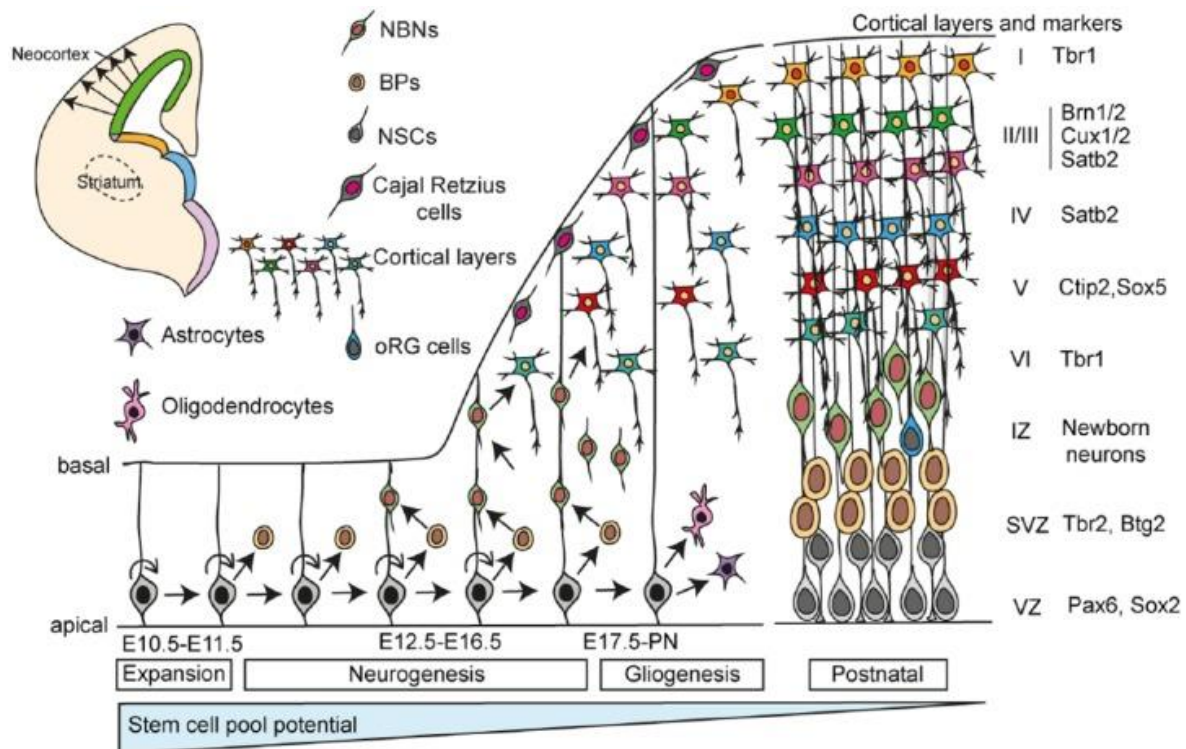


Fig. 1 Schematic illustration of corticogenesis in mice. This figure illustrates the lineages of cells that form the cortical layers during corticogenesis from embryonic day 10.5 (E10.5) to the postnatal period [14].

As indicated before, the correct formation of the cortex is a synergy of countless mechanisms like proliferation, differentiation and migration where the correct execution of each step is crucial for the following one. Even a single nucleotide change in essential genes is able to evoke a pathological phenotype as it can be seen in one type of lissencephaly. A study with 63 patients suffering from posteriorly predominant lissencephaly found that 77.5% carried a point mutation in the LIS1 gene [15]. The typical symptoms are mental retardation, epilepsy and spasticity likely due to deficits in neuronal migration [15]. Another congenital abnormality of cortical development that can be caused by a single point mutation is focal cortical dysplasia where the MTOR gene is affected. This disorder is the major cause for drug-resistant focal epilepsy [16]. The fact that a single point mutation in important genes can cause neurodevelopmental disorders makes transgenic mice an appropriate model.

1.3 Human embryonic stem cells in research and clinic

Investigations of human neurodevelopmental disorders have been greatly advanced by human embryonic stem cells (hESCs). hESCs are undifferentiated cells extracted from the inner cell mass of *in vitro* fertilized embryos [17]. These cells are pluripotent i.e. they have the capability to differentiate into cells from all three germ layers: ectoderm, endoderm and mesoderm, briefly speaking into all cell types. Early reports of the scientific use of pluripotent mouse embryonic stem cells (ESCs) date back to 1981 while the generation and use of stable hESCs lines was initially described years later in 1998. One of the first stable stem cell lines is the H1 embryonic stem cell line which was also used in one part of this work [18]. There are ethical debates about the scientific generation and use of hESCs due to the non-viability of the blastocyst after hESC extraction [19]. However, experiments with already generated stem cell lines are common use nowadays, although researchers need to obtain specific approval for experiments in Germany. The potential of ESCs in research is tremendous because their pluripotency makes them valuable for all sorts of niches in life science. For example, gene-edited stem cells were differentiated *in vitro* into vital neurons and were then morphologically investigated [20]. More recently, transplantation of ESC-derived neural crest cells promoted motor recovery after spinal cord injury in rats [21]. Such experiments in the laboratory are the basis for translating scientific knowledge into clinical trials and therapies. Meanwhile in the clinic, stem cell therapy is used in trials for several pathologies, e.g. in the recovery of eyesight, treatment of spinal cord injury and osteonecrosis. [22,23].

One unique *in vitro* model to investigate human embryonic development is the organoid. An organoid is a multicellular, self-assembled tissue derived from stem cells which were differentiated into specific cells characteristic for the organ the organoid is supposed to represent. Manifold types of this 3D cell culture model have been developed the last decade

with the purpose to mimic different organs or tissues [24]. The cerebral organoid is the most commonly used organoid model for studying brain development. The continuous attempt to replace animal studies with *in vitro* models is one major aspect and goal of scientific research (“3R principle”) but the intricacy of the mammal brain complicates this task. Typical *in vitro* assays comprise experiments with cultures of one or two different cell types at maximum, if not primarily derived from animals. Indeed, this experimental setup can’t nearly reflect the actual state and function of the complex mammal brain. Therefore, a more complex and representative *in vitro* method was much needed.

The first steps towards brain organoid cultures have been done by Watanabe *et al.* in 2005 who generated 3D cultures of different brain regions e.g. the forebrain [25]. Later, Lancaster *et al.* dedicated their research activities to the field of brain organoids. They not only found a way to reproducibly generate organoids with several brain regions inside one particular organoid but also managed to successfully model microcephaly disorder with organoids [26]. Their enhanced technique to produce cerebral organoids is based on the previous work from Watanabe *et al.* [27]. Lancaster *et al.* for example invented the technique to embed organoids in matrigel in order to improve neuroepithelial differentiation. Their latest protocol of how to reproducibly generate human cerebral organoids has been published in 2019 and is also the protocol that has been used in the present thesis [28]. Furthermore, work from this group has demonstrated that human cerebral organoids have common features with an embryonic mouse brain like the early cortical layers during corticogenesis (Fig. 2). As mentioned before, there are multiple types of organoids that have been established since Watanabe *et al.* paved the way in 2005. By this time, organoids were already generated mimicking different tissues of intestines, pancreas, liver, kidney, lungs and more [29]. Organoids in general are generated by using either a commercially available stem cell line (e.g. H1 or H9 hESCs) or by using induced pluripotent stem-cells derived directly from the patient. The benefit of patient-derived stem cells is that one can generate patient-specific organoids to study individual pathological mechanisms [30].

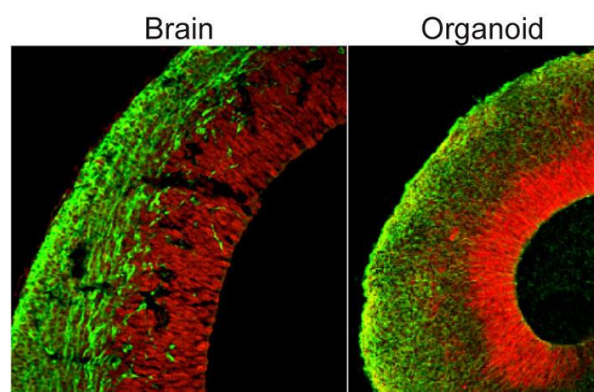


Fig. 2 Cerebral organoids can show structures similar to the embryonic mouse cortex. Immunofluorescence image of a cross-section of an embryonic mouse cortex and a human cerebral organoid. It shows neural progenitors in red and neurons in green [31].

1.4 Neural cell adhesion molecule L1/L1CAM

Cell adhesion molecules are particularly important for CNS development. The major classes of CAMs are the cadherins and protocadherins, integrins and the immunoglobulin superfamily [32]. Many gene mutations affecting members of these families have been identified as causative for neurodevelopmental disorders [33-35]. The neural cell adhesion molecule L1 or L1CAM (Fig. 3) is one of the most prominent CAMs implicated in neurodevelopmental disorders and is thus of clinical relevance [36-38]. L1CAM is a transmembrane type 1 glycoprotein and belongs to the immunoglobuline superfamily together with CHL1, Neurofascin and NrCAM.

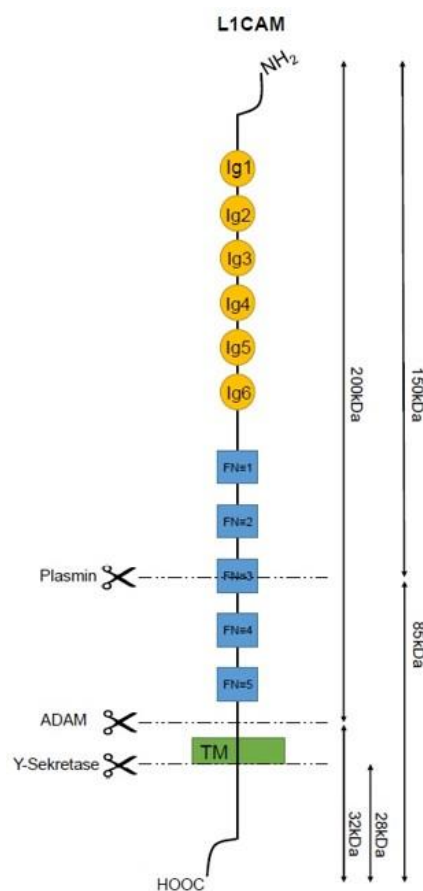


Fig. 3 Schematic structure of L1CAM. This schematic illustration of the L1CAM protein displays its extra-, intracellular and transmembrane domain (TM) with several cleavage sites and the sizes of L1CAM fragments after proteolytic cleavage in kDa.

This predominantly axonal protein comprises a large extracellular domain with 5 fibronectin type 3 domains, 6 immunoglobuline like domains, a transmembrane domain and a short cytoplasmic domain. Its expression is regulated by the zinc finger transcription factor RE-1-Silencing Transcription factor (REST) [39]. Mostly, L1CAM exists in two isoforms in human and mice generated by alternative splicing [40]. Neurons usually only express the full-length protein while non-neuronal cells express an isoform lacking the exons 2 and 27 [41]. After

translation and maturation of the protein it is transported to the cell surface via endosomes and fixated in the membrane by binding to cytoskeletal proteins like ankyrin [42,43]

L1CAM is involved in several processes besides the eponymous function of cell adhesion like the generation of transmembrane signals via tyrosine kinase receptors. Moreover, L1CAM is essential for proper neural development, due to its involvement in axon growth, axon pathfinding, neuronal migration, fasciculation and synaptogenesis [44-46]. Not only in the developing but also in the adult brain L1CAM is involved in important tasks like the establishment of neuronal networks and functions including synaptic plasticity [47]. Numerous ways have yet been elucidated how L1CAM transmits signals. L1CAM can elicit signaling through homo- and heterophilic interactions with other members of the immunoglobuline superfamily and RGD-dependent or independent binding of integrins [46]. Further, L1CAM-mediated signaling can be triggered via proteolytic cleavage of L1CAM, e.g. by ADAM10, TACE and Plasmin [48]. On the one hand, the ectodomain of L1CAM is released into the extracellular space after cleavage where it binds to e.g. integrins [49]. On the other hand, the intracellular domain translocates to the nucleus upon cleavage, where it serves as a transcriptional modulator, possibly via direct binding to nuclear proteins or interaction with transcription regulators such as MECP2 [50,51]

1.5 L1 syndrome

As mentioned above, L1CAM has been implicated with neurodevelopmental disorders. Over 350 frameshift, nonsense and missense mutations have been identified in the human *L1CAM* gene [41,52]. Nonsense and missense mutations are known to cause heterogeneous neurological conditions jointly referred to as L1 syndrome. Nonsense mutations in the *L1CAM* gene result in a truncated protein and missense mutations that influence the structure of the extracellular *L1CAM* domain are known to cause severe pathologies more often than missense mutations in the intracellular domain. Changes in the genomic sequence are usually point mutations resulting in an amino acid exchange. The mutations L1-R184Q (Arginine → Glutamine at pos. 184), L1-W635C (Tryptophane → Cysteine at pos. 635) and L1-I37N (Isoleucine → Asparagine at pos. 37) cause a retention in the endoplasmic reticulum (ER) and therefore prevent the translocation to the cell surface [47,53,54]. Other pathological mechanisms have been reported for mutations of L1-D202. L1D202Y (Aspartic acid → Tyrosine at pos. 202) for example impairs homophilic interactions at the cell surface [54]. Transgenic mice expressing this mutation on a L1 null background exhibit corpus callosum agenesis, retardation, motor dysfunction and hydrocephalus [55]. Additionally, there is a human mutation called L1D202N where an aspartic acid has been exchanged to an asparagine at position 202 (Fig. 4). In contrast to other mutations, the presentation at the cell surface is not affected here which makes it accessible for L1CAM mimetics [36]. L1D202N has already been described in two caucasian families where the males show intellectual disabilities. Both mutations of L1D202 are known to cause L1 syndrome [56].

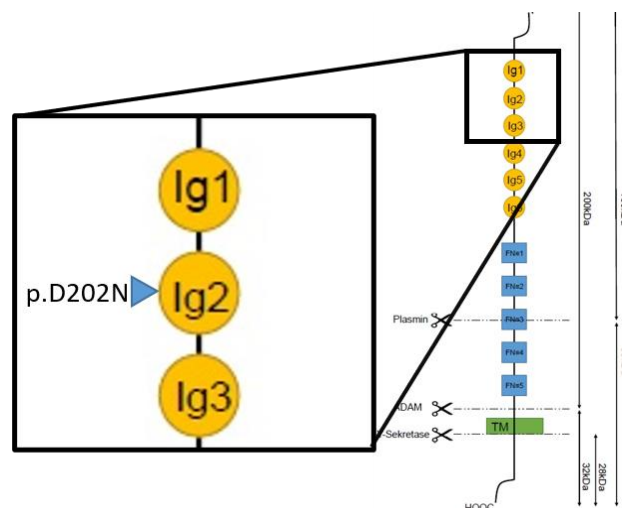


Fig. 4 Mutation site of L1D202N. This schematic illustration shows the position of the human mutation L1D202N in the second Ig-domain known to cause L1 syndrome.

The L1-syndrome or CRASH-syndrome is a rare X-linked developmental disorder characterized by the pathological features **C**orpus callosum agenesis, **R**etardation, **A**dducted thumbs, **S**pastic paraplegia and **H**ydrocephalus (CRASH). Medical treatments are restricted to symptomatic relief and the underlying mechanisms remain to be elucidated. The most common pathology in L1 syndrome is the X-linked hydrocephalus with an incidence of 1 in 30.000 males. Most patients undergo neurosurgery at young age to reduce the intracranial pressure and the ventricular volume by draining excess cerebrospinal fluid (CSF) through a shunt to the abdomen. Adducted thumbs are usually not treated by surgery but by applying a splint instead (Fig. 5A) [5]. Due to the X-linked heredity males are more affected than females and develop a more severe pathological phenotype [36]. Up to now, the origin of L1-linked dilated ventricles is unknown. According to theories, one possibility is that the reduced integrity of the white matter (as seen by corpus callosum agenesis) might lead to a reduced integrity of the ventricle causing hydrocephalus (Fig. 5B) since both pathologies are known to be connected [57-59].

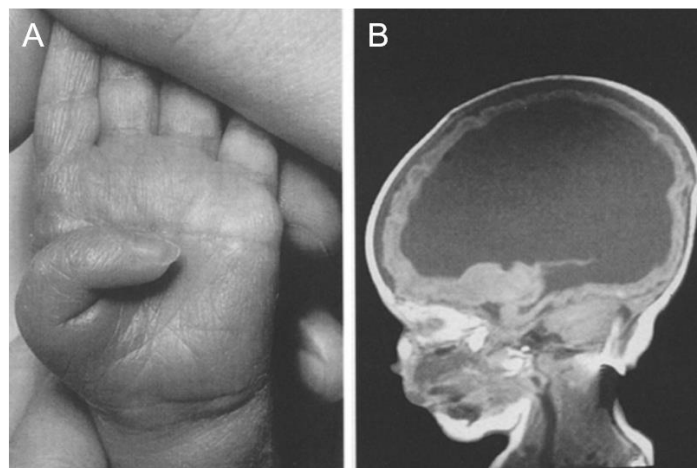


Fig. 5 Pathological phenotype of L1 syndrome. This illustration shows common pathological features of L1 syndrome. L1 syndrome pathologies involve (A) adducted thumbs and the (B) X-linked congenital hydrocephalus in newborns [60].

At least the mystery about one specific type of X-linked hydrocephalus has already been solved which is called X-linked hydrocephalus with stenosis of the aqueduct of sylvius or HSAS. As its name implies this type of L1-related hydrocephalus occurs due to the occlusion of a canal that connects the third and the fourth ventricle which reduces the circulatory flow of CSF. CSF is produced by epithelial tissue in the brain called choroid plexus (CP) which is also known to be involved in the formation of some types of hydrocephalus [61,62].

As already mentioned before, the agenesis/dysgenesis of the corpus callosum is one of the phenotypes of L1 syndrome. L1CAM is known for its necessity in axon growth, axon pathfinding and cell migration [44-46] and L1-deficient neurons or neurons expressing the

L1D202N mutant show deficits performing these tasks. In its most extreme form and dependent on the genetic background, axons in L1 knockout mice (L1KO) can show deficits to cross the hemispheres properly due to guidance issues where they end up in non-/dysfunctional axon clusters called Probst bundles (Fig. 6C+D).

Additionally, axons are supposed to cross the hemisphere at the medulla which is also reduced in brains of L1KO mice. These axons continue growing on the same hemisphere due to not being able to cross and stop at some point. This inefficient axon growth contributes to the motor dysfunctions seen in L1 syndrome patients.

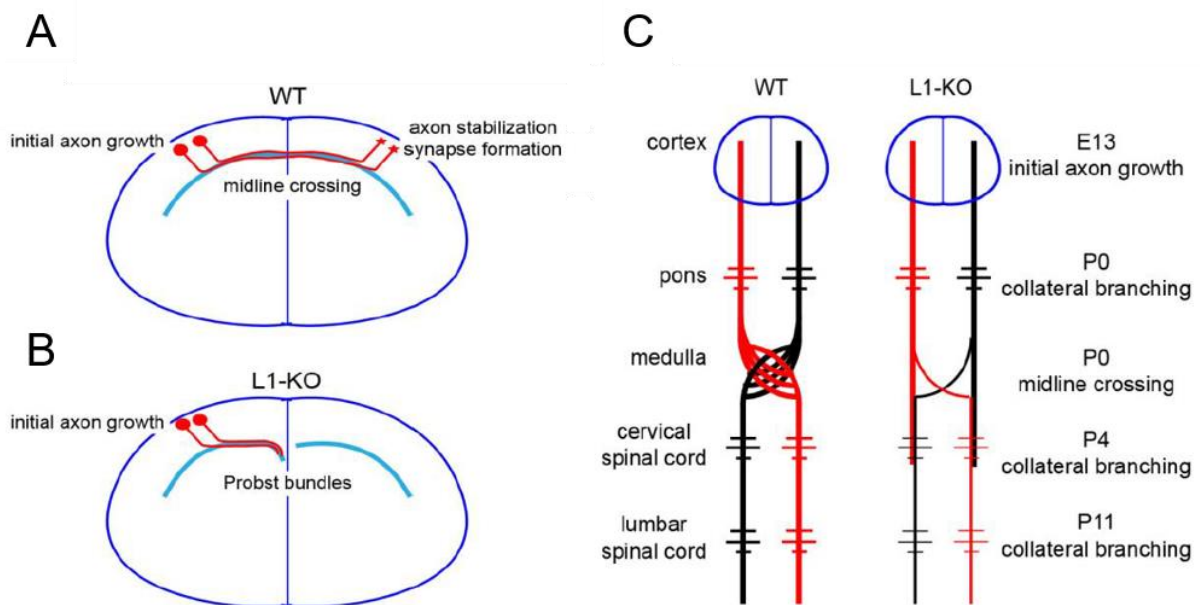


Fig. 6 Axonal guidance deficits in L1KO mice. (A) Normal midline crossing of axon fibers during neural development in control mice and (B) formation of Probst bundles in L1KO mice due to deficits in axonal guidance. (C) Murine development of the corticospinal tract from E13 to P11 of WT (left) and L1KO mice (right). Image by Schachner *et al.* outlining data from Demyanenko *et al.* and Cohen *et al.* [63,64].

1.6 Investigation of L1CAM in animal models

For the most part of scientific research the number one species used to model any sort of disease is the house mouse or *Mus musculus*. It is mostly preferred over other animal models like *Caenorhabditis elegans*, *Drosophila melanogaster* or *Danio rerio* because of their physiology which is very similar to the human. However, investigations of L1CAM function were already performed in all these animals and loss-of-function studies revealed L1 syndrome-like phenotypes (Table 1).

In this work we characterized two different mouse models for L1 syndrome called L1KO and L1D201N mice. L1KO mice were generated and initially investigated by Bartsch *et al.* in 2001 [65]. Here, the L1CAM protein was knocked out by an insertion of a tetracycline-controlled transactivator into the second exon of the *L1CAM* gene causing an interruption of the open reading frame which results in the production of a loss of function protein. Different research groups stated that these mice can display hydrocephalus and deficits in axon guidance. L1D201N mice exhibited an induced mutation in the *L1cam* gene (c.604G > T) causing a substitution from an aspartic acid (D) to an asparagine (N) in the amino acid sequence at position 201 [36]. This mutation can also be found in human patients at position 202, respectively [55,56] and does not affect the localization on the cell surface [36]. Their pathologies have not been characterized yet since it is a new mouse line generated by Schachner *et al.* [36]. *C. elegans* is another well investigated animal model known for its good accessibility to genetic modifications. The role of L1CAM homologues LAD-2 and SAX-7 were analyzed in *C. elegans* by several groups. For example, a *lad-2* knockout displayed altered axon guidance and neuronal migration while *sax-7* mutant nematodes showed altered neuronal positioning. Similar observations were made in *Drosophila* where a knockout of the L1CAM homologue Neurologin showed altered axon guidance. Interestingly a knockdown of the L1 homologue *l1camb* in *Danio rerio* revealed pathologies resembling the human L1 syndrome including hydrocephalus and altered axon growth.

Table 1 L1CAM animal models

name	animal model	pathologies	references
<i>L1cam</i> knockout	<i>mus musculus</i>	hydrocephalus altered axon guidance	Rolf <i>et al.</i> 2019 [65] Cohen <i>et al.</i> 1998 [64]
<i>lad-2</i> knockout	<i>C. elegans</i>	altered axon guidance altered neuronal migration	Chen and Zhou 2010 [66]
<i>sax-7</i> mutant	<i>C. elegans</i>	altered neuronal positioning	Chen and Zhou 2010 [66]
<i>Nrg</i> knockout	<i>Drosophila m.</i>	altered axon guidance	Martin <i>et al.</i> 2008 [67]
<i>l1camb</i> knockdown	<i>Danio rerio</i>	hydrocephalus altered axon growth myelination defects	Linneberg <i>et al.</i> 2019 [68]

1.7 Genomic sequencing and Gene ontology analysis

A major part of this work comprises Next Generation Sequencing (NGS) of murine brain tissue and human cerebral organoids. Historically, it was a long way from the first discovery of nucleic acids to the development of techniques to determine the nucleic composition of a sequence. The double helix structure of DNA was discovered in 1953 by Watson & Crick [69]. From then it took 24 years to develop a first sequencing method called Sanger sequencing named after the developer Frederick Sanger. This method was only suitable for DNA analysis and is based on the usage of di-deoxynucleotide triphosphates as well as gel electrophoresis. All technical innovations after Sanger sequencing in 1977 are summarized as Next Generation Sequencing. The Roche 454 device was developed in 2005 and allowed pyrosequencing which is based on the measurement of different Luciferase activities depending on the nucleotide in the sequence. Two years later in 2007 the Illumina technology was developed which is also the technology used in this work. Big milestones in genomic sequencing were the sequencing of whole genomes of different organisms beginning with *Drosophila melanogaster* and *Arabidopsis thaliana* in 2000 [70]. In 2003, sequencing of the whole human genome was finished successfully as part of the Human Genome Project which started back in 1990 using the Sanger method [70]. A major improvement in clinical research was the whole-genome sequencing of an acute myeloid leukemia sample in 2008. It demonstrated the capability of sequencing to identify pathology-related mutations and targets for medical treatments [71]. It was also a first step to switch from a phenotypic treatment approach to individual “precision medicine” which is common use in clinical trials of cancer therapeutics nowadays [72].

In this work we used RNA-seq data and subjected it to Gene Ontology (GO) analysis. The intention of the GO system is to establish an overall computational model of biological systems. It started back in 1998 as a union of researchers who investigated the genomes of *Drosophila melanogaster*, *Mus musculus* and *Saccharomyces cerevisiae*. These researchers collaborated to establish the GO system to uniformly describe the function of homologous genes. The main components of this system are the GO terms which represent specific classes of mechanisms in the organism like biological functions and pathways. Currently, the GO association is funded by the National Human Genome Research Institute in the US [73,74]. In this work different online tools were used for GO analysis: Pantherdb [75], GOrilla [76,77] and REVIGO [39].

1.8 Key points of this work

In this work we firstly characterized adult L1 syndrome mice called L1D201N and L1KO by motor function and behavior tests. Cryosectioned mouse brains were then analyzed by ventriculometry and the extent of the corpus callosum was assessed. Further, we subjected RNA samples extracted from adult L1 syndrome mouse brains to NGS. We also analyzed E16 L1KO brains by immunohistochemistry and qPCR analyses. As an *in vitro* model for L1 syndrome we generated L1CAM-deficient human cerebral organoids and subjected them to RNA-seq. The evaluation of human cerebral organoids revealed a L1CAM-related regulation of WNT signaling which we further assessed in a β -Catenin nuclear translocation assay using HEK-cells.

2. Material and Methods

2.1 Materials

Table 2 Chemicals and substances

4',6-diamidino-2-phenylindole (DAPI)	ThermoFisher Scientific, USA
Abs.Blue QPCR Sybr Green Mix	ThermoFisher Scientific, USA
Accutase	Sigma-Aldrich, Germany
Acetic acid	Carl Roth, Germany
APS	Sigma-Aldrich, Germany
Aqua steril	Braun, Germany
B27+RA	ThermoFisher Scientific, USA
B27-RA	Life Technologies, Germany
bFGF	Peprotech, Germany
bovine serum albumin (BSA)	Sigma-Aldrich, Germany
chameleon protein ladder	Li-Cor Biosciences, Germany
chloroform	Roth, Germany
Cresylviolet	Merck, Darmstadt
Cutsmart buffer	NEB, England
Cytoseal	ThermoFisher Scientific, USA
Ddel	NEB, England
DMEM	Gibco, Darmstadt
Entellan embed medium	VWR, Germany
Ethanol absolut	Roth, Germany
fetal calf serum	Life Technologies, USA
fetal calf serum	Gibco, Germany
hydrogen chloride	Roth, Germany
Instamed PBS Dulbeco	Biochrom, Germany
Insulin solution human	Sigma-Aldrich, Germany
isopropyl alcohol	Roth, Germany
Jet prime	Polyplus, Illkirch, France
Liquid nitrogen	Air Liquide, Germany
lithiumchloride	VWR, Germany
Luxol fast blue	Sigma-Aldrich, Germany

Matrigel	Corning
MEM	Gibco, Germany
Mercaptoethanol	Sigma-Aldrich, Germany
Methanol abs.	Merck, Darmstadt
mTeSR1	StemCell Technologies, Germany
N2 supplement	Life Technologies, Germany
NEG50	ThermoFisher Scientific, USA
NP-40	ThermoFisher Scientific, USA
PageRuler protein ladder	ThermoFisher Scientific, USA
paraformaldehyde	Merck, Darmstadt
penicilline/streptomycine	Life Technologies, USA
phosphatase inhibitor	Sigma-Aldrich, Germany
PrimaQuant buffer	Steinbrenner Laborsysteme, Germany
protease inhibitor	Sigma-Aldrich, Germany
Roti Histofix	Roth, Germany
Roti-Histol	Carl Roth GmbH, Germany
Rotiphorese acrylamide	Roth, Germany
skimmed milk powder	Roth, Germany
sodium chloride	Roth, Germany
sodium dodecylsulfate (SDS)	Roth, Germany
SYBR green buffer	ThermoFisher Scientific, USA
tetramethylethylenediamine (TEMED)	Carl Roth, Germany
thiazovivin	Sigma-Aldrich, Germany
tris-hydroxymethyl-aminomethane (tris)	Roth, Germany
Triton X-100	Sigma-Aldrich, Germany
Trypsin-EDTA	Sigma-Aldrich, Germany
Tween-80	Sigma-Aldrich, Germany
Tween-80	Roth, Germany
Xylol	Roth, Germany
β -mercaptoethanol	Roth, Germany

Table 3 Buffers and media

cresylviolet	stir 5 g cresylviolet in 100 ml ethanol abs. 30 min at 50 °C, ad. 500 ml Aqua, filter solution
4 % paraformaldehyde	70 °C 125 ml ddH ₂ O, 10 g PFA, 0.25 ml 10 M NaOH, filter solution, 125 ml 0.2 M phosphate buffer
1x phosphate buffered saline (PBS)	9.55 g Instamed PBS/ 1000 ml Aqua st.
SDS-loading buffer	30 g Tris, 140.4 g Glycin, 10 g SDS in 1 L H ₂ O
two 10 % separating mini gel	3.3 ml acrylamide, 4.1 ml H ₂ O, 2.5 ml Lower buffer, 5 µl TEMED, 150 µl APS
two 5 % stacking gel	1.25 ml acrylamide, 2.4 ml H ₂ O, 1.25 ml Upper buffer, 5 µl TEMED, 75 µl APS
Blotting buffer	25 ml 25 mM Tris-HCl (pH 8.3), 14.4 g 192 mM Glycin in 20 % methanol
10x TBS	60.6 g Tris, 87.6 g NaCl, 1 M HCl
50 ml 10 % Transfection medium	45 ml DMEM + 5 ml FCS + 0.5 ml Pen/Strep
Primary antibody-solution western blot	antibodies diluted in 2.5 % skimmed milk-TBS
Secondary antibody-solution western blot	1:15000 in 2.5 % skimmed milk-TBS
Radio Immuno Precipitation Assay buffer (RIPA)	150 mM NaCl, 50 mM Tris-HCl (pH8), 1 % Nonidet P-40, 0.1 % SDS, 1 tablet phosphatase and protease inhibitor each in 10 ml RIPA
SCF buffer	20 mM HEPES (pH7.4), 10 mM KCl, 2 mM MgCl ₂ , 1 mM EDTA, 1 mM EGTA
1x TBST	1x TBST + 1:1000 Tween-20
Genotyping digestion buffer	10 µl buffer A, 5 µl buffer B, 35 µl H ₂ O
Lower buffer	1.5 M Tris-HCL (pH 8.8), 0.1 % SDS
Upper buffer	0.5 M Tris-HCL (pH 6.8), 0.1% SDS
LFB solution	1g LFB, 1000ml 95% isopropyl alcohol, 5 ml acetic acid
Neural induction medium	1 % (v/v) N2 supplement, 1 % (v/v) GlutaMAX supplement, 1 % (v/v) MEM-NEAA solution in DMEM/F12 with 1 µg/ml heparin
differentiation medium-RA	0.5 % (v/v) N2 supplement, 1 % (v/v) B-27-RA supplement without vitamin A, 1 % (v/v) GlutaMAX supplement, 0.5 % (v/v) MEM-NEAA solution in 1:1 DMEM/F12:Neurobasal medium, insulin 2.5 µg/ml, 3.5 µl/l neat 2-mercaptoethanol, 100 U/ml penicillin and 100 µg/ml streptomycin
differentiation medium+RA	0.5 % (v/v) N2 supplement, 1 % (v/v) B-27+RA supplement with vitamin A, 1 % (v/v) GlutaMAX supplement, 0.5 % (v/v) MEM-NEAA solution in 1:1 DMEM/F12:Neurobasal medium, insulin 2.5 µg/ml, 3.5 µl/l neat 2-mercaptoethanol, 100 U/ml penicillin and 100 µg/ml streptomycin

Table 4 Devices

2100 Bioanalyzer	Agilent, Germany
AxioCam MRc 5 farbig	Zeiss, Germany
Cell counting chamber	Carl Roth, Germany
Chemical weighing scale L2200P	Sartorius laboratory, Germany
Cryosectioning blades	Apollo, Plano, Germany
Cryotome HM560	Microm, Germany
Ethovision XT	Noldus, Netherlands
Evos FL inverted microscope	Fisher Scientific, Germany
GE NanoVue spectrometer	GE Healthcare Systems, USA
Glomax Plate Reader	Promega, Germany
Ikamag RH magnetic stirrer	Janke und Kunkel, Germany
LightCycler 480	Roche Diagnostics, Germany
LSM 510 confocal microscope	Zeiss, Germany
Master Thermocycler	Eppendorf, Germany
New Brunswick Galaxy 170R incubator	Eppendorf, Germany
Odyssey Sa Imaging System	Li-Cor Biosciences, Germany
Orbital shaker KM CO2	Edmund Bühler, Germany
Pipet Boy	Hirschmann, Germany
Pipets	Eppendorf, Germany
QIAxcel Advanced	Qiagen, Germany
Qubit	Invitrogen, Germany
Rotamax 120 shaker	Heidolph, Germany
Rotanta/RP centrifuge	Hettich, Germany
RotaRod	Harvard Apparatus, USA
Stemi 305 stereo microscope	Zeiss, Germany
Stemi microscope 305	Zeiss, Germany
Thermomixer	Eppendorf, Germany
Tissue Lyser MM300	Qiagen, Germany
Trans-Blot Turbo Blotting System	BioRad, Germany
VF2 Vortexer	Janke und Kunkel, Germany
Water bath GFL	GFL-Gesellschaft für Labortechnik, Germany

Table 5 Consumables

12-well plates	VWR, Germany
12-well ULA plates	Sigma-Aldrich, Germany
15ml falcon tubes	Greiner, Germany
50ml falcon tubes	Greiner, Germany
60mm petri dish	Greiner, Germany
96-well plates	VWR, Germany
96-well ULA plates	Sigma-Aldrich, Germany
cell culture flasks	Greiner, Germany
cell culture plates	Greiner, Germany
cell strainer	Miltenyi, Germany
DAKO pen	Agilent, Germany
Eppendorf reaction tubes	Greiner, Germany
nitrocellulose membrane	Merck Millipore, USA
object slides	Thermo Scientific, USA
Parafilm	Sigma Aldrich, Germany
PCR plate seals	Biozym, USA
PCR plates	Biozym, USA
pipet tips	Greiner, Germany
serological pipets	Greiner, Germany
serological pipettes	Greiner, Germany
syringe needles	Braun, Germany

Table 6 Primary Antibodies

Immunogen	Used in	Conjugate	Host	Clone/order-no	Concentration	Producer
L1CAM	WB	-	rabbit	HPA005830	1:1000	Sigma, Germany
L1CAM	IHC	-	rabbit		1:1000	Fritz Rathjen, MDC, Berlin
GFP	WB	-	rabbit	ab290	1:500	Abcam, Germany
Sox2	IHC	-	rabbit	AB5603	1:500	Millipore, Germany
Pax6	IHC	-	rabbit	Poly19013	1:500	Biologend, Germany
Claudin5	IHC	-	rabbit	34-1600	1:500	Invitrogen, Germany
Ki67	IHC	-	rat	SolA15	1:500	eBioscience, Germany
Tbr2	IHC	-	rat	Dan11mag	1:250	Thermofisher, Germany
H3 histone	WB	-	rabbit	9715	1:2000	Cell Signaling, Germany
GAPDH	WB	-	ms	6C5	1:10000	Origene, Germany

Table 7 Anti IgG secondary antibodies

Reactivity	Used in	Conjugate	Host	Concentration	Producer
mouse	WB	IR Dye 680RD	goat	1:15000	Li-Cor, Germany
rabbit	IHC	AlexaFluor488	goat	1:500	ThermoFisher, Germany
rabbit	IHC	AlexaFluor633	goat	1:500	ThermoFisher, Germany
rabbit	WB	IR Dye 800RD	goat	1:15000	Li-Cor, Germany
rabbit	WB	IR Dye 680RD	goat	1:15000	Li-Cor, Germany
rat	IHC	AlexaFluor488	goat	1:500	ThermoFisher, Germany
rat	IHC	AlexaFluor568	goat	1:500	ThermoFisher, Germany

Table 8 Kits

DC Protein assay	Bio-Rad, Germany
My Taq Extract-PCR Kit	BioCat, Germany
Polyplus jetPrime transfection kit	VWR, Germany
QuantiTect reverse transcription kit	Qiagen, Germany
RNA Library Prep Kit for Illumina	NEB, England
Rneasy plus extraction kit	Qiagen, Germany

Table 9 PCR primer

mouse primer	5' --->3'	amplicon size (bp)	gene accesssion number
Aqp1-F	AGACACTCTGACAAGCTGAC	187	NM_007472.2
Aqp1-R	TCCCTCACTTTCACTCCTCC		
Aqp4-F	GGAGAAGAGAAGAAGGGGAAAG	181	NM_001317729.1
Aqp4-R	TGTAACAAGGTGTGAAGCAAG		
BAX-F	AGACAGGGGCCTTTTTGCTAC	137	NM_007527.3
BAX-R	AATTCGCCGGAGACTCG		
Casp3-F	TGGTGATGAAGGGGTCATTTATG	105	NM_001284409.1
Casp3-R	TTCGGCTTTCCAGTCAGACTC		
Gap43-F	AGGAGCCTAAACAAGCCGAT	150	NM_008083
Gap43-R	CGTCTACAGCGTCTTTCTCCTC		
Ppia F	GCGTCTSCTTCGAGCTGTT	146	NM_008907
Ppia R	RAAGTCACCACCCTGGCA		
Trp53-F	CCCCTGTCATCTTTTGTCCCT	137	NM_011640
Trp53-R	AGCTGGCAGAATAGCTTATTGAG		
VGlut2-F	ACTATGCGCAGAATCCGTCT	177	NM_080853
VGlut2-R	GCTTCTTCTCCAGCACCCCTGTA		
human primer	5' --->3'	amplicon size (bp)	gene accesssion number
h-DCX-F	TTGCCCTGTCTAATTTTGCC	135	NM_000555.3
h-DCX-R	AAAAGGGGCACTTGTGTTTG		
h-GAP43-F	AAGAGAGAGAAGGAAAGGAGAG	118	NM_001130064.2
h-GAP43-R	GAAAACAACCCAGAGACCAG		
h-GFAP-F	AGAGATCCGCACGCAGTATG	81	NM_002055.5
h-GFAP-R	TCTGCAAACCTTGAGCGGTA		
h-Grin2a-F	CAACCATCTCAGCATCGTC	155	NM_001134407.3
h-Grin2a-R	ATTTCTTCACATTCATCCCCTC		
h-Pax6-F	ATTTTGTGTGAGAGCGAGCG	246	NM_000280.4
h-Pax6-R	TCTCAGATTCTATGCTGATTGGT		
h-PPIA-F	CCCACCGTGTCTTCGACATT	275	NM_021130
h-PPIA-R	GGACCCGTATGCTTTAGGATGA		
h-Sox2-F	CCCAGCAGACTTCACATGT	151	NM_003106.4
h-Sox2-R	CCTCCCATTTCCCTCGTTTT		
h-vGAT-F	ATTGCGACGACCTCGACTTT	265	NM_080552.3
h-vGAT-R	ACGAACATGCCCTGGATGG		
h-vGluT2-F	TCAGATTCGGGAGGCTACA	175	NM_020346.3
h-vGluT2-R	TGGGTAGGTCACACCCTCAA		

Table 10 Software

CLC Workbench	Qiagen, Germany
GOrilla	http://cbl-gorilla.cs.technion.ac.il/
Illustrator 2020	Adobe, USA
ImageJ	NIH Image, USA
ImageStudio	Li-Cor, USA
Panther GO	Gene Ontology Phylogenetic Annotation Project
Prism	GraphPad, USA
REVIGO	http://revigo.irb.hr/
PyRat	Scionics

2.2 Methods

2.2.1 Animal husbandry and assessment of L1CAM-mutant mice

L1KO and L1D201N mouse lines were provided by Melitta Schachner, ZMNH, Hamburg and maintained in the animal facility 905 in the University Medical Center Mainz with 12h day/night cycles with food and water *ad libitum*. 8-9 week old mice from the L1KO and L1D201N lines were investigated in the initial assessments. Male and female mice hemi-/heterozygous for L1CAM as well as corresponding wildtype littermate controls were subjected to neurological motor function and behavioral tests. In order to analyze E16 embryonic mice, overnight breedings were performed. In each cage two heterozygous (-/+) females and one wildtype (+/y) male mouse were united in the afternoon and separated the next morning, which counts as day 1. On day 16, the pregnant mice were transported to the laboratory to dissect the embryos.

All animal experiments were performed in compliance with institutional guidelines of the Johannes Gutenberg-University Mainz, Germany and approved by the Animal Ethics Committee of the Landesuntersuchungsamt Rheinland-Pfalz (protocol numbers G 18-1-097).

2.2.2 Generation of L1CAM mutant mouse lines

In L1KO mice, the L1CAM protein was knocked out by an insertion of a tetracycline-controlled transactivator into the second exon of the *L1CAM* gene causing an interruption of the open reading frame which results in the production of a loss of function protein. Technically this mutation is a knock-in that causes a knockout but it is further referred to as L1KO. This mouse line was originally generated and initially investigated by Bartsch *et al.* in 2001 [65]. L1D201N mice exhibited a missense mutation in the *L1CAM* gene (c.604G > T) causing a substitution from an aspartic acid (D) to an asparagine (N) in the amino acid sequence at position 201 [36], which can also be found in human patients at position 202 [55,56] and does not affect the localization on the cell surface [36].

2.2.3 Genotyping of transgenic mice

With 3 weeks of age the pups of mouse litters were separated from the parents and divided by gender into new cages with 5 animals each. While separating males from females ear biopsies were taken for genotyping. DNA extraction and PCR analysis were performed with MyTaq™ Extract-PCR Kit (BioCat). Due to the tissue size, 50 µl extraction buffer per sample was prepared instead of 100 µl according to the original protocol (10 µl buffer A, 5µl buffer B, 35µl water). The tissue/extraction buffer-mix was incubated at 75 °C for 5 min and deactivated at 95 °C for 9 min. The suspension was centrifuged at 17000 g for 1 min to pellet cellular debris. The supernatant was transferred to a new tube and stored at -20 °C until PCR analysis. The PCR cycles are shown in Table 11. The L1KO PCR protocol requires 39 cycles, while the L1D201N protocol requires 45 cycles.

Table 11 Genotyping PCR program

1. 95 °C (initial denaturation)	3 min
2. 95 °C (denaturation)	15 sec
3. 60 °C (Annealing)	15 sec
4. 72 °C (Extension)	1 min
5. GoTo 2. Rep.39 or 45	
6. 72 °C Final Extention	3 min
7. 4 °C	∞

Additionally, L1D201N PCR products had to be incubated with restriction endonucleases before gel electrophoresis, so the mix in Table 12 was prepared.

Table 12 L1D201N restriction endonuclease mix

Cutsmart buffer (NEB)	3 µl
Ddel 10000 u/ml (NEB)	0.2 µl
H ₂ O	11.8 µl
total	15 µl

15 μ l restriction endonuclease mix + 10 μ l PCR product were incubated at 37 °C for 60 min and analyzed with the Qiaxcel Advanced System (Qiagen). Only hemizygous males, heterozygous females and corresponding wildtype littermate mice were subjected to behavioral, histological and molecular biological analysis which was the reason for genotyping. The genotyping result can display PCR amplicons of different sizes (Fig. 7) which are used to distinguish between control (+/+ or +/y) and mutant (-/+ or -/y) mice. For the L1KO line, +/y male or +/+ female mice display an amplicon with a size of 350 bp while -/y males display an amplicon with a size of 450 bp. L1D201N +/y males and +/+ females mice display two bands with a size of 200 bp and 150 bp due to enzymatic cleavage of the amplicon by the restriction enzyme DdeI while mutant male mice show a non-cleaved amplicon with a size of 350 bp.

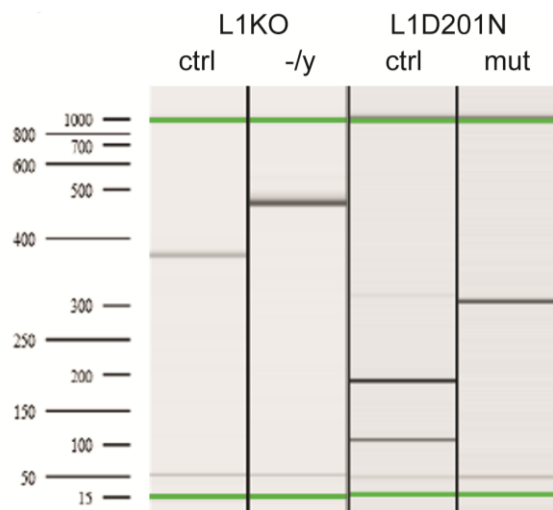


Fig. 7 Genotyping of L1CAM-mutant mice. PCR genotyping result showing the amplicons of L1KO and L1D201N male mice. The Y-axis represents the basepair marker to identify the genotype of each mouse.

2.2.4 Motor function and behavior tests

The genetically modified 8-9 week-old mice either have a mutation (L1D201N) or a knockout of the L1CAM (L1KO) gene and were used as a mouse model for the human L1 syndrome. To investigate their pathological phenotype the mice were subjected to several tests that elucidate the extent of neurological deficits. The mice were subjected to a 13-point motor function test called neurological deficit score (NDS, Table 13), a RotaRod test (RR) modified from Tsender *et al.* [78] and a widely used camera-assisted Open Field Test (OFT) using EthoVision technology [79].

Neurological deficit score

1. Startle reflex:

The mouse receives a NDS point if it does not startle at the sound of a handclap. It is important, that the mouse does not see the actual procedure of clapping so it is only an auditory reflex.

2. Seeking behavior:

The mouse receives a NDS point if it does not show seeking behavior mostly shown by sniffing and walking around.

3. Walking straight line:

The mouse receives a NDS point if it is not able to walk a straight line.

4. Walking beams

The mouse has to walk over wooden beams with the widths 3, 2 and 1 cm in descending order in a height of about 10 cm. The mouse receives an NDS point if foot misplacements occur, i.e. that one or more feet slip from the beams. It receives 2 NDS points if it falls down or does not walk over the beam at all.

5. Balance/grip strength

The mouse receives a NDS point if it is not able to grip a round stick with all paws for 10 seconds. The same applies for a square stick.

6. One foot/hemiparesis

The mouse receives a NDS point if it has a visible one-foot-paresis and two points if it shows a hemiparesis.

Table 13 NDS scoresheet

Animal ID:				
		Day 1	Day 2	Day 3
		date	date	date
1. Reflexes				
startle reflex	Present (0)			
	Absent (1)			
If the mouse is not moving at all, clap your hands once above the mouse; did it react?				
2. General behavioral deficit?				
Seeking behavior	Present (0)			
	Absent (1)			
Walk straight	Present (0)			
	Absent (1)			
3. Coordination				
Beam walking 3 cm	Score (0-2)			
Beam walking 2 cm	Score (0-2)			
Beam walking 1 cm	Score (0-2)			
Criteria: 0 point: normal movement				
1 points: feet misplacements / unstable movement				
2 points: sits down / stops moving on beam / falls down				
4. Balance				
Round stick	Score (0-1)			
Square stick	Score (0-1)			
Criteria: 0 point: Can grip the stick with 4 paws for 10 seconds				
1 points: turn the stick: can it do that again, or is a paw (hemiparesis) "hanging out"				
5. Motor deficit				
Paresis	Absent (0)			
	One foot (1)			
	Hemiparesis (2)			
Total score (13pts max)				

RotaRod

The Rota-Rod device (Harvard Apparatus, Fig. 8) was utilized to investigate motor ability of the mice. Their performance was evaluated by their ability to stay on a rotating rod with increasing rotation speed over time. When the mouse reached its limits and is not able to stay on the moving rod anymore it falls down onto a plate which automatically stops the time-counter. The cylindrical rod with a diameter of 3 cm starts spinning with 4 rpm and increases up to 40 rpm during 5 min maximum experiment time. In our experience it takes some practice for the mice to know what they are supposed to do in this test. For this reason, two days of practice were performed before the actual 3 days of testing. Each mouse was tested two times per day and the best daily score has been subjected to statistical analysis.

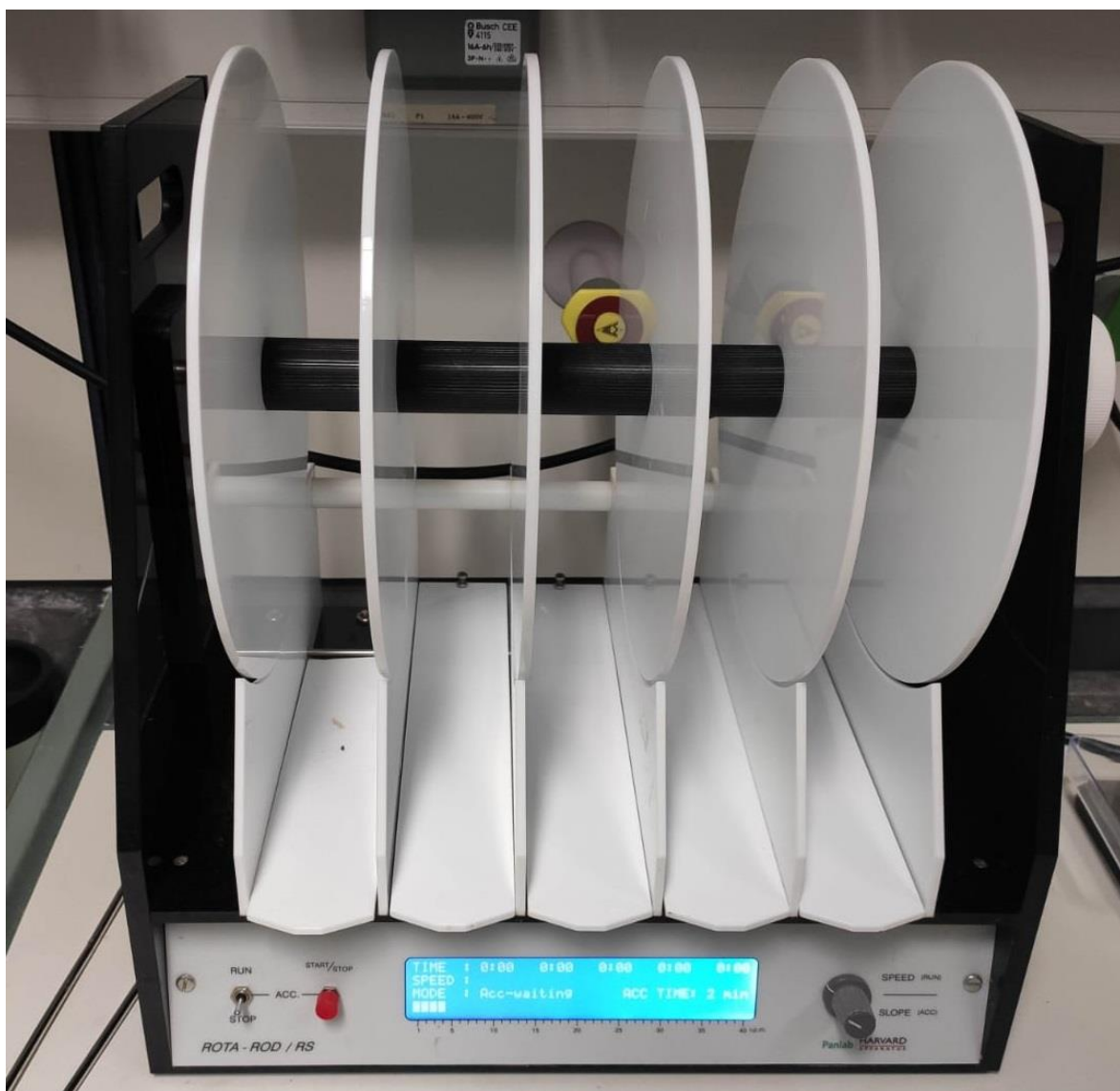


Fig. 8 RotaRod device for motor function test. The RotaRod device by Harvard Apparatus was used to assess motor function deficits of transgenic mice. The device consists of a cylindrical rod with increasing rotation speed. The mouse is placed on top of the rod and time is recorded until the mouse falls down and triggers a switch that stops the time-counter.

EthovisionXT Open Field Test

The Ethovision XT setup (Noldus) was used to evaluate behavioral abnormalities between control and mutant mice in an OFT. The setup consists of a grey cube 40x40x40 cm with an open top and a camera that tracks the mouse running inside the cube from an aerial perspective (Fig. 9).



Fig. 9 Ethovision XT Open field test setup for behavioral investigation. The Noldus Ethovision XT setup was used to perform behavioral analysis on transgenic mice. The cubes dimensions are 40x40x40 cm. The high-definition camera observes the field area and tracks the mice from above.

The software tracks the velocity and distance the mouse covers during the 3 min timeframe of the experiment. In the beginning of the test the mouse was placed in the center of the cage (Fig. 10A). The provided software is able to identify the nose, body and tail of the mouse and generates a virtual circle with a diameter of 20 cm (Fig. 10B). After starting the trial (Fig. 10C) the 3 min recording time begins with a 1 second delay to make sure the investigators hand is not recorded which can cause errors otherwise. The principle of this test is that healthy, unconditioned mice would immediately leave the open area in the center in search for a safer place like walls or corners as a result of anxiety behavior. Mice that have developed an abnormal phenotype due to genetic modifications might not be as anxious as the controls and don't leave the circle as fast. Also, differences in movement activity can be investigated by measuring velocity and distance which the software is tracking. Initially this test was performed as an Exit of Circle test, which is why different zones were drawn on the floor image in the software (Fig. 10B).

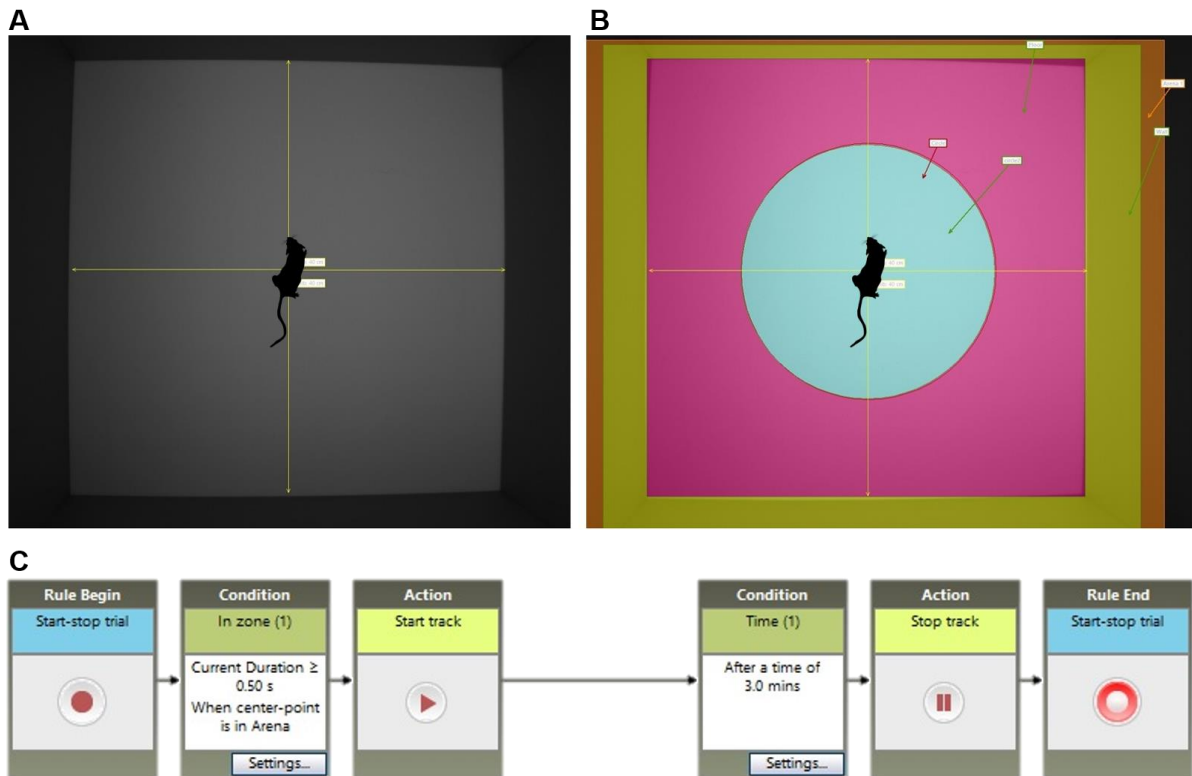


Fig. 10 Trial layout in EthovisionXT software. (A) Background image of the cubes floor also showing the mouse in the middle. Each arrow indicates a length of 40 cm. (B) Illustration of different zones in the cube of the initial Exit of Circle test (turquoise= inner circle, pink= floor, yellow= walls, orange=outside the cage). (C) Recording layout of the 3 min OFT trial.

2.2.5 Mouse killing, brain dissection and storage

Adult mice

After the mice were subjected to motor function and behavioral analysis they were sacrificed and their brains were collected. Herefore, each mouse was anesthetized with 4 % isoflurane for 1 min until deep narcosis occurred and then sacrificed by cervical dislocation. The brain was collected after decapitation by opening the cranial bone with a scissor. 2 incisions from the foramen magnum to the auditory canals and one from the foramen magnum along the sagittal and interfrontal suture to the frontonasal suture exposed the brain. The brain was then collected and flash frozen on powdered dry ice (-80 °C). The brains were then stored in plastic bags at -30 °C until cryosectioning.

E16 embryo mice

16 days after impregnation the pregnant females were anesthetized with 4 % isoflurane until deep narcosis occurred and sacrificed by cervical dislocation. The peritoneum was opened so that both arms of the uterus were exposed. All embryos, still enclosed by the uterus and amniotic sac, were carefully retrieved from the amniotic sac and decapitated. The embryos heads were flash frozen on powdered dry ice (-80 °C) and stored in plastic bags at -30 °C until cryosectioning. Tail biopsies were taken after sacrifice for genotyping. Only wildtype

(+/+ and +/-) and male hemizygous mice (-/-) were subjected to cryosectioning, as well as immunohistochemical and molecular biological analysis.

2.2.6 Cryosectioning

Adult mice

To further process the brains for immunohistochemical and molecular biological analyses, consecutive coronal sections were prepared at -20 °C using a cryotome (Microm) as already reported [80]. The brain was placed on a metallic plate in a 90° angle with the cerebellar site first and then completely covered with NEG-50 embedding medium to stabilize the tissue integrity during sectioning. Of each brain, 16 sections with a thickness of 12 µm were collected for stainings and eight section-stacks with a specific thickness (6x40 µm) were collected in cryotubes for RNA analysis. The first section (layer 1/ 0 µm) was collected in a layer where the two areas of both olfactory bulbs are equal in size to the two areas of the frontal cortex (approx. Bregma +3 mm). Every 500 µm a section was collected until n=16. Starting from layer 6/ 2500 µm, section-stacks were collected for RNA analysis. The lower third of the stack was discarded while the upper part was divided into the left and right hemisphere of the brain. One hemisphere for RNA and one hemisphere for protein analysis. The stacks of each side were collected in different cryotubes, kept in liquid nitrogen (Air Liquide) for transport and stored at -80 °C while cryosections were stored at -20 °C until analysis.

E16 embryo mice

In addition, also brains of E16 mice were cryosectioned with a similar protocol as used for adult mice. Of each brain, 16 consecutive sections with a thickness of 12 µm were collected for stainings and two section-stacks with a specific thickness (8x12 µm) were collected in cryotubes for RNA analysis. The first section (layer 1/ 0 µm) was collected in a layer where the areas of both olfactory bulbs are equal in size to the frontal cortex. Every 150 µm one section was collected until n=16. At layer 6/800 µm, section-stacks were collected for qPCR analysis (16x12 µm) and again at layer 9/1500 µm. The stacks were transported in liquid nitrogen (Air Liquide) and stored at -80 °C while cryosections were stored at -20 °C until analysis.

2.2.7 Nissl/cresyl violet staining

For the quantification of ventricle sizes in cryosections of transgenic mice Nissl stainings were performed as described previously [80]. Cresyl violet binds to basophile structures like DNA and RNA which is why mostly nuclei and the rough endoplasmic reticulum are stained. These stainable cell compartments are called Nissl bodies and due to their high density in

neurons, neuronal structures can be analyzed with this technique. 12 staining containers were prepared under a fume hood, with 3x 70 % ethanol, 2x aqua dest., 2x 96 % ethanol, 2x ethanol absolute, 2x Roti-Histol and one container with cresylviolet. Cryosections were airdried for 1 h at RT. Then, the slides were incubated in 70 % ethanol for two minutes to slowly rehydrate the tissue, followed by a 10 min incubation in cresylviolet. Afterwards, the slides were shortly drenched two times each in 70 % ethanol, 96 % ethanol and 100 % ethanol. The slides were then placed in Roti-Histol for 5 min and another 2 min in new Roti-Histol and embedded with Entellan (VWR) afterwards. Imaging was performed using a stereo microscope (Zeiss).

2.2.8 Luxol fast blue/Nissl staining

Most Luxol fast blue stainings were kindly performed by Nicole Roder from the institute of neuropathology at the University Medical Center Mainz led by Prof. Clemens Sommer. The following protocol was used to stain the myelin sheath as well as grey matter and nuclei:

At first, the cryosections were thawed for 10 min at RT. The sections were transferred to a staining cuvette, sealed with parafilm and incubated overnight in LFB solution at 60 °C in a water bath. The next day, all sections were washed with 75 % isopropyl alcohol (Roth), followed by tap distilled water. Differentiation of the staining was performed in 75 % ethanol and repeated until the desired staining was reached. Then, the slides were washed again with distilled water, followed by 5 min incubation in cresylviolet solution and a washing step with distilled water again. Afterwards, the slides were dehydrated in 70 %, 2x 96 % and 2x 100 % isopropyl alcohol for a few seconds. Lastly, the slides were incubated 2x in Xylo (Roth) and embedded with Cytoseal (ThermoFisher).

2.2.9 Immunohistochemical labeling

Immunohistochemical labelings were performed as described previously [80]. All following incubation steps were performed at RT if not described otherwise. Cryosections were thawed for 30 min and 3 sections per slide were surrounded with DAKO pen (Agilent) as a liquid blockage. The cryosections were then fixed in 4 % PFA (Merck) for 10 min and washed 2x 5 min with 1x PBS (Biochrom) on a horizontal shaker (Heidolph). Afterwards, the sections were incubated in blocking solution for 60 min in a wet chamber and then with the primary antibodies overnight at 4 °C. The next day, the slides were rinsed 3x 5 min with PBS and incubated with the secondary antibodies for 60 min in the dark. Afterwards the slides were washed 3x 5 min again and embedded with Roti-Histofix (Roth).

2.2.10 RNA extraction from brain tissue and cDNA synthesis

RNA was extracted with the RNeasy plus universal kit (Qiagen) as previously described [80]. The cryosections inside the cryotubes were decanted in 2 ml reaction tubes filled with 0.9 ml Qiazol reagent and a metallic sphere. Afterwards, the tissue was minced in a Tissue Lyser (Qiagen) 2x1 min at a speed of 20 Hz and then incubated for 5 min at RT. After incubation 100 µl DNA eliminator was added to the suspension and vortexed for 15 s. Then, 180 µl of chloroform (Roth) was added to the suspension and vortexed for 15 s. After incubating the samples for 2-3 min at RT the tubes were centrifugated for 15 min at 4 °C to separate the suspension into 3 phases. The colorless, clear phase on top contains the RNA and was transferred into new tubes prefilled with 600 µl 70 % ethanol (Roth) to precipitate the RNA. The RNA/ethanol-mix was pipetted into centrifugatable columns and centrifugated for 15 s at 8000 x g at RT. Subsequently, 700 µl RWT buffer was added onto the column and centrifugated again for 15 s at 8000 x g at RT. 500 µl RPE buffer was added to the column and centrifugated again for 15 s at 8000 x g at RT. In the following step, 500 µl RPE buffer was added and centrifugated for 2 min at 8000 x g at RT to wash the membrane and to dry the column. Lastly, 30-50 µl RNase free water was pipetted on the membrane and centrifugated for 1 min at 8000 x g to elute the RNA into a 1.5 ml reaction tube.

For RNA extraction of cell culture samples, the culture medium was removed, the cells were rinsed two times with PBS and resuspended with 450 µl of Trizol/Quiazol. The following extraction steps are similar to the RNA extraction protocol from cryosections, besides that the volume of buffers were reduced by 50 % and RNeasy microcolumns were used. The RNA concentration and purity was determined with the NanoVue spectrometer (GE Healthcare) at 260 nm and 280 nm. The RNA samples could then be stored at -80 °C until use. After RNA extraction, cDNA was synthesized with the QuantiTect reverse transcription kit (Qiagen). 1 µg of extracted RNA was diluted in RNase-free water with a final volume of 12 µl. 2 µl of gDNA W-buffer was added and incubated at 42 °C for 8 min in a thermocycler to eliminate genomic DNA. For the reverse transcription a mastermix with 1 µl of Quantiscript reverse transcriptase, 4 µl of Quantiscript RT-buffer and 1 µl of reverse transcription-primermix per sample was prepared and added to the 14 µl RNA from the gDNA elimination step. The reverse transcriptase-RNA-mix was incubated for 30 min at 42 °C to synthesize the cDNA followed by an inactivation of the reverse transcriptase at 95 °C for 3 min. The cDNA was diluted 1:2 with H₂O and stored at -80 °C until further analysis.

2.2.11 qPCR gene expression analysis

Quantitative polymerase chain reaction (qPCR) was performed using either SYBR Green mix (Thermo Fisher Scientific) or PrimaQuant (Steinbrenner) as described previously [80]. Each sample was investigated in duplicates and amplified with a Lightcycler 480 (Roche). All primers were applied from Eurofins MWG Operon or Qiagen and are listed in Table 9. For relative quantification, a standard curve of all target genes was generated and the absolute copy numbers were normalized to the absolute copy numbers of Peptidylprolyl Isomerase A (PPIA), a housekeeping gene which is functioning as a control gene.

2.2.12 Preparation of human cerebral organoids

All incubation phases were performed at 37 °C, 5 % CO₂. In order to generate L1CAM-deficient (L1KO) and control human cerebral organoids two types of H1 human embryonic stem cells (hESCs) were used. Both cell lines were provided by [REDACTED] Department of Biological Sciences University of Notre Dame. In L1KO hESCs Exon 3 was removed from the L1CAM gene by Cre-recombinase resulting in a conditional knockout, whereas the Cre-recombinase is not active in control hESCs and L1CAM is expressed completely [20]. L1KO and control hESCs were subjected to the organoid preparation protocol of Sutcliffe and Lancaster [28]. hESCs were cultured on solidified 25 % Matrigel/MEM medium with mTeSR1+Supplement (StemCell) until the culture is approximately 60-70 % confluent. On day 0, the cells were detached with 4 °C Accutase (Sigma-Aldrich) and replated in a 96-well Ultra Low Attachment (ULA, Corning) plate with 9000 cells in 150 µl mTeSR1+Supplement + 4 ng/ml bFGF (Peprotech) + 1 µM Thiazovivin (Sigma-Aldrich) per well. Living cell numbers were measured using trypan blue and a Neubaur counting chamber (Roth). On day 3, half of the medium was removed and 150 µl of mTeSR1+Supplement without bFGF or Thiazovivin was added. Approximately on day 6, the embryoid bodies had formed and were transferred into a 24-well ULA plate with 500 µl neural induction medium (Table 3). Depending on the morphology and size, on day 10-12 the organoids were coated with Matrigel (Corning) and further cultured in 60 mm petri dishes (Greiner) with 7 ml differentiation medium without retinoic acid. At day 13-15 the Matrigel coating was removed and the organoids were cultured in differentiation medium with retinoic acid on an orbital shaker (Edmund Bühler) until the end of the experiment at day 60.

2.2.13 β-Catenin nuclear translocation assay and subcellular fractionation

On day 1, 3x10⁶ HEK cells were seeded on a 10 cm petri dish and transfected with the vectors β-Catenin-GFP, ER-RFP and/or L1CAM the following day. The β-Catenin-GFP protein consists of the green fluorescent protein coupled to β-Catenin which facilitates the monitoring of intracellular β-Catenin transport. After transfection of ER-RFP the cells express

RFP which is fused to the signaling sequence of calreticulin and KDEL (ER retention signal). ER-RFP is used as a negative control here. On day 3, half the cultures were treated with 25 mM LiCl for 24 h to induce nuclear translocation of β -Catenin-GFP and trigger WNT signaling. After 24 h the cells were washed two times with 1x PBS, resuspended in 500 μ l Subcellular fractionation (SCF) buffer and incubated on ice for 15 min. SCF (protocol by Abcam) is a technique that facilitates the separation of nuclear and cytoplasmic protein fractions by centrifugation. The cell suspension was then resuspended with a 1 ml syringe using a 30 gauge needle (Braun) for 10 times and incubated on ice for 20 min. The samples were centrifuged at 720 g for 5 min afterwards. The pellet contains the nuclei while the supernatant was transferred into a fresh tube and contains the cytoplasm, membrane and mitochondria. The pellet was resuspended with 500 μ l fractionation buffer and resuspended with a 1 ml syringe using a 25 gauge needle (Braun). The pellet which contains the nuclei was resuspended with TBS/0.1 % SDS and sonicated for 3 s on ice. Protein concentration of the nuclear and cytoplasmic lysates was determined with DC Protein Lowry Assay (BioRad).

2.2.14 Protein extraction

To obtain total protein lysates from cultivated cells, cell culture medium was discarded and the cells were rinsed two times with 1x PBS. Then, an appropriate amount of RIPA buffer was added according to the size of the wells and number of the cells. With a cut-off tip the cells were scraped off the wells bottom and resuspended with the buffer. The lysis suspension was then centrifuged at 17000 g (Hettich) for 5 min to spin down non-soluble cellular debris. Protein concentration of the supernatant was determined with Lowry DC protein assay (BioRad).

2.2.15 Lowry DC protein assay

To ensure that the same amount of protein was loaded on the sodium dodecyl sulfate (SDS) gel for the Western Blot, the protein concentration was measured beforehand with the Lowry DC protein assay (BioRad) as described previously [28]. The assay works with a color reaction where the reaction mix becomes bluer with increasing protein concentration. An 8-point bovine serum albumin standard (BSA, Sigma-Aldrich) was prepared from a range of 0 mg - 3 mg/ml. All samples and standards were measured in duplicates in a 96-well plate (VWR). For each well 5 μ l of protein sample, 49 μ l of reagent A, 1 μ l of reaction S and 200 μ l of reagent B is needed. When all combined, the mixture was incubated for 12 min at RT in the dark and analyzed with the Glomax Plate Reader (Promega) at 750 nm.

2.2.16 SDS-PAGE and Western Blot

In order to investigate protein expression levels SDS-polyacrylamide gelelectrophoresis (SDS-PAGE) was performed followed by a western blot as described previously [80]. According to the protein concentrations determined with Lowry DC assay, the proteins were diluted in new tubes with PBS and 5x Laemmli buffer. The Laemmli buffer contains β -mercaptoethanol (Roth) to break disulfide bonds and also SDS (Roth) to linearise the protein structure and give them a negative charge, so that all proteins travel to the anode during electrophoresis. After the protein/Laemmli buffer mix was prepared, the samples were incubated at 95 °C for 5 min to destroy the quaternary and tertiary structure. Usually, 25 μ g of total protein was loaded on a 10 % polyacrylamide gel with Chameleon (Li-Cor) and PageRuler protein ladder (ThermoFisher). The electrophoresis was performed at 0.04 A in an electrophoresis chamber filled with running buffer until the smallest desired protein is almost exiting the separating gel. Afterwards, the stacking gel was removed and the proteins were blotted from the gel on a nitrocellulose membrane (Merck) with the Transblot Turbo system (BioRad) for 7 min. The membrane was then blocked with 2.5 % skimmed milk (Roth) for 60 min and incubated with the primary antibody solution overnight at 4 °C on a shaker. On the next day, the membranes were washed with PBS 2x 5 min and incubated with the secondary antibody solution (secondary antibody 1:15000 in 2.5 % skimmed milk) for 60 min in the absence of light. Lastly, the membranes were rinsed again 3x 5 min with PBS and analyzed with Li-Cor Odyssey Infrared Imaging system using the software ImageStudio. Here, the signal intensities of the different protein bands were determined. The signals of the target proteins were then normalized to the signals of the housekeeping proteins GAPDH or H3 in Microsoft Excel and subjected to statistical analysis in Graphpad Prism.

2.2.17 NEBNext Ultra™ II RNA Library Prep for Illumina and NGS

Total RNA from mouse cryosections or human cerebral organoids extracted with RNeasy plus universal kit (Qiagen) were subjected to Next Generation Sequencing (NGS). For this reason, concentrations of total RNA were measured using Qubit (Invitrogen) and the RNA Integrity Number (RIN) was assessed for quality control using a 2100 Bioanalyzer (Agilent). The detailed protocol to generate RNA libraries can be obtained from the supplier homepage (international.neb.com). In brief, mRNA was captured from the total RNA pool using a NEBNext Poly(A) mRNA Magnetic Isolation Module (Invitrogen) included in the library preparation kit. Then, RNA libraries were prepared using the NEBNext Ultra™ II RNA Library Prep Kit for Illumina (New England Biolabs). Concentration and integrity of libraries were again measured by Qubit and Bioanalyzer. Sequencing depth was 150×10^6 reads per sample. First investigation and sorting of RNA-seq data was performed using the software CLC Genomics workbench (Qiagen). Here, the data could be sorted by fold change and

difference of mean expression values. Also, principal component analysis was performed with this tool. Final data was then exported as Microsoft Excel sheets for further analysis.

2.2.18 Statistics

Statistical analysis was performed using Graphpad Prism software. Statistical outliers were identified using ROUT-test and removed. Normal distribution of data sets was tested with Shapiro-Wilks test. *P* values of parametric data sets were calculated by t test and *p* values of non-parametric data sets were calculated by Mann-Whitney *U*-test. *P*<0.05 was declared to be a significant effect (shown with 1 asterisk *). *P* values below 0.01 are illustrated with 2 asterisks (**), *p* values below 0.001 with 3 asterisks (***) and *p* values below 0.0001 with 4 asterisks (****). *P* values of 0.05<*p*<0.1 were described as a statistical trend. All results are shown as mean values ±SEM.

2.3 Acknowledgements

Animal husbandry was performed by the animal care attendants of the building 905, 13th floor and my colleagues [REDACTED] and [REDACTED]. Mouse genotyping was performed by my colleague [REDACTED]. Most LFB stainings were performed by [REDACTED] from the Institute of Neuropathology.

3. Results

As outlined in the introduction, gene mutations in human L1CAM can cause L1 syndrome characterized by pathological features like congenital hydrocephalus, corpus callosum agenesis, spastic paraplegia, adducted thumbs and mental retardation. These phenotypes manifest to varying degrees which is also reflected in different mouse lines mutated in *L1cam* [36,81,82]. Due to X-chromosomal inheritance of the L1 syndrome, human male individuals as well as male mice show a more severe phenotype than females.

In the present thesis, initially two mouse lines were characterized which supposedly mimic the human phenotype of the L1 syndrome, namely L1KO and L1D201N mice.

3.1 Low numbers of hemizygous mutant males in litters

According to the classical mendelian distribution when one is breeding heterozygous females (-/+) with hemizygous males (+/y) there is a 25 % chance of hemizygous male or heterozygous female mice (Fig. 11A) in the litters. While we bred and genotyped the animals for the study we observed that only few pups were hemizygous males. For this reason, the actual yield of genotypes was calculated using the breeding history data derived from PyRat (Scionics). Analysis of this data revealed that out of all L1KO mice (n=596) bred in our animal facility only 9.06 % mice were hemizygous males (n=54, Fig. 11B). The other three genotypes were quite equally distributed with 29.36 % control males (n=175), 31.88 % control females (n=190) and 29.7% heterozygous females (n=177). Even more flagrant is the percentage of hemizygous males in L1D201N litters with only 3.67 % (n=16) of all bred mice (n=436). The other three groups were quite equally distributed again with 33.94 % control males (n=148), 29.59 % control females (n=129) and 32.8 % heterozygous females (n=143).

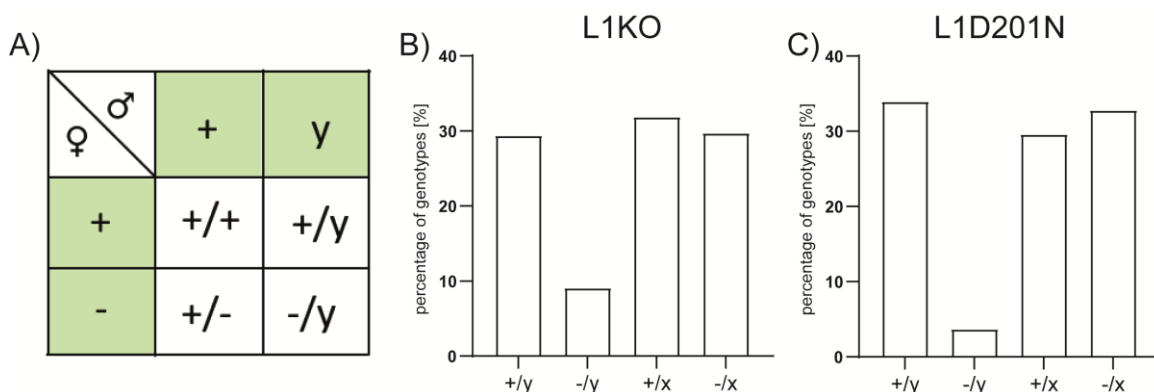


Fig. 11: Mendelian distribution of L1 adult mice. (A) Schematic illustration of the expected mendelian genetics of the breeding strategy of wildtype male (+/y) and heterozygous female mice (+/-), resulting in wildtype female (+/+), hemizygous male mice (-/ y), as well as wildtype male and heterozygous female mice. (B+C) Actual yield of genotypes in adult (B) L1KO and (C) L1D201N litters. Values are shown as percentages of all genotyped mice from our animal facility.

3.2. Neurological alterations in L1D201N mutant mice

Heterozygous females, hemizygous males and their corresponding control animals were subjected to behavioral and motor function tests. Initial investigations to characterize the mice comprised the OFT, assessment of the NDS and evaluating their performance on the RR. These tests should unveil deficits that we would expect to occur in an appropriate mouse model for L1 syndrome such as motor and behavioral dysfunctions, since human patients frequently show symptoms like spastic paraplegia. The OFT focusses on locomotor activity and anxiety behavior of the mice while the NDS and RR were used to measure motor deficits. During the 3 min experiment, the EthovisionXT software tracked the mice and the total distance the mice traveled in the cage was recorded. Additionally, EthovisionXT software also saves the mouse trackings in video files. Those videos were rewatched to manually count the rearing activity of the mice.

Assessments showed that L1D201N mutant male mice exhibited a higher NDS compared to their littermate wildtype controls (Fig. 12A, +/y: 0.29 ± 0.1 , L1D201N: 3.33 ± 0.51 , $p=0.0006$). Although the mutant male mice showed significant deficits, there was no obvious effect in endurance on the RR (Fig. 12B, +/y: 45.71 ± 14.46 s, L1D201N: 19.67 ± 7.22 s, $p=0.155$). Assessment via OFT revealed an increased locomotor activity of L1D201N mutant male mice compared to the controls (Fig. 12C, +/y: 628 ± 163.6 cm, L1D201N: 1204 ± 128.7 cm, $p=0.024$). Analysis of rearing activity showed no difference between mutant males and the controls (Fig. 12D, +/y: 8.2 ± 4.2 , L1D201N: 8.4 ± 2.38 , $p=0.968$). In the initial experiments also female mice were investigated. L1D201N female mice did not show an increased NDS compared to their corresponding control littermates (Fig. 12E, +/+ : 0.92 ± 0.24 , L1D201N: 0.58 ± 0.3 , $p=0.524$). Additionally, their endurance on the RR was also not different compared to control mice (Fig. 12F, +/+ : 51.5 ± 5.07 s, L1D201N: 49.5 ± 12.22 s, $p=0.883$). However, OFT of female mutant mice showed increased locomotor activity compared to controls (Fig. 12G, +/+ : 831.7 ± 67.29 cm, L1D201N: 1107 ± 83.87 cm, $p=0.0284$). Investigation of rearing activity did not reveal any difference between mutant and control female mice (Fig. 12H, +/+ : 9.5 ± 3.47 , L1D201N: 12.33 ± 3.98 , $p=0.603$).

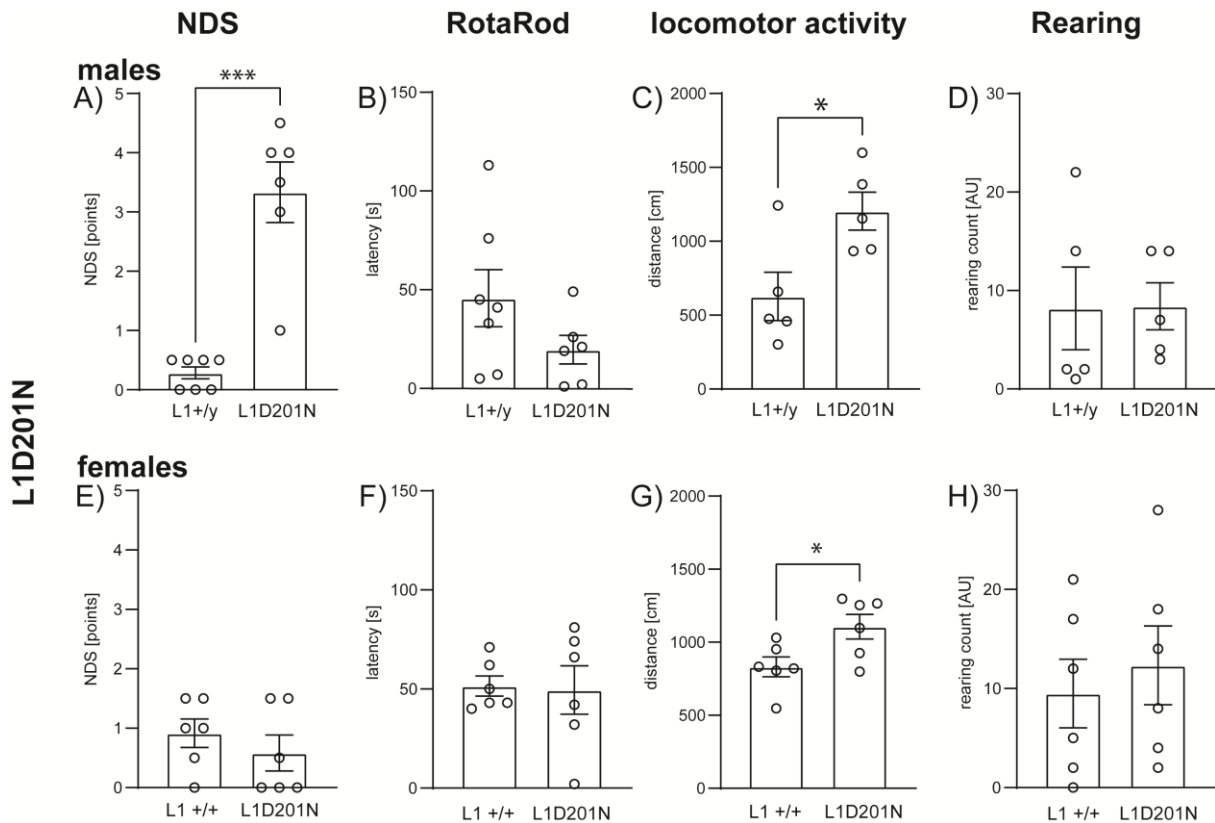


Fig. 12 Increased NDS and locomotor activity in L1D201N mutant males. (A-H) Neurological assessment of L1D201N male and female mice, including (A+E) Neurological Deficits Score, (B+F) RotaRod, (C+G) locomotor activity and (D+H) rearing counts. Graphs show the individual values \pm SEM. *P* values were calculated by Mann-Whitney *U* test (* $p < 0.05$, *** $p < 0.001$).

3.3 Neurological deficits in L1KO mutant male mice

The same behavioral and motor ability tests which were performed to study L1D201N mice were also performed to compare hemizygous male and heterozygous female L1KO mice with wildtype littermate controls. NDS assessment revealed increased neurological deficits in hemizygous L1KO male mice compared to their littermate controls (Fig. 13A, +/y: 0.28 ± 0.09 , -/y: 1.85 ± 0.28 , $p < 0.0001$). Investigation of the endurance on the RR did not show any handicaps of the mutant male mice compared to the controls (Fig. 13B, +/y: 21.56 ± 6.07 s, -/y: 16.5 ± 3.48 , $p = 0.469$). Further, hemizygous L1KO male mice displayed a trend towards increased locomotor activity compared to their wildtype littermate controls (Fig. 13C, +/y: 630.7 ± 73.1 cm, -/y: 1262 ± 285.9 cm, $p = 0.0726$). Additionally, the number of rearings was reduced in hemizygous L1KO male mice, however, this difference did not reach statistical significance (Fig. 13D, +/y: 11.5 ± 2.74 , -/y: 5.57 ± 2.72 , $p = 0.0559$). Female L1KO mutant mice showed elevated deficits compared to the controls but this difference did not reach statistical significance (Fig. 13E, +/+ : 0.22 ± 0.12 , -/x : 0.61 ± 0.16 , $p = 0.0901$).

Further, female mutant and control mice did not show alterations in their RR performance (Fig. 13F, +/+ : 44.56±8.75 s, -/x: 32.00±4.64 s, $p=0.223$). Finally, female mutant mice did not show altered locomotor activity (Fig. 13G, +/+ : 934±143.3 cm, -/x: 884.4±47.04 cm, $p=0.77$) and no difference to control mice regarding their rearing counts (Fig. 13H, +/+ : 9.17±3.48, -/x: 9.83±2.78, $p=0.884$).

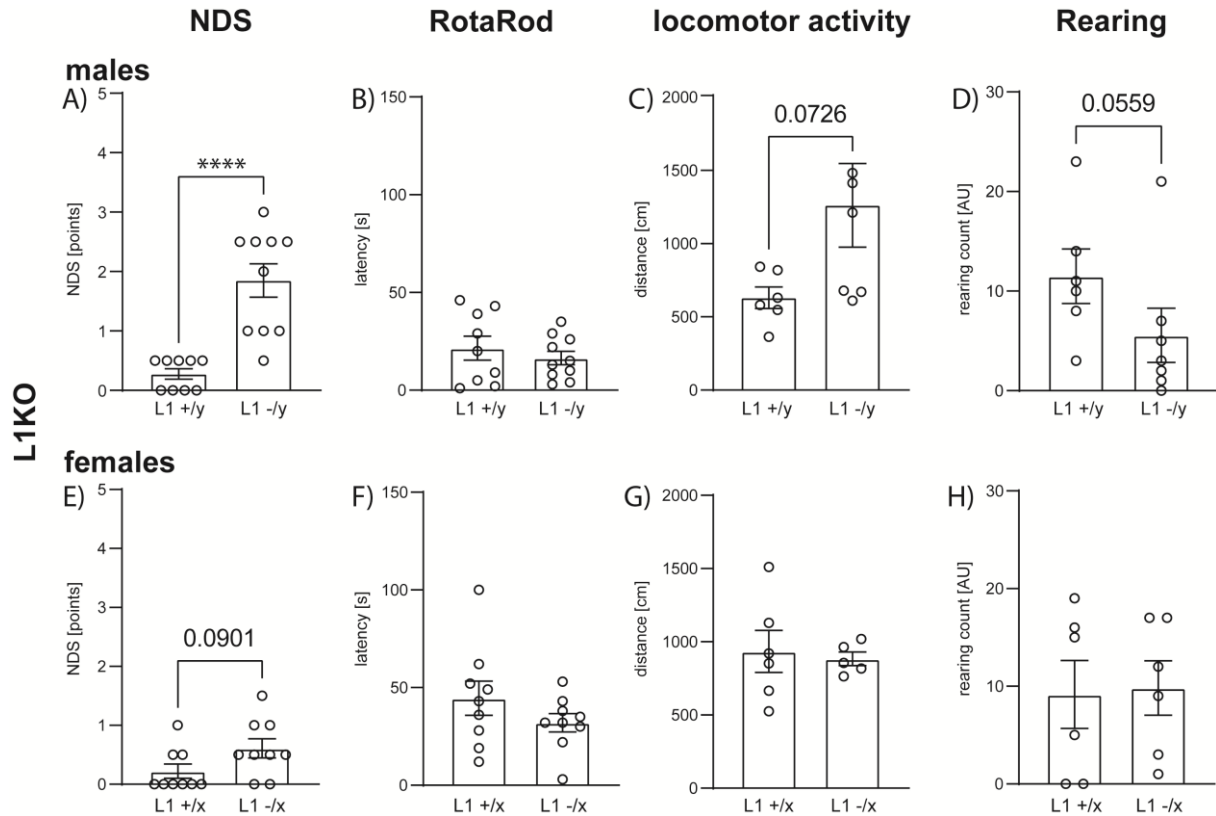


Fig. 13 Increased NDS in L1KO male mice. (A-H) Neurological assessment of L1KO male and female mice, including (A+E) Neurological Deficits Score, (B+F) RotaRod, (C+G) locomotor activity and (D+H) rearing counts. Graphs show the individual values ±SEM. P values were calculated by Mann-Whitney U test (**** $p<0.0001$)

3.4 Altered travel paths in mutant male mice

The OFT revealed increased locomotor activity in L1D201N mutant mice and a trend towards increased locomotor activity in hemizygous L1KO males. We hypothesized a potential difference in exploration and anxiety-like behavior of the mutant mice since it was already shown that *L1cam*-deficiency can cause an altered anxiety-like behavior [52,83]. To test this assumption, heatmaps of OFT data were created which visualize the position of the mouse during the OFT (Fig. 14). Here, the mouse's travel path can be investigated and due to the colorization also their most preferred locations inside the cage during the experiment. In general, mice show aversions to large, brightly lit, open and unknown environments and therefore prefer to stay in close proximity to the safe corners and along the walls [84]. The presented heatmaps show the data of representative mice, whose locomotor activity was similar to the overall group mean value.

The heatmaps of L1D201N and wildtype littermate male mice indicated that the wildtypes preferred to stay close to the walls of the experimental cage while mutant mice also ran across the mid area and along the whole cage. The same observation was made in L1KO males where mutant males spend more time in the open area than the wildtypes. The travel paths of L1D201N and L1KO female mice did not show an obvious difference between mutant and wildtypes.

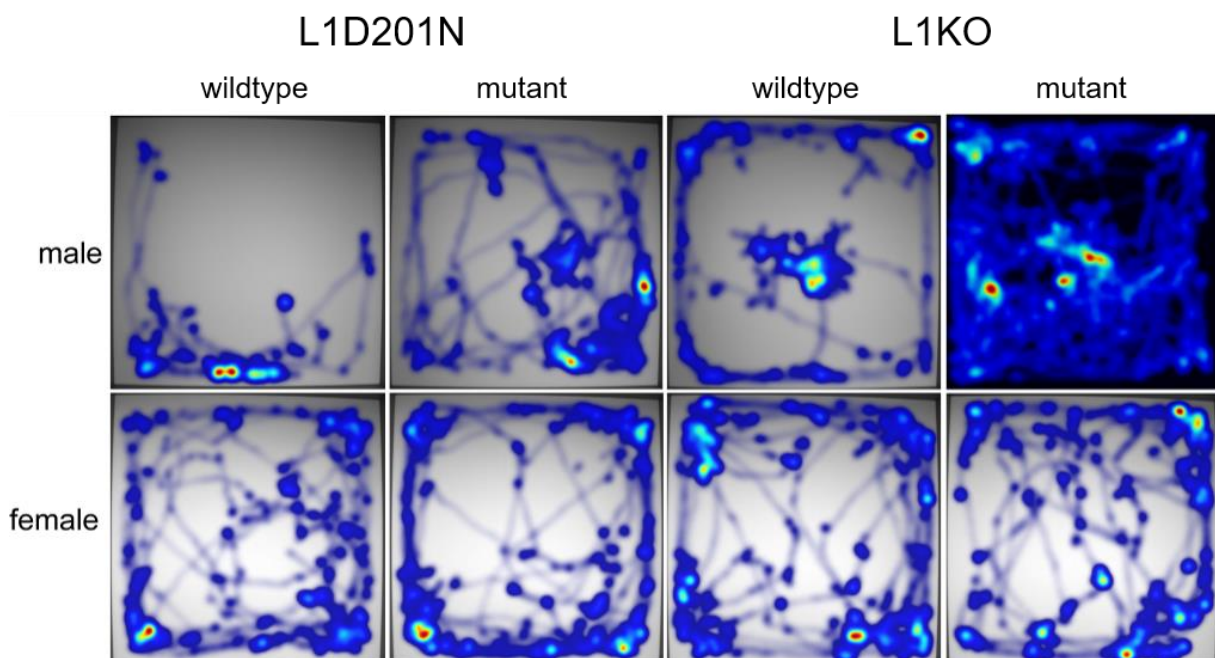


Fig. 14 Altered travel paths in mutant male mice. EthovisionXT software visualized the walking paths of L1KO and L1D201N mice in heatmaps using the data generated in the OFT (n=2/genotype). The heatmaps point out the paths and also the locations the mice were mostly located during the 3 min experiment period (blue=short length of stay, red= long length of stay).

3.5 L1D201N male mice show enlarged ventricles

Congenital hydrocephalus and hypoplasia of the corpus callosum occur frequently in the human L1 syndrome. To investigate whether these features also occur in the mouse models, we assessed ventricle sizes and the thickness of the corpus callosum in Nissl stained cryosections. Since male but not female mutant mice showed behavioral alterations, the following investigations of this work were restricted to male mutants and their control mice.

Serial cryosections were prepared and subjected to Nissl stainings. Here, sizes of the lateral ventricles were measured in two sections for each animal (n=3-7) at Bregma -0.34 mm and -2.46 mm in Nissl stained cryosections (Fig. 15A). The ventricle sizes are presented as percentages of the section area. Volumetric measurements of L1D201N male ventricles revealed enlarged ventricles in mutant mice at Bregma -0.34 mm compared to the controls (Fig. 15B, +/y: 3.16 ± 0.42 %, -/y: 7.45 ± 1.89 %, $p=0.033$). There was no difference between mutant and control ventricle sizes at Bregma -2.64 mm (Fig. 15C, +/y: 1.97 ± 0.75 %, -/y: 5.23 ± 1.86 %, $p=0.164$). However, it was noticed that the mean ventricle size was more than twofold increased in L1D201N mice at both Bregma levels accompanied by a remarkably high variation of ventricle size in individual L1D201N mutants.

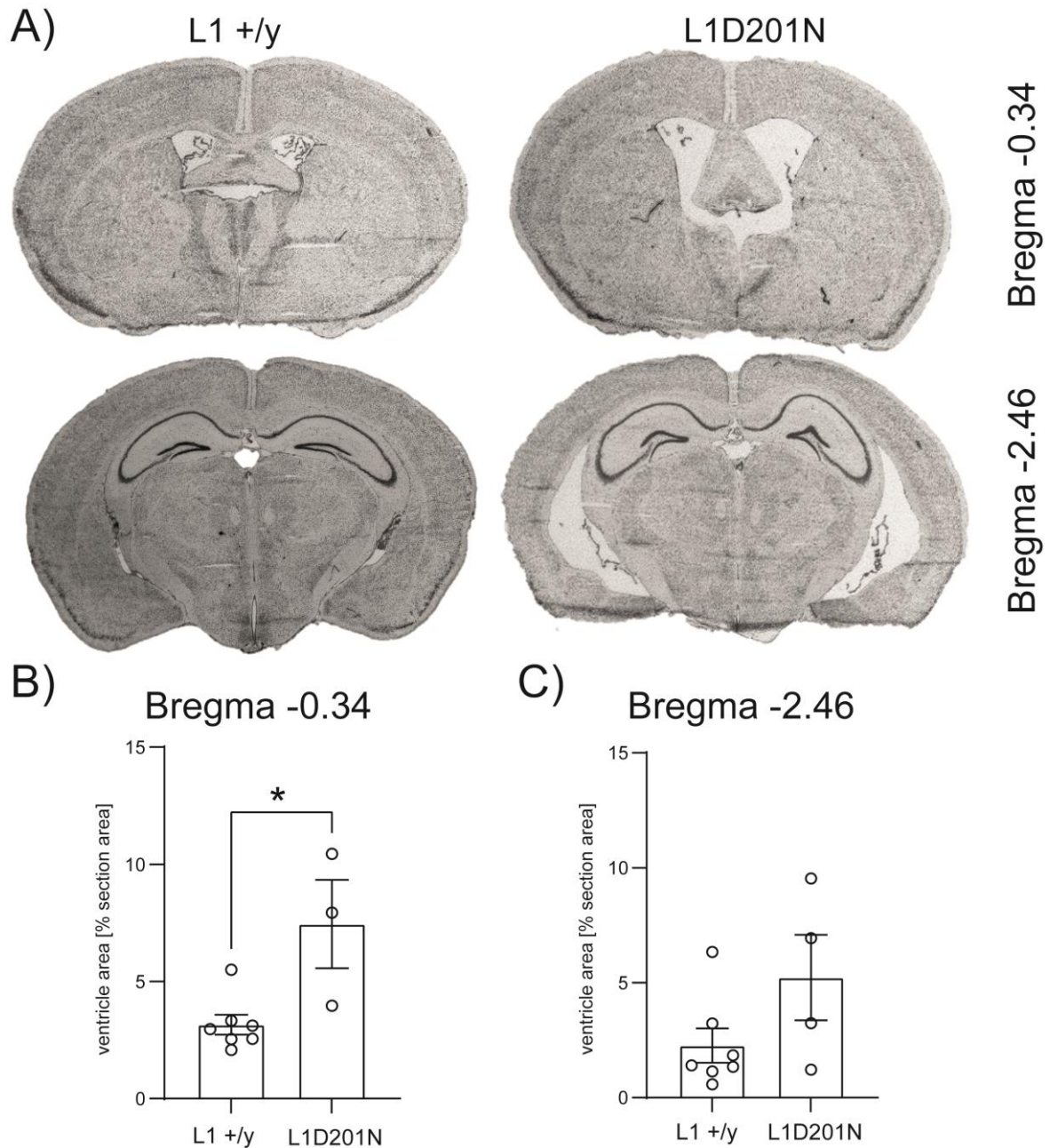


Fig. 15 L1D201N male mice show enlarged ventricles. Histological analysis of ventricle sizes was performed with (A) Nissl stainings of L1D201N control and mutant male brain sections Images were taken with Zeiss binocular at Bregma -0.34 and -2.46 and ventricle sizes were measured using Zeiss software ZEN. (B) Statistical analysis of ventriculometry in L1 +/y (n=7) and L1D201N males (n=3) at Bregma -0.34. (C) Statistical analysis of ventriculometry in L1 +/y (n=7) and L1D201N males (n=4) at Bregma -2.46. Graphs show the individual values \pm SEM. *P* values were calculated by Mann-Whitney *U* test (* $p < 0.05$)

3.6 L1KO mutant mice do not show enlarged ventricles

Similar to L1D201N mice ventricle sizes of L1KO mice were also assessed in Nissl-stained cryosections (Fig. 16A). Measurements of L1KO ventricles at Bregma -0.34 mm showed no difference between mutant and control mice (Fig. 16B, +/y 2.05 ± 0.14 %, -/y 2.19 ± 0.24 %, $p=0.612$). The ventricle size at Bregma -2.46 mm also did not show a significant difference between L1KO mutant and control mice, although there was a slight trend towards larger ventricles in L1KO mice (Fig. 16C, +/y 0.98 ± 0.2 %, -/y 1.39 ± 0.13 %, $p=0.1025$).

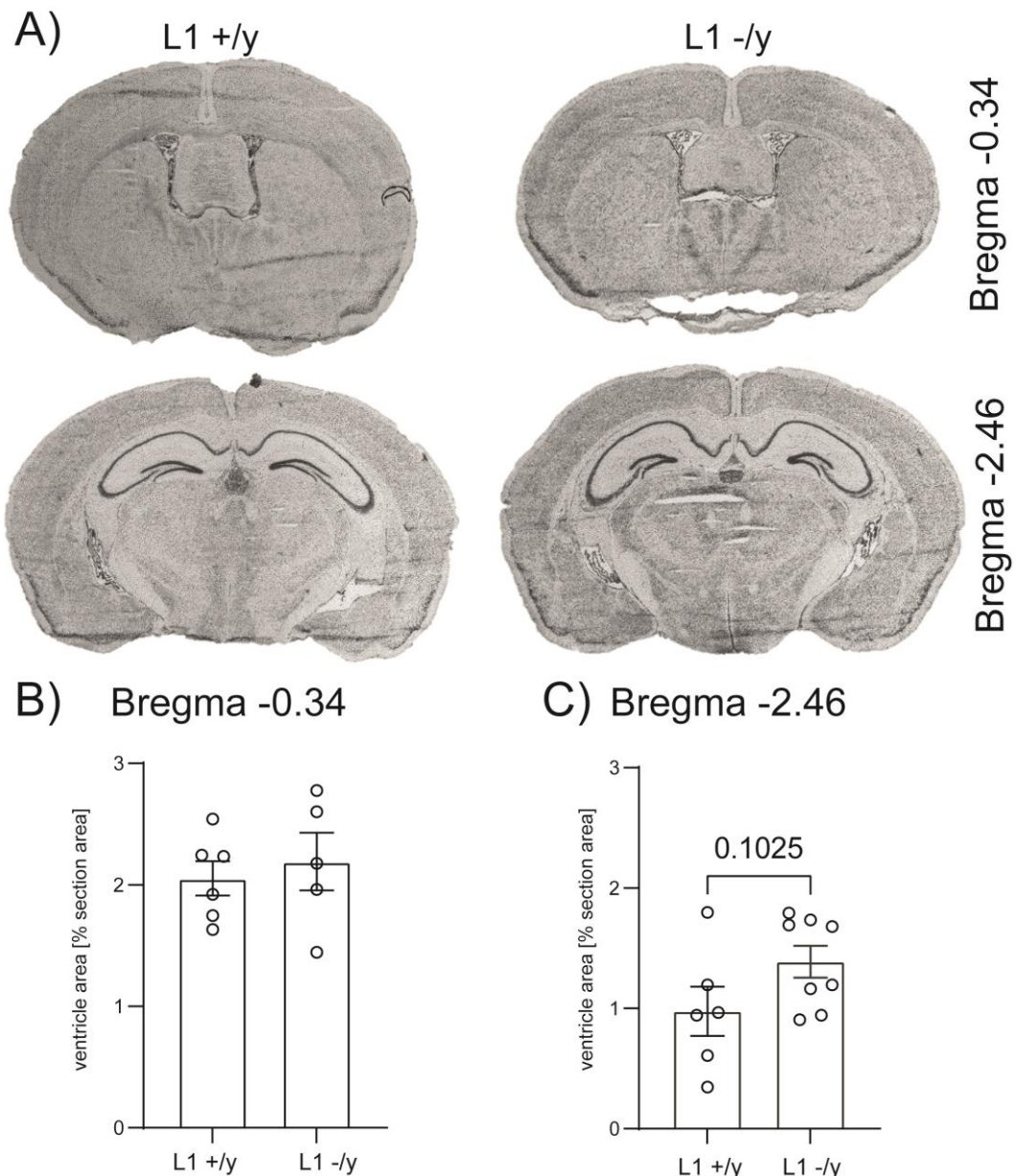


Fig. 16 Unaltered ventricle sizes in L1KO mice. (A) Histological analysis of ventricle sizes was performed with Nissl stainings. Images were taken with Zeiss binocular at Bregma -0.34 and -2.46 and ventricle sizes were measured using Zeiss software ZEN. (B) Statistical analysis of ventriculometry in L1 +/y (n=6) and L1 -/y mice (n=5) at Bregma -0.34. (C) Statistical analysis of ventriculometry in L1 +/y (n=6) and L1 -/y mice (n=8) at Bregma -2.46. Graphs show the ventricle sizes in percent of the section area \pm SEM. *P* values were calculated by t test.

3.7 Thinned corpus callosum in L1D201N and L1KO mutant mice

L1CAM is essential for important developmental processes like axonal pathfinding and dendritic arborization [20,85]. A frequently arising pathological phenotype in L1 syndrome patients is an agenesis or dysgenesis of the corpus callosum which can be attributed to aforementioned processes. To examine whether this pathological feature of L1 syndrome is present in our mouse models LFB stainings were performed that stain the myelin sheath of oligodendrocytes. Here, the thickness of the callosal commissure was measured which is one of the largest structure of white matter in the human brain [2]. Cryosections of both, L1KO and L1D201N mice from Bregma -2.46 mm were subjected to staining and microscopy. The extent of the medial as well as the lateral corpus callosum was measured using ZEN software. Measuring points are illustrated with arrows in L1WT and L1 mutant sections exemplarily (Fig. 17).

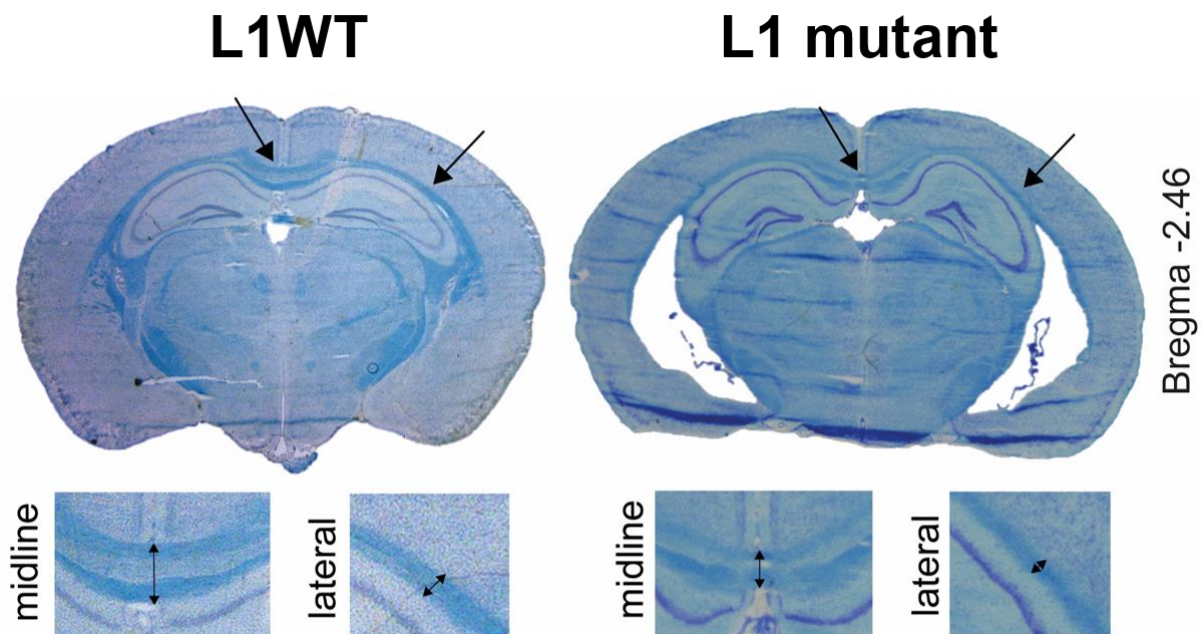


Fig. 17 Measurement of callosal thickness. The thickness of the corpus callosum was measured in LFB stained cryosections of L1D201N and L1KO mice at Bregma -2.46. Data was collected from medial and lateral corpus callosum indicated by black arrows.

Assessment of the corpus callosum via LFB stainings revealed that L1D201N mutant males exhibit a smaller callosal commissure at the midline between the hemispheres (Fig. 18A, +/y 0.42 ± 0.02 mm, L1D201N 0.35 ± 0.02 mm, $p=0.045$). Additionally, the thickness of the lateral corpus callosum was reduced in L1D201N mutant males compared to control mice. (Fig. 18B, +/y 0.15 ± 0.01 mm, L1D201N 0.1 ± 0.01 mm, $p=0.0033$). Assessment of the L1KO mouse line also displayed a thinned callosal tract at the midline in L1KO mutant males compared to controls (Fig. 18C, +/y 0.43 ± 0.02 mm, -/y 0.39 ± 0.01 mm, $p=0.045$). In addition, the lateral corpus callosum of L1KO mice was reduced at Bregma -2.46 (Fig. 18D, +/y 0.13 ± 0.01 mm, -/y 0.08 ± 0.01 mm, $p=0.0023$).

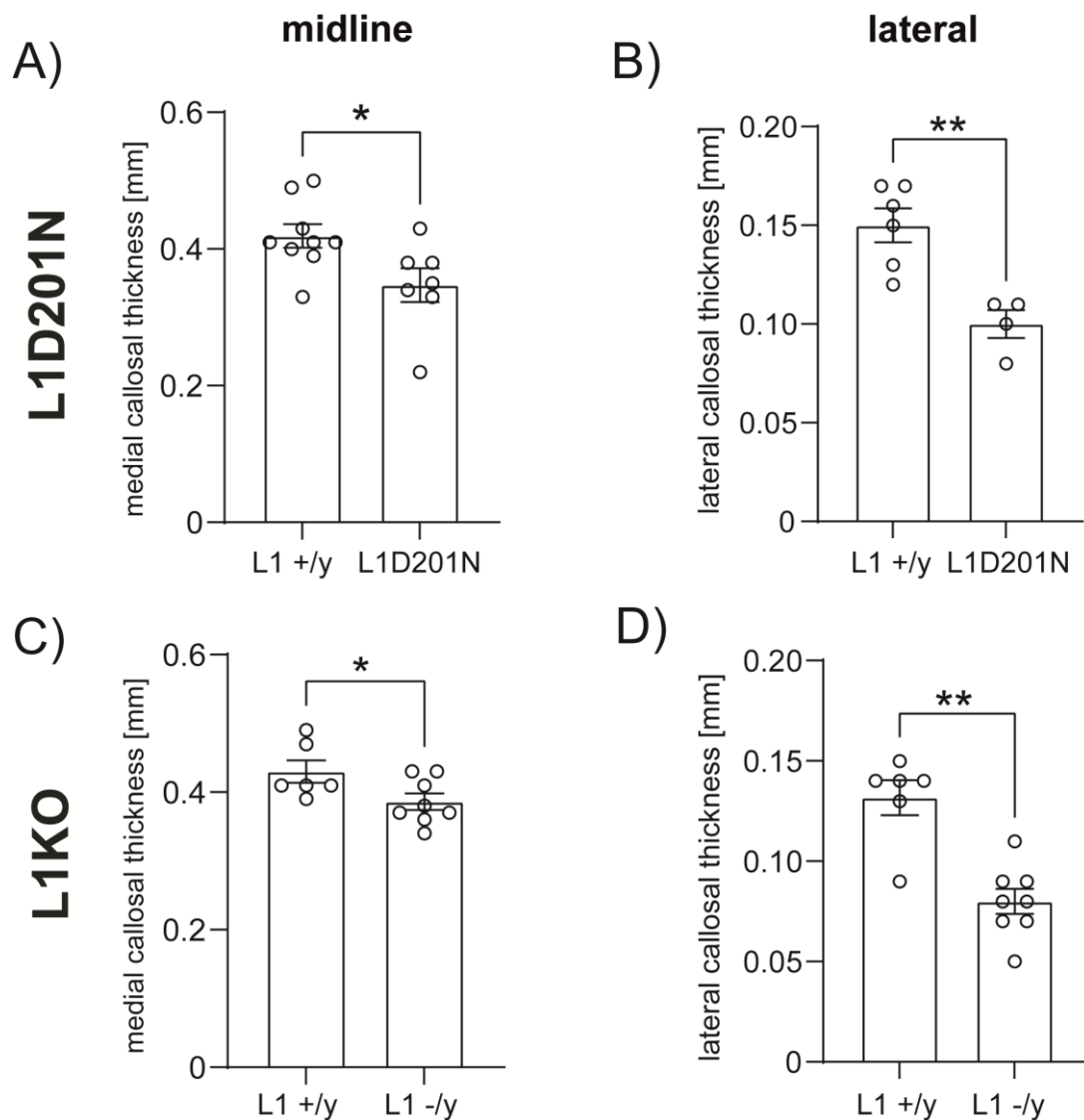


Fig. 18 Thinned corpus callosum in L1D201N and L1KO mutant males. (A-D) Statistical analysis of histological investigation of the corpus callosum in L1D201N and L1KO males. Measurements were conducted at the (A) medial corpus callosum of L1 +/y (n=9) and L1D201N mutant males (n=7) and the (B) lateral corpus callosum of L1 +/y (n=6) and L1D201N mutant males (n=4). (C+D) Investigation of the (C) medial and (D) lateral corpus callosum of L1 +/y (n=6) and L1KO mutant males (n=8). Graphs show the individual callosal thicknesses in mm \pm SEM. *P* values were calculated by t test (A-C, **p*<0.05, ***p*<0.05) and Mann-Whitney *U* test (D, ***p*<0.05)

Taken together, behavioral assessments of L1D201N and L1KO mice revealed locomotion deficits and neurological deficits as determined by locomotion tracking and the NDS, respectively. However, Rotarod performance did not reveal differences of L1 mouse mutants as compared to wildtype littermates. Neuroanatomical characterization revealed enlarged ventricles in L1D201N mutant males but not in L1KO mutant males, whereas both L1 mutant mouse lines exhibited hypoplasia of the corpus callosum. The high individual variability of the determined values suggest that the phenotype variety observed even in intrafamilial cases of human L1 syndrome [86] is also resembled in the mouse model.

3.8 Principal component analysis of transcriptomes from adult L1KO mutant mice

L1CAM is involved in various pathways related to CNS development such as proliferation, neurogenesis, axon pathfinding and more [52,85,87]. Mutations in the human *L1CAM* gene can cause L1 syndrome with heterogeneous pathological features of varying degrees, most prominently congenital hydrocephalus, agenesis of the corpus callosum, and spastic paraplegia. In behavioral assessments of L1KO mice we already pointed out motor and behavioral dysfunctions. Moreover, histological investigations revealed a mild hypoplasia of the corpus callosum in L1KO mutant males. As an attempt to investigate the underlying mechanisms for those pathological features evoked by *L1cam* deficiency, RNA-seq transcriptomics of adult L1KO mutant and wild-type male brain tissue was performed. For this purpose, 4x240 µm thick coronal brain cryosections were collected between Bregma +0.5 mm and -2.0 mm and processed for RNA extraction. RNA samples were subjected to library preparation for Illumina which again were subjected to RNA-seq and gene expression values were integrated to CLC Workbench for further analysis. The investigation of L1D201N mice was discontinued from this point, due to insufficient numbers of adult hemizygous male pups in the breedings.

Principal component analysis (PCA) is a statistical method that can be used for exploratory data analysis. In general, PCA can be used to reduce the size of data sets by analysing the variance of these data sets. It is able to evaluate data sets like gene expression values, which makes it a suitable method to identify and remove outliers in the data sets [88]. PCA revealed, that among the 10 integrated data sets, 3 data sets were removed for being subjectively defined as outliers: 2 WT and 1 KO data set.

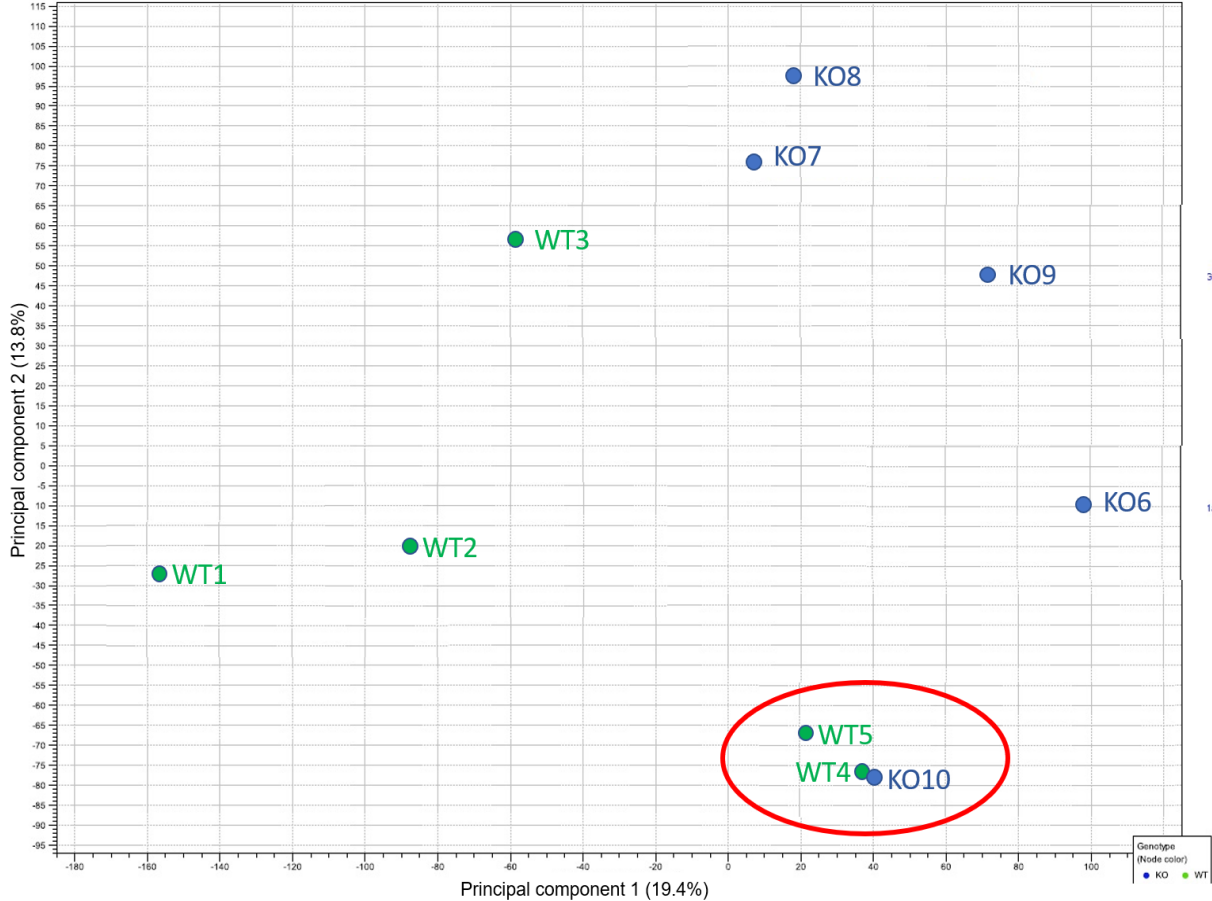


Fig. 19 Principal component analysis. PCA displayed the composition of RNA-seq data sets and was used to detect and remove outliers. This graph shows the 3 outliers (encircled in red) in L1KO (blue) and L1WT (green) RNA-seq datasets. PCA was performed using CLC Genomic Workbench.

3.9 L1KO males display more down-regulated than up-regulated DEG

A volcano plot is a visualization of data that illustrates its distribution by plotting the significance (p -value) versus fold-change of gene expression values in a coordinate system. In our case, it displays how many genes are up- or downregulated in RNA-seq data of L1KO mice. All values were included, where a fold change and p value could be calculated. The values are plotted as log-values. Volcano plotting revealed that more genes were down-regulated than up-regulated in L1KO mutant mice as compared to wildtype controls (Fig. 20, 10116 (41.8 %) higher in L1KO and 14058 (58.2 %) lower in L1KO). All highly differentially expressed genes (DEG) with a negative log p -value higher than 2 were highlighted in red. Among those 1250 red highlighted genes, 318 genes were upregulated (25.44 %) and 932 genes (74.56 %) were downregulated in L1KO mutant mice.

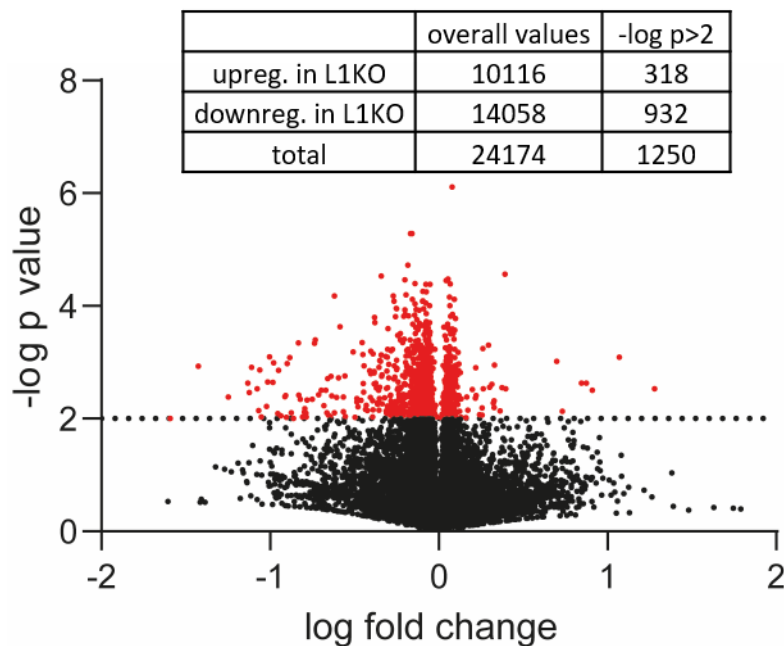


Fig. 20 Imbalanced ratio of up- and downregulated genes in L1KO mutant males. This volcano plot displays the distribution of RNA-seq data, by showing the negative log p value (Y-axis) and the log fold change (X-axis) of each gene. A total of 24174 genes were integrated. The Volcano plot was generated using GraphPad Prism. P values were calculated in GraphPad Prism. P values above a negative log(2) value were highlighted in red.

3.10 Panther GO analysis showed changes in “cellular processes”, “binding” and “WNT signaling”

In order to elucidate underlying processes and pathways that may contribute to the formation of the pathological phenotype typical for the human and murine L1 syndrome, RNA-seq data were subjected to Gene Ontology (GO) analysis. The principle of the GO database (<http://geneontology.org/>) is a systematic categorization of genes and their products concerning their special features regarding three criteria: biological processes, molecular function and pathways. In the following 3612 gene IDs of DEG ($p < 0.05$) were subjected to GO analysis with Panther [75,89] of which 3134 genes could be associated to GO terms that describe a specific function or process [90]. In each section of Panther analysis the most prominent processes or pathways were described exemplarily as well as the GO term and an example for the corresponding process or pathway. The calculated percentage in each analysis represents the percentage of DEG of the total number of annotations behind a GO term since each annotation links one specific gene product to a GO term. Therefore, the percentage gives information about the range of functions the genes behind a GO term have. When the percentage is higher, the genes behind a GO term have a lower range of different functions.

3.10.1 DEG between L1KO and WT males associated with “cellular processes”

In “biological processes”, the integrated genes are combined into groups according to their protein function and interaction with other proteins from integrated genes to conduct specific tasks that frame the GO term [75]. Panther then displays the number of genes found to belong to the same GO term. This analysis showed that the 3134 DEG are involved in 5505 biological processes (Fig. 21). 1745 genes are related to “cellular processes” (GO:0044237, e.g. cellular metabolic process) which is 2.33 % of all annotations (74807 annotations) in this GO term. Further, 1074 genes are associated with “metabolic process” (GO:0008152, e.g. organic substance metabolic process) which is 1.07% of all annotations (100042 annotations) in this GO term. 872 genes are allied to biological regulation (GO:0065007, e.g. regulation of biological process) which is 0.4 % of all annotations (216303 annotations) in this GO term. 420 genes are related to “localization” (GO:0051179, e.g. establishment of localization) which is 0.75 % of all annotations (55827 annotations) in this GO term. Taken together, most differentially expressed genes and also the highest percentage of differentially expressed genes were associated to “cellular processes” with 1745 of 3134 genes and 2.33%.

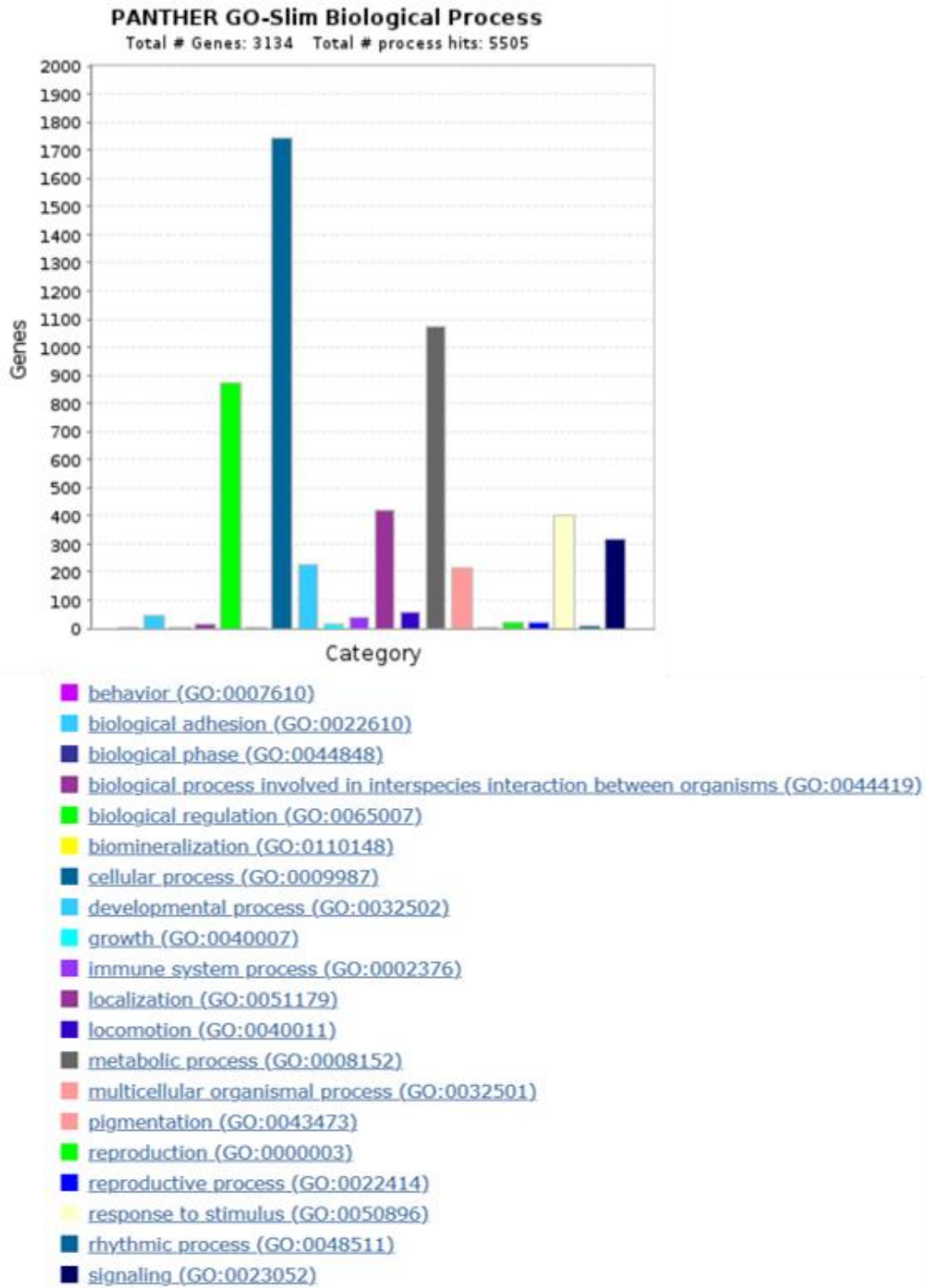


Fig. 21 Cellular processes altered in L1KO mutant males. Biological Process is one part of RNA-seq data analysis with the online tool Panther. 1745 of 3134 DEG were linked to cellular processes. The graph shows the number of genes that were matched to a specific GO term in biological processes.

3.10.2 DEG between L1KO and WT males associated with “binding”

In Panther’s “molecular function”, the online tool points to the specific protein function of the integrated genes or their immediate interaction partners “on a biochemical level” [75]. Analysis of the 3134 DEG with Panther’s molecular processes (Fig. 22) revealed 2358 altered molecular processes in L1KO mutant males. Here, 991 genes were associated with the GO term “binding” (GO:0005488, e.g. protein binding) which is 0.64 % of all annotations (155491 annotations) in this GO term. 661 genes were allied to “catalytic activity” (GO:0003824, e.g. hydrolase activity) which is 0.75 % of all annotations (88618 annotations) in this GO term. 173 genes were involved in “transcription regulator activity” (GO:0140110, e.g. DNA-binding transcription factor activity) which is 1.72 % of all annotations (10078 annotations) in this GO term. 127 genes were related to “molecular function regulator” (GO:0098772, e.g. enzyme regulator activity) which is 1.16 % of all annotations (10978 annotations) in this GO term. Taken together, most differentially expressed genes were associated to “binding” with 991 of 3134 genes while the highest percentage of regulated genes was found in “DNA-binding transcription factor activity” with 1.72 %.

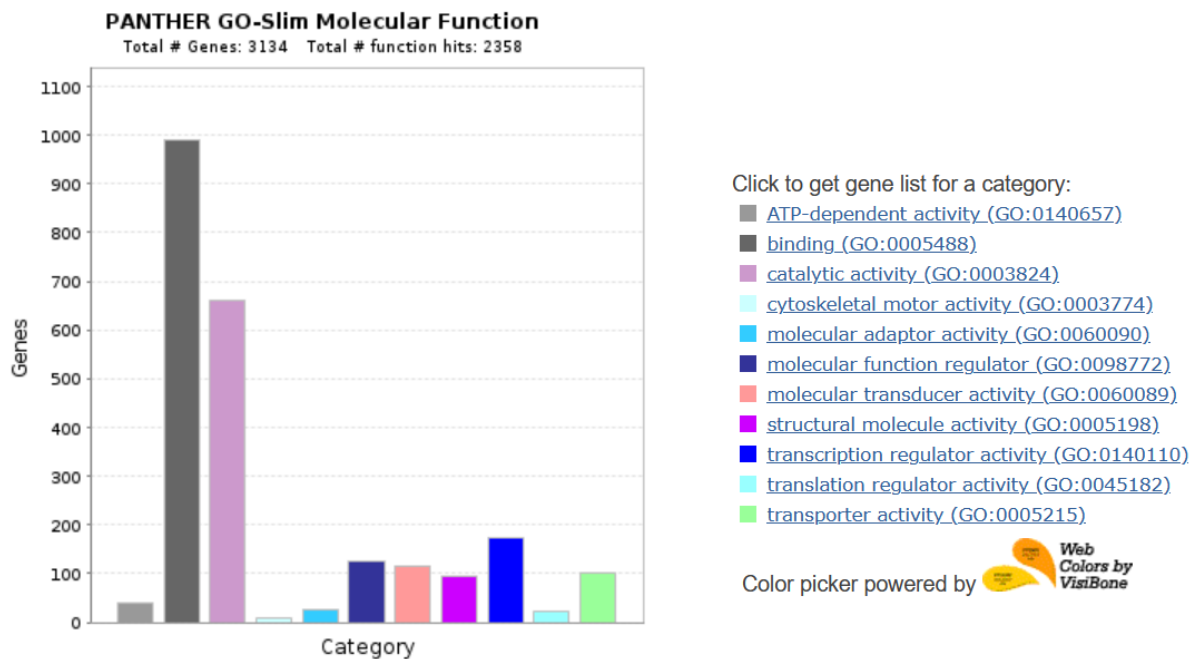


Fig. 22 Binding processes altered in L1KO mutant mice. Molecular function is one part of RNA-seq analysis with the online tool Panther. 991 of 3134 DEG were associated with “binding”, 661 with “catalytic activity”, 173 with “transcription regulator activity” and 127 gene IDs with “molecular function regulator”. The graph shows the number of genes that were matched to a specific GO term in molecular function.

3.10.3 DEG between L1KO and WT associated with “WNT signaling”

Panther’s pathway analysis uses the information generated in “biological processes” and additionally considers the “relationships between the interacting molecules”. Panther then displays the number of genes whose emerging proteins are functionally connected [75]. Panther’s pathway analysis showed that the 3134 DEG are involved in 1052 pathways (Fig. 23). Most DEG were found in “WNT signaling pathway” with 48 genes (P00057, e.g. Cadherin) which is 2.16 % of all annotations (2224 annotations) in this pathway. 39 genes were involved in “GnRH receptor pathway” (P06664, e.g. MAP3Ks) which is 16.53 % of all annotations (236 annotations) in this pathway. 34 genes were associated with “Inflammation mediated by chemokine and cytokine signaling pathway” (P00031, e.g. Myosin) which is 2.11 % of all annotations (1615 annotations) in this pathway and 32 genes were related to “Heterotrimeric G-protein signaling pathway-Gi alpha and Gs alpha mediated pathway” (P00026, e.g. Collagen) which is 2.98 % of all annotations (1075 annotations) in this pathway. Taken together, most differentially expressed genes were found in “WNT signaling pathway” with 48 of 3134 genes while the highest percentage of regulated genes was found in “GnRH receptor pathway” with 16.53 %.

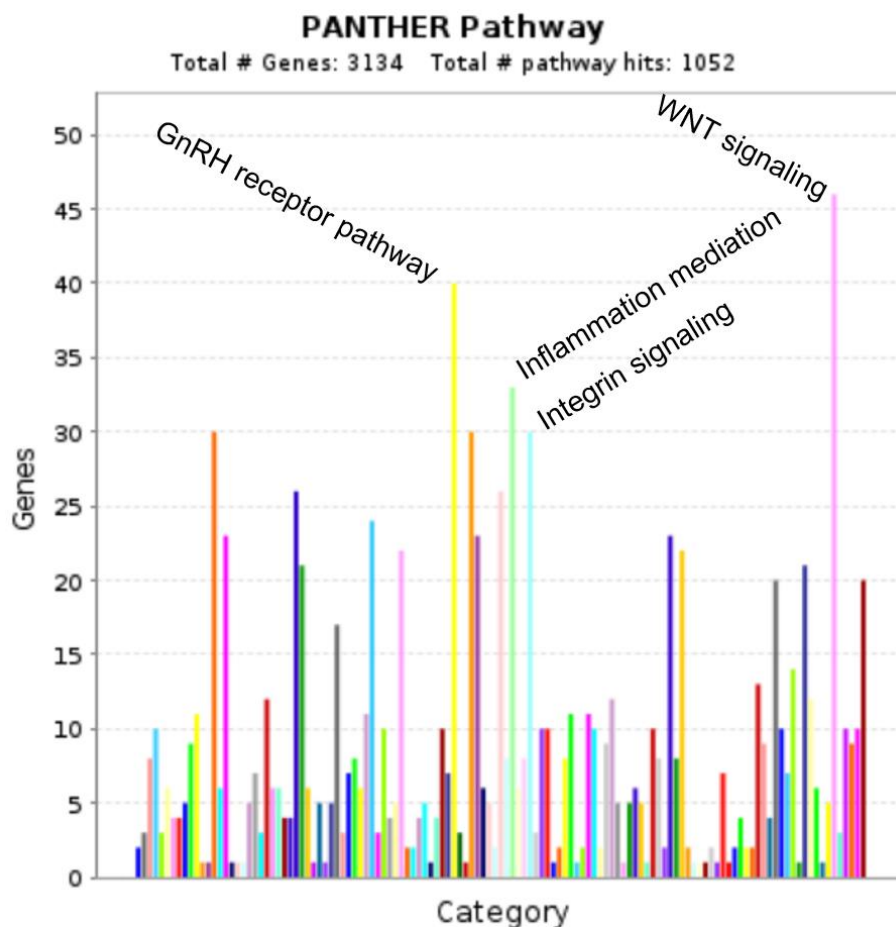


Fig. 23 WNT signaling pathway altered in L1KO mutant mice. Panther's pathways is one part of the RNA-seq data analysis with the online tool Panther. 48 of 3134 DEG were linked to “WNT signaling”, 39 to “GnRH receptor pathway”, 34 to “Inflammation mediated by chemokine and cytokine signaling pathway”, and 32 gene IDs to “Heterotrimeric G-protein signaling pathway-Gi alpha and Gs alpha mediated pathway”. The graph shows the number of genes, that were matched to a specific pathway.

3.11 Altered expression of TJP genes and genes involved in oligodendrogenesis

In addition to Gene Ontology analyses, RNA-seq expression levels of selected genes were investigated. There are multiple indications that the emerging hydrocephalus in the human L1 syndrome can be caused by dysfunctions in the CP which acts as a Blood-CSF-barrier [61,91,92]. The CP consists of epithelial cells in contrast to the BBB which is formed by endothelium [93]. Major components of the epithelial barrier integrity are tight junction proteins (TJP) and dysregulations in TJP expression can result in reduced integrity and hyperpermeability of the CP [94,95]. *Cldn5* and *Tjp1* expression levels were investigated here because their emerging proteins belong to the family of TJPs [96,97]. *Tjp1* is coding for the protein Zonula occludens-1 (ZO-1) and further known to be a marker for the apical membrane of epithelial cells [98]. *Lamb1* was included here because it is known to be a marker for the basal membrane of epithelial cells [99] indicating the relationship between the three genes.

On the one hand, gene expression levels of the tight junction gene *Claudin5* were significantly lowered in L1KO mutant male mice compared to their littermate wildtype controls (Fig. 24A, $p=0.0079$). On the other hand, the expression levels of *Tjp1* and *Lamb1* were both elevated in L1KO mutant male mice compared to their littermate wildtype controls (Fig. 24B *Tjp1* $p=0.0273$, Fig. 24C *Lamb1* $p=0.0456$).

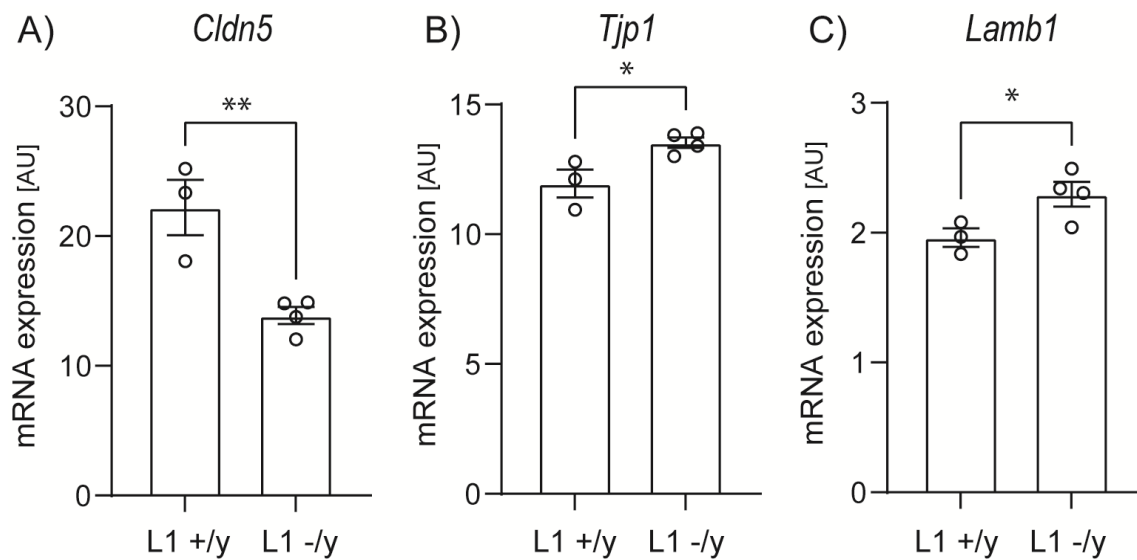


Fig. 24 Altered expression of TJP genes and *Lamb1*. Analysis of mRNA expression levels of (A) *Cldn5*, (B) *Tjp1* and (C) *Lamb1* in L1 +/y (n=3) and L1 -/y mice (n=4) revealed by RNA-seq. Graphs display mRNA expression values \pm SEM. *P* values were calculated by t test (* $p<0.05$, ** $p<0.01$).

The essential role of L1CAM in the regulation of proliferation, differentiation and myelination is undisputed [52,100]. For this reason, we looked for altered expression levels of marker genes known to be involved in named processes since we expected dysregulations in L1KO mutant mice here. Investigation of RNA-seq data showed altered expression of the neural progenitor marker *Sox2* and the markers *Nkx6.2*, *Olig1* and *Olig2* known to be involved in oligodendrogenesis. *Sox2* expression levels were decreased in L1KO mutant males compared to littermate controls (Fig. 25A, $p=0.0131$). *Nkx6.2* mRNA expression was elevated in L1KO mutant mice compared to controls but this difference did not reach statistical significance (Fig. 25B, $p=0.0603$). Expression levels of the oligodendrocyte marker *Olig1* were elevated in L1KO mutant mice compared to their littermate controls (Fig. 25C, $p=0.0298$) while *Olig2* expression was decreased in L1KO mutant mice compared to controls (Fig. 25D, $p=0.0277$).

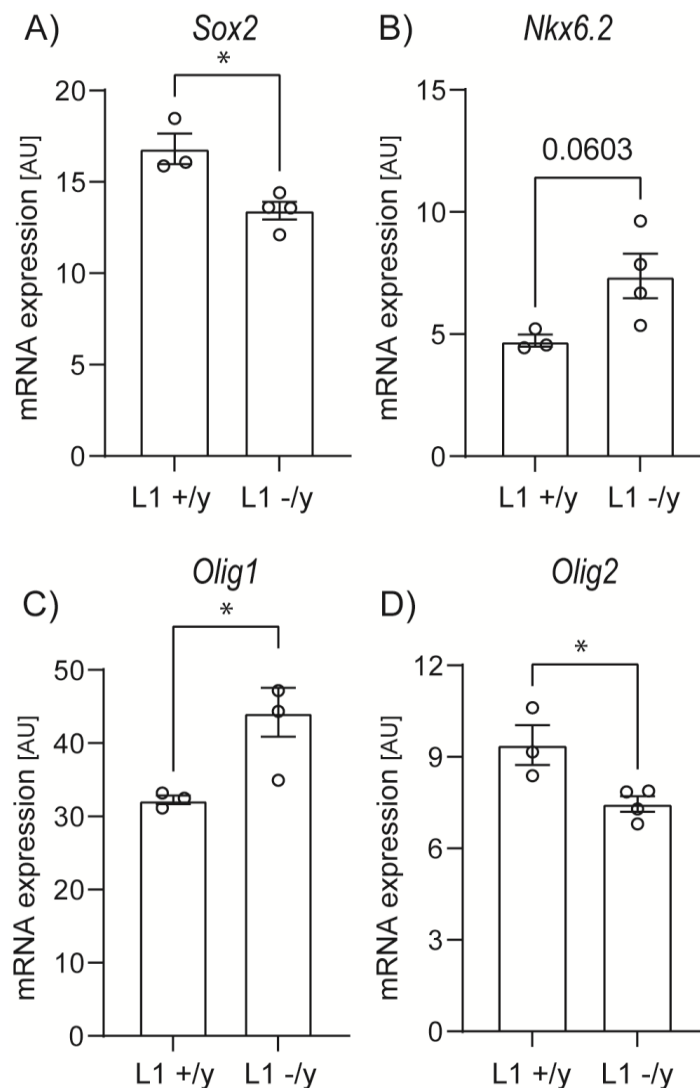


Fig. 25 Changed expression of genes involved in oligodendrogenesis. Analysis of mRNA expression levels of (A) *Sox2*, (B) *Nkx6.2*, (C) *Olig1* and (D) *Olig2* of L1 +/y (n=3) and L1 -/y mice (n=4) by RNA-seq. Graphs display mRNA expression values \pm SEM. *P* values were calculated by t test (* $p<0.05$).

3.12 L1CAM-deficiency increases lethality at late embryonic or neonatal stages

The results described above revealed a neurological phenotype of adult L1KO mutant males. They showed neurological deficits and behavioral abnormalities as well as neuroanatomical alterations. Subsequent gene expression analyses further suggested that the phenotype of L1KO mutant males may originate from disturbances of neurodevelopmental processes. The results are consistent with previous findings that L1 syndrome is a neurodevelopmental disorder [101,102]. Therefore, the next series of experiments was performed using embryonic stage 16 (E16) mice. For this purpose, we performed overnight breedings of wildtype male and heterozygous female mice. 16 days after conception, the pregnant mice were sacrificed and the embryos were dissected from the uterus. The embryos were then sacrificed by decapitation, their brains were collected and tail biopsies were taken for genotyping. Serial cryosectioning was performed following a specific sectioning protocol adapted from adult mice. These cryosections were then subjected to immunolabeling as well as qPCR analysis.

In order to investigate whether the onset of hypermortality observed in adult L1KO mutant mice is before E16 or not we first analyzed the yield of genotypes in litters of E16 overnight breedings. Wildtype male and female mice were combined in one column because they show identical amplicates in the L1KO genotyping PCR. According to Mendelian genetics a distribution of 25 % hemizygous males, 25 % heterozygous females and 50 % wildtypes was expected. Merging the genotypes from all E16 L1KO mice (n=57) revealed a yield of 38.6 % (n=22) wildtype female/male mice, 26.3 % (n=15) hemizygous male mice and 35.1 % (n=20) heterozygous female mice (Fig. 26).

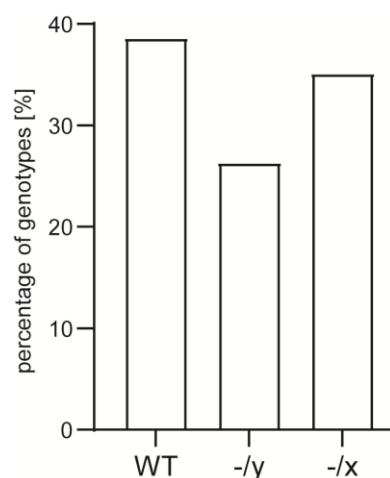


Fig. 26 Normal yield of hemizygous L1KO E16 males. This graph shows the percentages of the different genotypes in E16 L1KO litters (n=57): wildtype mice (WT), hemizygous males (-/y) and heterozygous mice (-/x).

3.13 E16 L1KO males show enlarged ventricles and altered expression patterns in the cortex and CP

In this work, we often referred to the congenital hydrocephalus when planning new experiments since it is a frequently emerging pathology in human L1 syndrome patients. There are several theories concerning the origin of this hydrocephalus. One is a dysfunction and hyperpermeability of the CP causing an overproduction of CSF [94,95] which we partially addressed in adult L1KO mice. Another possible origin for the murine hydrocephalus proposed by researchers is a malformation of cortical layers during corticogenesis. More precisely, they consider hydrocephalus as a consequence of a disruption of the ventricular zone [103]. The early onset of corticogenesis is around E10.5 while the division of the cortex into different layers starts around E12.5 and climaxes after E17.5 to the postnatal period [14]. Therefore, we chose E16 to be the timepoint of analysis to investigate cortical alterations in L1KO mutant males during corticogenesis.

For a better comparability of adult and embryonic L1KO mice, Nissl-stained cryosections of E16 mice were also subjected to ventriculometry (Fig. 27). Volumetry of cryosections revealed that L1KO mutant male mice (further referred to as L1KO) exhibited enlarged ventricles compared to littermate control mice (L1WT: 4.27 ± 0.27 %, L1KO: 5.75 ± 0.37 %, $p=0.0062$). We were not able to distinguish between wildtype females and males in a single *L1cam* PCR because they both show the same amplicons. Therefore, the wildtype females and males were combined as 'L1WT' here. Ventricle sizes were again illustrated as percentages of the whole section area.

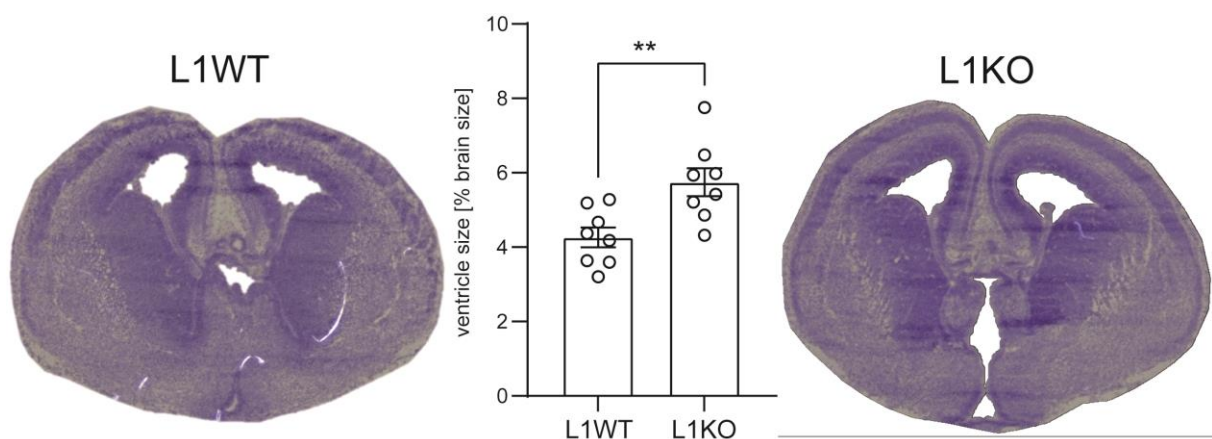


Fig. 27 Increased ventricle sizes in E16 L1KOs. Analysis of ventricular sizes of L1WT (left, n=8) and L1KO E16 mutant males (right, n=8) was performed in Nissl stainings. The Graph shows individual percentual ventricle sizes \pm SEM. *P* values were calculated by Mann-Whitney *U* test (** $p < 0.01$).

In order to investigate protein expression in L1KO and control mice on a cellular level, several immunostainings were carried out. In general, all shown images of immunofluorescent stainings were captured from the medial and dorsal subventricular area (Fig. 28, medial=red square, dorsal=yellow square).

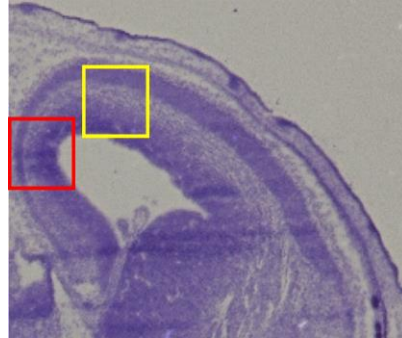


Fig. 28 Dorsal and medial cortical areas for analysis. Nissl staining of E16 cryosection to illustrate where images were taken in the medial (red square) and dorsal area (yellow square).

3.14 No L1CAM expression in L1KO E16 cortex

In order to see how L1CAM expression is distributed along the embryonic cerebral cortex we performed α L1CAM labelings (Fig. 29). The strongest L1CAM signal was found in the intermediate zone, whereas less signal was observed in the cortical plate and no L1 signal in the ventricular and subventricular zone (VZ/SVZ). Immunohistochemical analysis further showed, that there is no L1CAM expression in the L1KO cortex.

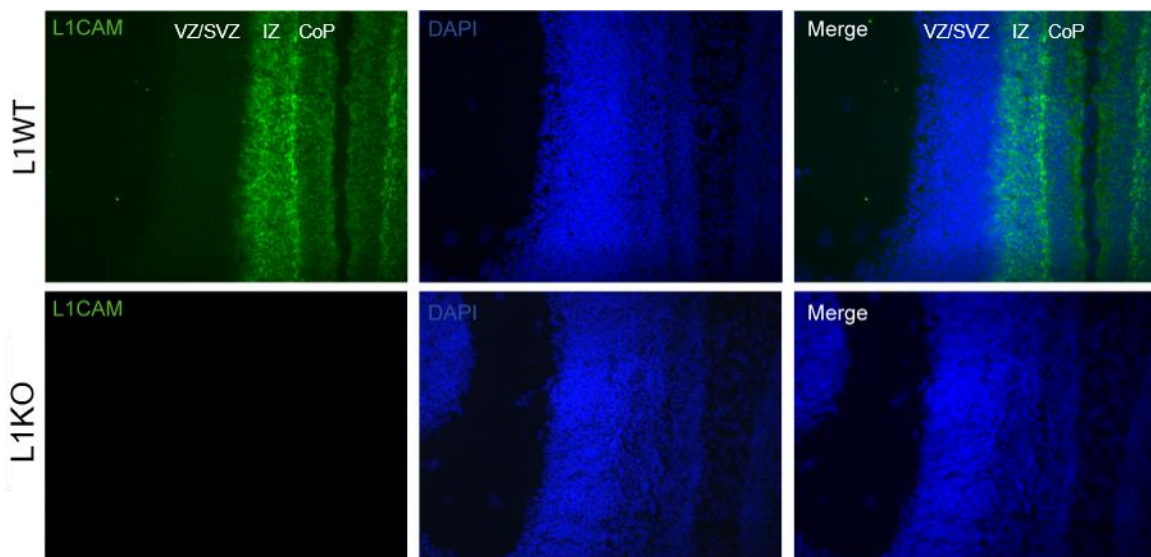


Fig. 29 No L1CAM expression in VZ/SVZ. Immunohistochemical validation of L1CAM expression in L1WT and L1 hemizygous male mice (L1KO). The images show the signals of α L1CAM (green), DAPI staining for nuclei (blue) as well as the merge image of both signals (Merge) in the ventricular and subventricular zone (VZ/SVZ), intermediate zone (IZ) and cortical plate (CoP).

3.15 Thinned SOX2 layer in L1KO mutant dorsal cortex

L1CAM is known to be involved in the regulation of proliferation, self-renewal and differentiation of neural stem and progenitor cells [52]. Alterations of these processes are very likely to occur in L1 syndrome which is why we tried to assess them by IHC. It was also shown that hydrocephalus in general can arise from a disruption of the VZ [103]. For these reasons we analyzed cortical layers where several types of neural progenitor cells reside using specific markers, among them the VZ. The VZ/SVZ markers SOX2, PAX6 and TBR2 were investigated by immunohistochemical labeling (Fig. 30). SOX2 and PAX6 are both transcription factors expressed in neural stem cells while in more differentiated progenitor cells PAX6 is expressed but not SOX2 anymore [12]. SOX2 expression by neural progenitor cells is mostly restricted to the VZ where it is essential for maintaining the progenitor state [104]. Analysis of dorsal and medial parts of the VZ immunolabeled by SOX2 revealed a thinner VZ in L1KO embryos compared to wildtype controls at dorsal sites (Fig. 30A, L1WT: $111.9 \pm 3.86 \mu\text{m}$, L1KO: $100.3 \pm 3.14 \mu\text{m}$, $p=0.0472$). However, there was no difference in the thickness of the SOX2-immunolabelled VZ at medial sites between wildtype and L1KO embryos (Fig. 30A, L1WT: $106.5 \pm 3.39 \mu\text{m}$, L1KO: $105.5 \pm 4.92 \mu\text{m}$, $p=0.871$). Further, the thickness of the medial VZ/SVZ was analyzed via PAX6 labeling which is expressed by cells located in the VZ but also in the SVZ to some extent [104]. There PAX6 is important for the regulation of self-renewal of neural stem cells [105]. PAX6 labelings showed no difference between control and L1KO (Fig. 30B, L1WT: $110.4 \pm 3.05 \mu\text{m}$, L1KO: $113.8 \pm 3.34 \mu\text{m}$, $p=0.47$). The dorsal part could not be investigated here due to inconsistent signals of PAX6 in both groups. In the cortex TBR2 is essential for the symmetrical division of intermediate progenitors in the VZ/SVZ to produce neurons [106]. Investigation of the VZ/SVZ via TBR2 labeling displayed no difference between L1WT and L1KO mice in the medial (Fig. 30C, L1WT: $104 \pm 1.12 \mu\text{m}$, L1KO: $103.4 \pm 2.93 \mu\text{m}$, $p=0.859$) as well as the dorsal area (Fig. 30C, L1WT: $136 \pm 3.01 \mu\text{m}$, L1KO: $131.1 \pm 4.76 \mu\text{m}$, $p=0.417$). Overall, the analysis of the cortical layers did not reveal major differences between L1WT and L1KO mice. However, SOX2 immunostaining showed a decreased abundance of this marker in the dorsal part of the VZ in L1KO at E16.

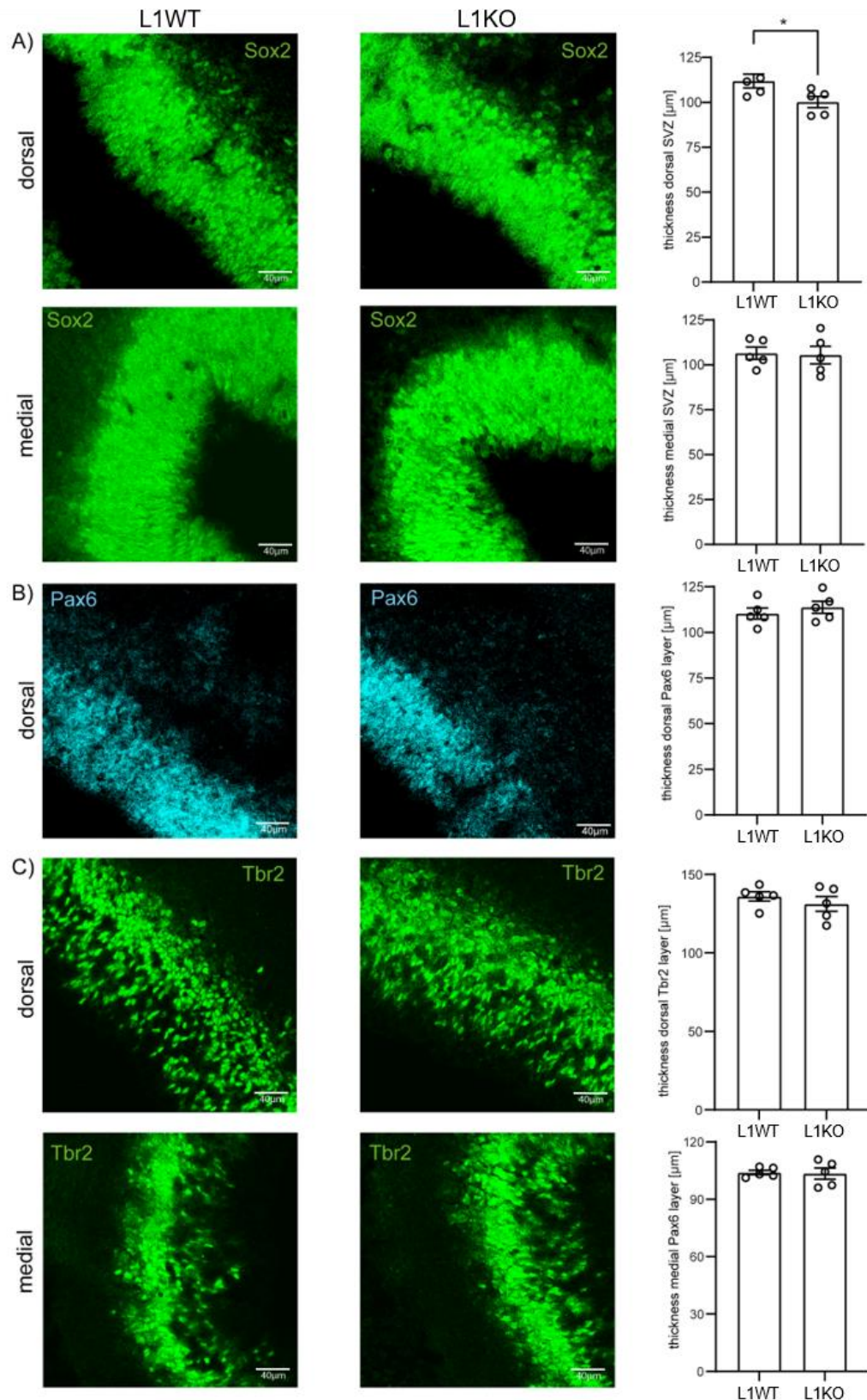


Fig. 30 Thinned SOX2-layer in L1KO mutant dorsal cortex. (A-C) Representative immunostainings of cortical markers and their assessment regarding the thickness of each stained layer. (A) Immunohistochemical analysis of α SOX2 to measure the size of the ventricular zone in E16 cryosections dorsal and medial from the ventricle. (B) Immunohistochemical analysis of α PAX6 that also represents the ventricular zone. (C) Immunohistochemical analysis of α TBR2 in the dorsal and medial embryonic cortex that mostly represents the subventricular zone. Individual values are displayed as thicknesses in $\mu\text{m} \pm \text{SEM}$. *P* values were calculated by *t* test ($*p < 0.05$), $n = 5/\text{genotype}$.

3.16 Less KI67⁺ cells in the L1KO choroid plexus

In general, epithelial and endothelial cells serve as a barrier between two compartments. The respiratory epithelium for example prevents pathogens, allergens and debris from entering the body through the air we breathe. It is also involved in their clearance of foreign particles [107]. Further, endothelial cells like vascular endothelial cells can be found inside the whole blood and lymphatic system. They are involved in multiple essential mechanisms like fluid filtration in the kidneys, blood vessel tone, hemostasis, neutrophil recruitment, and hormone trafficking [108]. Tight junctions are a major component in executing these tasks by controlling permeability of adjacent cells, together with adherens junctions and desmosomes (Fig. 31). They are obligatory for cellular stability and preserving cell polarity [109].

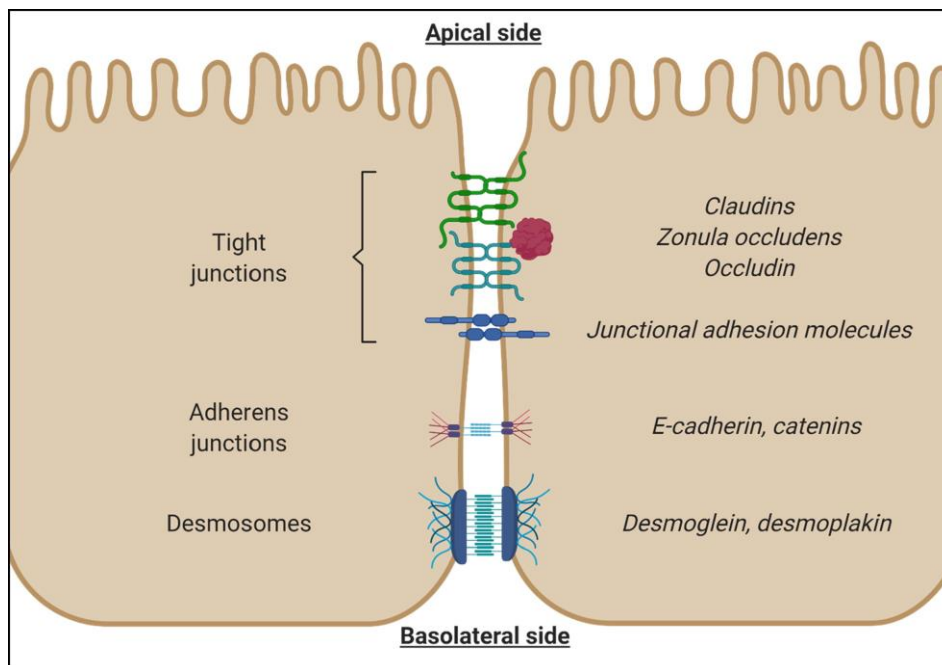


Fig. 31 Junctions and desmosomes. Schematic illustration of adjacent epithelial cells that are connected by tight junctions, adherens junctions and desmosomes. These proteins act as a paracellular barrier and control the paracellular permeability and are essential for the BBB and blood-CSF-barrier [110].

Inside the brain, TJPs are mostly known for their vital function in the blood brain barrier, blood-CSF barrier, the arachnoidal barrier and in combination with adherens junctions for the integrity of the neural tissue [111,112]. The family of TJPs comprise the Claudins, Zona occludens proteins, Occludin and Junctional adhesion molecules (JAMs). Among these, the largest group are by far the Claudins with 27 members, followed by JAMs with only 4 sub-family members [111,112]. Altered expression levels of Claudins or mutations in the encoding genes have been related to pathologies [97,113].

The CP can be found in every brain ventricle. It is a highly vascularized epithelial tissue, serving as a link between blood and CSF where the majority of CSF is produced [114]. In the embryonic CP, the tight junction gene of CLAUDIN-5 is highly expressed and is commonly utilized as a marker for epithelial cells [115]. The secretion of CSF depends on the generation of an osmotic gradient by carbonic anhydrase and Na⁺/K⁺ ATPase. Water is then able to follow the gradient through integral membrane proteins called Aquaporins. For example, Aquaporin1 (AQP1) is expressed in epithelial cells of the CP, while AQP4 is expressed in astrocytes that embrace the capillaries of the CNS. AQP1 is, together with 12 other proteins, a family member of water channels [116]. However, aquaporins are reportedly shown to be involved in some types of brain swelling, cancer, epilepsy and skin diseases [117]. The underlying mechanisms of the L1-dependent hydrocephalus has not yet been completely elucidated. In this approach we assumed a possible origin of enlarged ventricles in the CP which was already shown in a different mouse model of hydrocephalus [62]. Here, we assessed the number of KI67⁺ proliferating cells as well as CLAUDIN-5 expression in the E16 CP of L1WT and L1KO mice since CLAUDIN-5 was already suggested to be involved in the formation of hydrocephalus [62]. KI67 is a DNA-binding protein and a common marker for proliferating cells (genecards). Immunolabeling of the embryonic CP revealed a reduced number of KI67⁺ cells in the CP of L1KO mice compared to littermate controls (Fig. 32, L1WT: 13±1.05, L1KO: 9.25±0.75, *p*=0.0282). Secondary, expression of the TJP CLAUDIN-5 was investigated by IHC which showed less signal in the L1KO CP (Fig. 32, L1WT: 14.12±2.15 %, L1KO: 9.08±1.05 %, *p*=0.0683). However, this difference did not reach statistical significance. Additionally, there was no difference in size between L1KO and wildtype CP (data not shown, *p*=0.167).

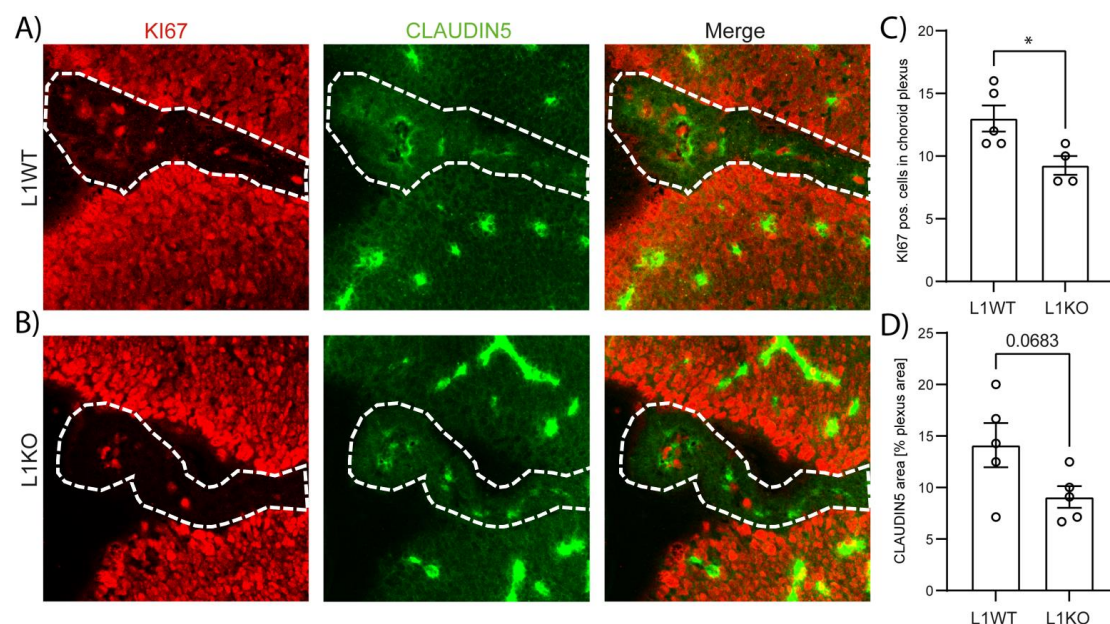


Fig. 32 Less KI67⁺ cells in L1KO choroid plexus. IHC analysis of α KI67 and α CLAUDIN-5 in the CP of (A) E16 control mice and (B) E16 L1KO mice. CP indicated by dotted lines. (C) Assessment of KI67 positive cells in the CP of E16 L1WT (n=5) and L1KO mutant mice (n=4). (D) Assessment of CLAUDIN-5 positive structures per CP area (%; n=5/genotype). Individual values are displayed as mean \pm SEM. *P* values were calculated by t test (**p*<0.05).

3.17 No major changes of mRNA expression of selected genes in E16 L1KOs

In order to assess mRNA expression levels in E16 L1KO brain tissue, qPCR analyses of several targets were performed which we suspected to potentially be altered in L1KO mutant mice. We performed qPCR analyses since RNA-seq of our E16 RNA samples did not give any relevant significant information due to technical issues. L1CAM is known to be essential for synaptogenesis and axonal growth [118,119] which is why we investigated *Gap43* RNA levels for being a growth cone marker [120]. *Vglut2* (*Slc17a6*) was included as an addition to *Gap43* because it encodes for a vesicular glutamatergic transporter located in growth cones [121]. Further, the gene expression levels of *Trp53*, *Bax* and *Casp3* were analyzed by qPCR to gain further insight into apoptosis. According to animal studies concerning hydrocephalus, apoptosis is the major mechanism for the degeneration of neuronal cells there [122]. The RNA levels of Aquaporin 1 and 4 were included here because they are known to be involved in some types of hydrocephalus and possibly contribute to the enlarged ventricles we observed before.[123,124].

qPCR analysis revealed that *Vglut2* was differentially expressed in E16 L1KO mice (Fig. 33). Its RNA levels were increased in E16 L1KO mutant brains but this difference did not reach statistical significance. The RNA expression levels of all other investigated targets were unaltered between E16 L1KO and control brain tissues.

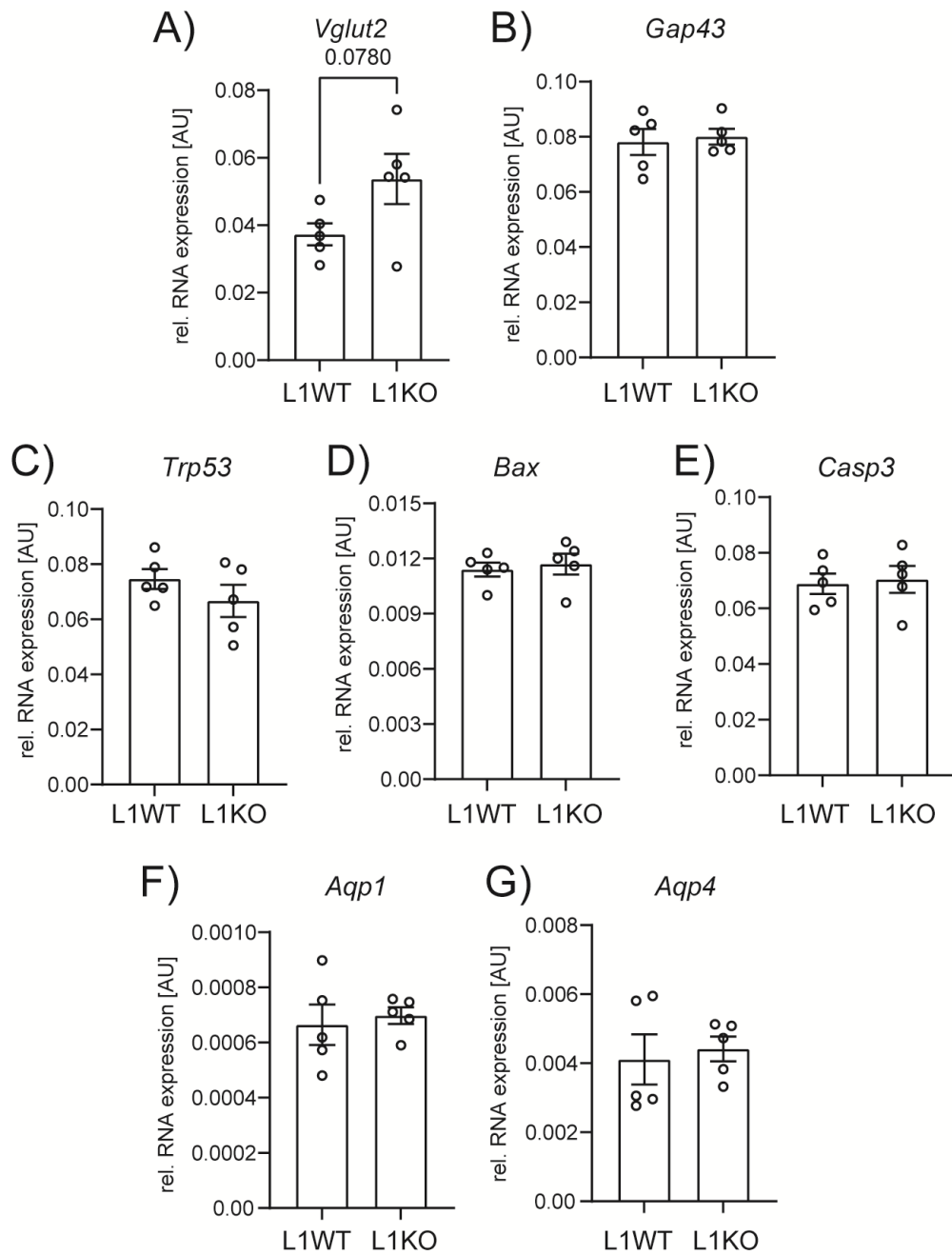


Fig. 33 Gene expression analyses of E16 L1WT and L1KO mice. (A-G) qPCR analysis of E16 L1WT and L1KO mice. RNA expression levels of (A) *Vglut2*, (B) *Gap43*, (C) *Trp53*, (D) *Bax*, (E) *Casp3*, (F) *Aqp1* and (G) *Aqp4*, were assessed (n=5/genotype). Individual values are shown as relative expression values normalized to *Ppia*. P values were calculated by t test.

3.18 Almost no expression of L1CAM in L1KO hESCs

In popular (scientific) journals, cerebral organoids are described as *in vitro* mini brains. Although they are able to show features of brain areas, e.g. some cortical structures they lack the complexity of tissues and networks present in the actual brain. The generation of human cerebral organoids starts with a batch of patient-derived induced pluripotent stem cells or with a commercially available hESC line. In this work we used two stem cell lines, that were genetically modified from the commercially available stem cell line H1. One stem cell line is deficient for L1CAM while the second one normally expresses L1CAM and serves as a control. Initially, to confirm L1 deficiency in our L1KO hESCs, protein lysates of stem cell cultures were subjected to western blot analysis. (Fig. 34). The blot displayed a strong signal of L1CAM (~220 kDa) in control hESCs and almost no signal in L1KO hESCs.

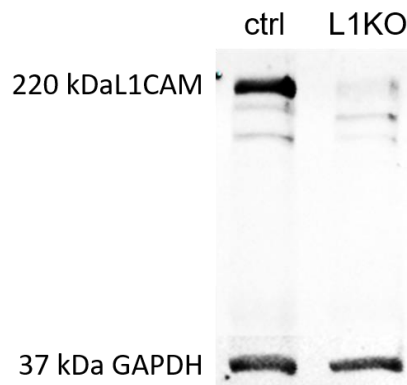


Fig. 34 Almost no expression of L1CAM in L1KO hESCs. Western Blot analysis of α L1CAM (220 kDa) of control and L1KO hESC protein lysates. α GAPDH signal was used (37 kDa) as a housekeeping reference.

Human cerebral organoids were already used in several studies as a model for neurological diseases like microcephaly or lissencephaly [125,126]. In this work, cerebral organoids were generated from a L1KO hESC as an attempt to establish a human *in vitro* model for L1 syndrome since patient samples are inaccessible and also in regard to the 3R principle to reduce animal experiments. Our aim was to test whether L1KO cerebral organoids can mimic the pathological phenotype of the human L1 syndrome in parts. Further, we aimed to compare L1KO organoids to the murine L1 syndrome model and look for similarities that may indicate a successful alternative for animal models. The first timepoint of organoid size analysis was 6DIV because then all cells were in a complex and embryoid bodies had already formed there. The following weeks different media with different proneural ingredients were added to the 3D cultures to promote neural differentiation. Every other day images were taken with a binocular (Evos) and the organoids cross section area was measured.

3.19 Growth of cerebral organoids peaked after 28DIV

With ongoing incubation of the organoid cultures, the organoid grows in size due to proliferative processes. The progression of growth can be a determining factor for the timepoint of analysis. In this work, the timepoint of molecular biological analysis was chosen to be 60DIV because this is the phase where also astrocytes can be present since they usually do not form earlier than that [127]. Images were taken every few days with a microscope during the first 3 weeks and then once a week (Fig. 35A). The size of the organoid was assessed by outlining the organoids borders and measuring the outlined area in ImageJ. The values are plotted in a column graph and presented in mm² (Fig. 35B). Analysis of the organoid growth showed that the growth increased exponentially from 6DIV to 17DIV (Fig. 35B 6DIV: 0.529±0.02 mm², 12DIV: 1.025±0.05 mm², 17DIV: 2.566±0.16 mm²) and then slowed down at 21DIV (21DIV: 2.774±0.0.78 mm²). The size peaked at 42DIV but there was no significant size change after 17DIV (28DIV: 3.066±0.11 mm², 35DIV: 3.091±0.0.16 mm², 42DIV: 3.154±0.0.11 mm², 49DIV: 2.42±0.0.09 mm², 56DIV: 2.624±0.18 mm²). The size differences reached statistical significance at 12 to 17DIV ($p=0.0029$). The graph combines values from 3 batches of organoids.

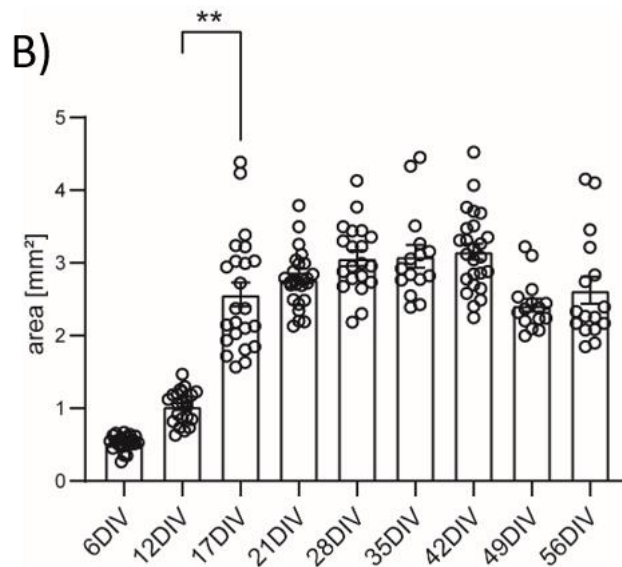
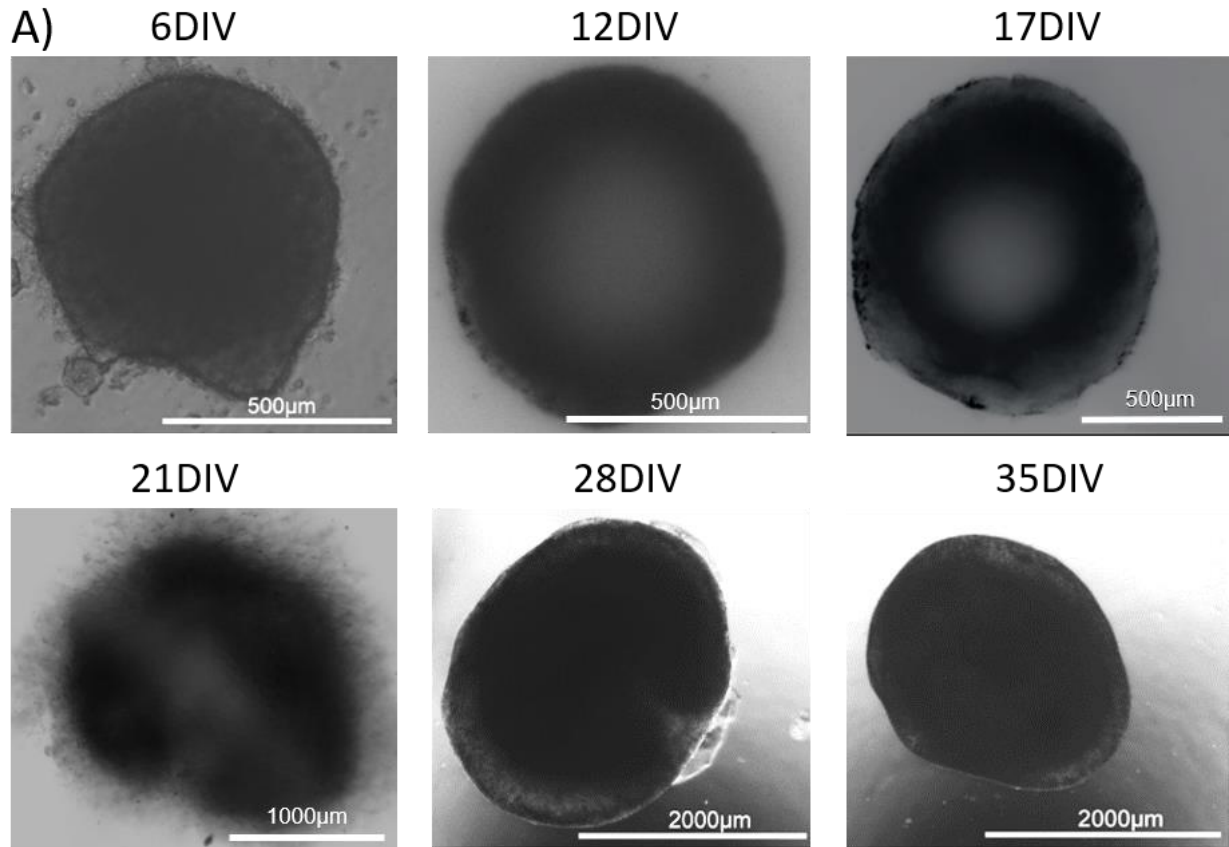


Fig. 35 Size of cerebral organoids peaked after 42DIV. (A) Representative images of organoids after 6DIV to 35DIV. Images of the timepoints 42DIV, 49DIV and 56DIV were not shown since the size did not change significantly after 21DIV. (B) Assessment of the size of 6DIV (n=23), 12DIV (n=22), 17DIV (n=23), 21DIV (n=25), 28DIV (n=21), 35DIV (n=16), 42DIV (n=26), 49DIV (n=17), 56DIV (n=17) old organoids. Individual values are displayed as $\text{mm}^2 \pm \text{SEM}$. *P* values were calculated by Kruskal Wallis test.

3.20 *PAX6* and *VGLUT2* expression altered in L1KO cerebral organoids

In order to investigate the RNA expression levels of selected targets in 60DIV cerebral organoids several qPCRs were performed (Fig. 36). We investigated the expression levels of the progenitor markers *PAX6* and *SOX2* because *L1CAM* is known to be involved in proliferation and differentiation of progenitor cells in the cortical VZ [52]. Also, previous investigations in the present thesis revealed a thinned *SOX2* layer in the E16 L1KO dorsal cortex. The involvement of *L1CAM* in proliferation and differentiation of e.g. progenitor cells was also the reason for the investigation of *GFAP* and *DCX*. *GFAP* encodes for the glial fibrillary protein and is mostly known as a marker for astrocytes but also as a marker for some early neural progenitor cells. However, *DCX* is a marker for immature neurons [128] where we also assumed dysregulated expression levels due to *L1CAM*-deficiency. Since qPCR analyses of E16 L1KO brain tissue indicated a trend towards an increased *Vglut2* expression ($p=0.07$) we also analyzed other targets of glutamate signaling in organoids. Therefore, we performed qPCR analyses of *GRIN2A*, encoding for a NMDA receptor subunit and *VGLUT2*, encoding for a vesicular glutamate transporter in growth cones to be able to make assumptions about glutamate signaling in organoids. As a counterpart for those excitatory signaling markers we analyzed *VGAT* by qPCR which encodes for the vesicular GABA transporter [129]. Lastly, *GAP43* expression was investigated again due to its relationship with *L1CAM* in growth cone development [130,131].

The illustrated values display the relative RNA expression normalized to the housekeeping gene *PPIA*. qPCR analysis revealed that the relative RNA expression of *PAX6* is lowered in L1KO organoids compared to controls (ctrl: 0.000067 ± 0.000029 , KO: 0.000048 ± 0.000037 , $p=0.0068$). Investigation of *VGLUT2* showed that its expression is increased in L1KO organoids compared to control organoids (ctrl: 0.00033 ± 0.00005 , KO: 0.00138 ± 0.00037 , $p=0.0233$). Further, RNA expression levels of *SOX2*, *GFAP*, *DCX*, *VGAT*, *GRIN2A* and *GAP43* were not differentially expressed in L1KO organoids compared to control organoids (*SOX2* $p=0.7813$, *GFAP* $p=0.6051$, *DCX* $p=0.6135$, *VGAT* $p=0.4206$, *GRIN2A* $p=0.1861$, *GAP43* $p=0.1626$).

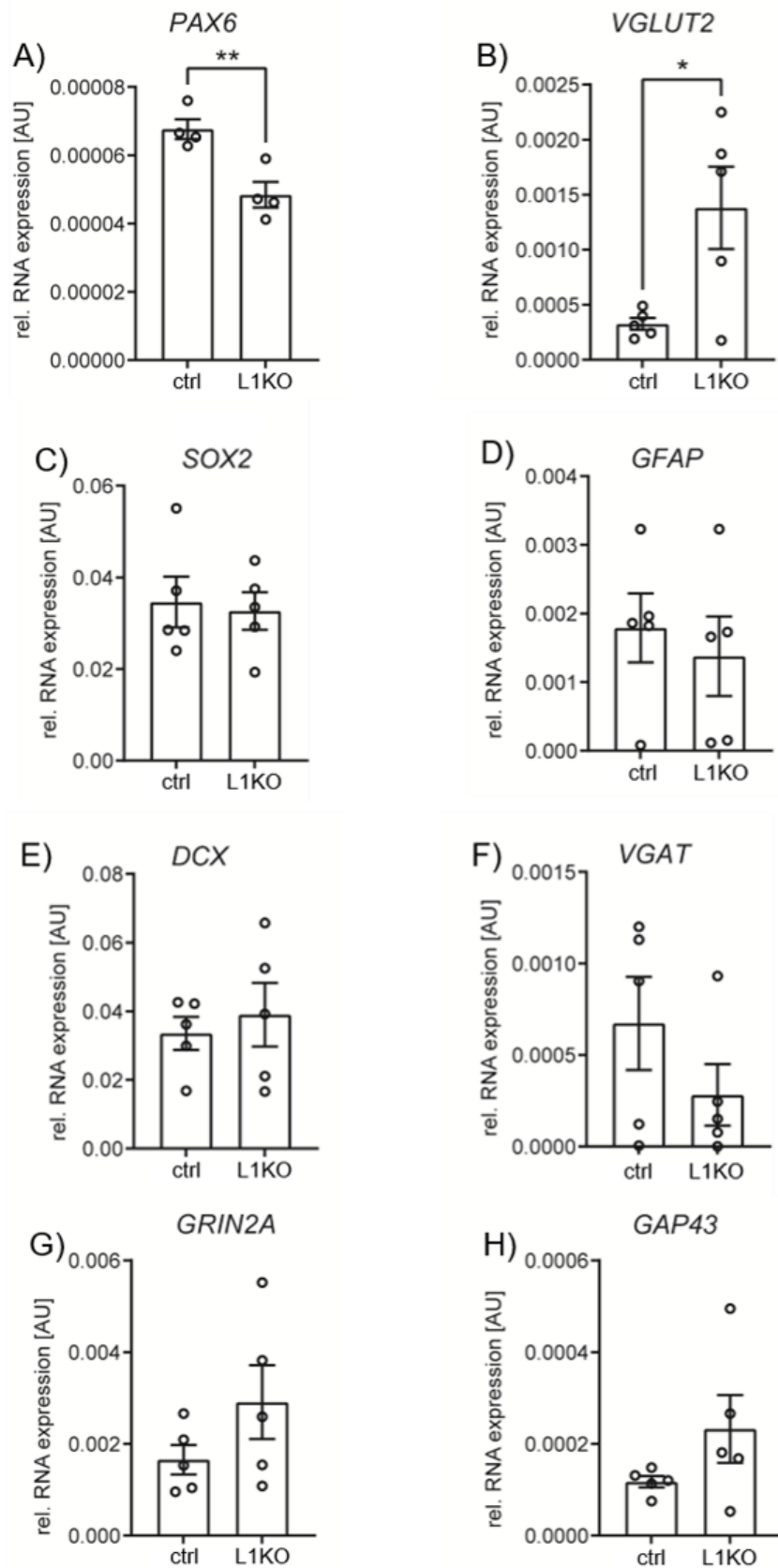


Fig. 36 *PAX6* and *VGLUT2* expression altered in L1KO organoids. qPCR analysis of (A) *PAX6*, (B) *VGLUT2*, (C) *SOX2*, (D) *GFAP*, (E) *DCX*, (F) *VGAT*, (G) *GRIN2A* and (H) *GAP43* of control and L1KO human cerebral organoids. Individual values are displayed as relative gene expression values normalized to the housekeeping gene *PPIA* \pm SEM. *P* values were calculated by t test (A-E, G+H, **p*<0.05, ***p*<0.01) and Mann-Whitney *U* test (F).

3.21 Principal component analysis of transcriptomes from human cerebral organoids

As an attempt to test whether L1KO organoids share features of the human L1 syndrome as modelled in L1KO mutant mice, we subjected RNA samples of 60DIV control and L1KO organoids to RNA-seq. The role of L1CAM in the regulation of proliferation and differentiation of hESCs and progenitors was described multiple times. For example, a downregulation of L1CAM causes premature differentiation of neural progenitors [52]. For this reason, we assumed that RNA-seq of human cerebral organoids reveals altered pathways involved in proliferation and differentiation. We performed similar analyses of organoid RNA-seq data as we did in adult L1KO mice including PCA, GO analysis and investigation of selected genes. Out of the 10 integrated RNA-seq data sets of organoids one control and one L1KO data set were removed because they were subjectively defined as outliers after PCA analysis (Fig. 37). RNA samples of the initial L1KO and control embryonic stem cultures were also subjected to RNA-seq with 1 sample each to assess whether stem cells show major differences in expression levels compared to each other and to cerebral organoids. PCA of hESC RNA samples showed no striking difference between L1KO and WT cell lines.

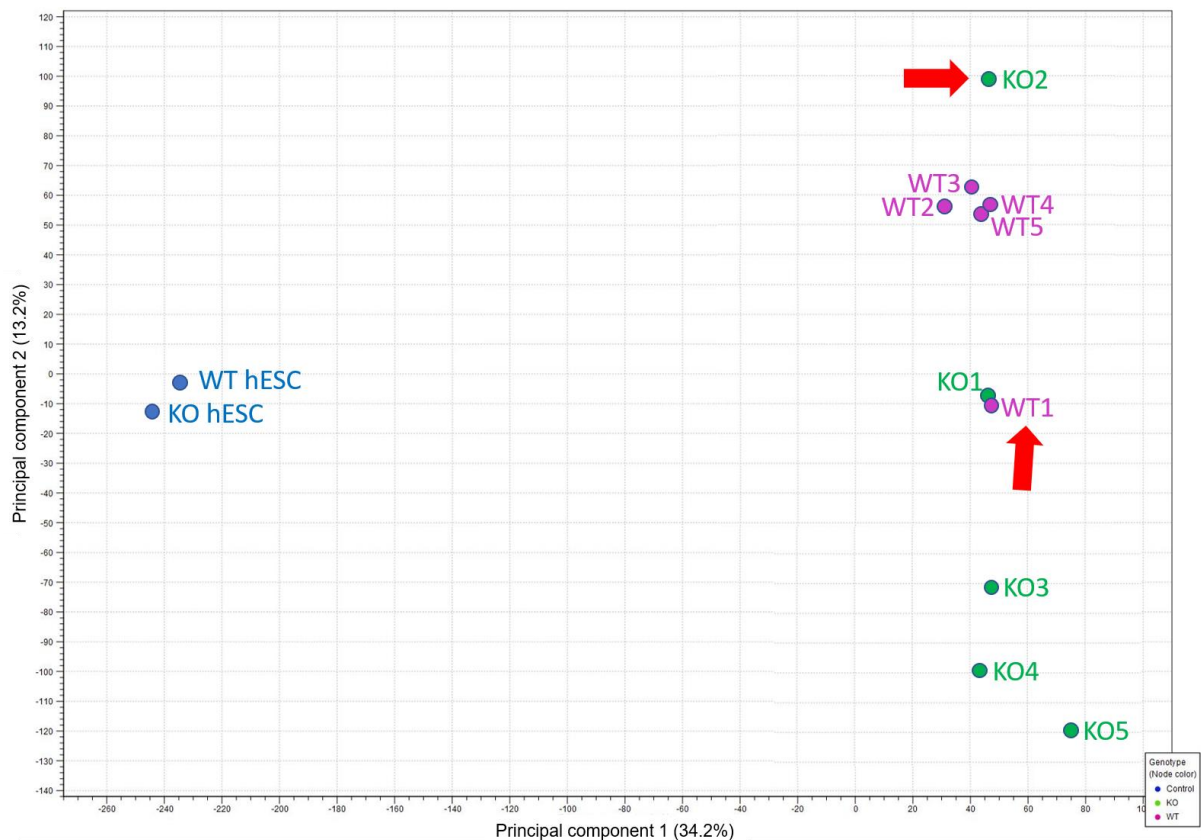


Fig. 37 Principal component analysis detects 2 outliers. Principle component analysis revealed 2 outliers (red arrows) in L1KO (green) and control (purple) RNA-seq data sets. PCA was performed using CLC Genomic Workbench.

3.22 Imbalanced ratio of up- and downregulated genes in L1KO organoids

A volcano plot is a method to visualize data distribution by plotting the p values versus the fold change of gene expression values in a coordinate system. In our case, the volcano plot gives information about the ratio of up- or downregulated in RNA-seq data sets of L1KO organoids. All fold change values were included where a calculation of fold change and p value was possible (27729 genes). The values were plotted as log-values.

Volcano plotting revealed that more genes were up-regulated than down-regulated in L1KO organoids as compared to controls (Fig. 38, 15793 (56.95 %) higher in L1KO and 11936 (43.05 %) lower in L1KO). All DEG with a negative log p -value higher than 2 were highlighted in red. Among those 3010 DEG with $\log p > 2$, 1178 genes were upregulated (39.14 %) and 1832 genes (60.86 %) were downregulated in L1KO mutant mice.

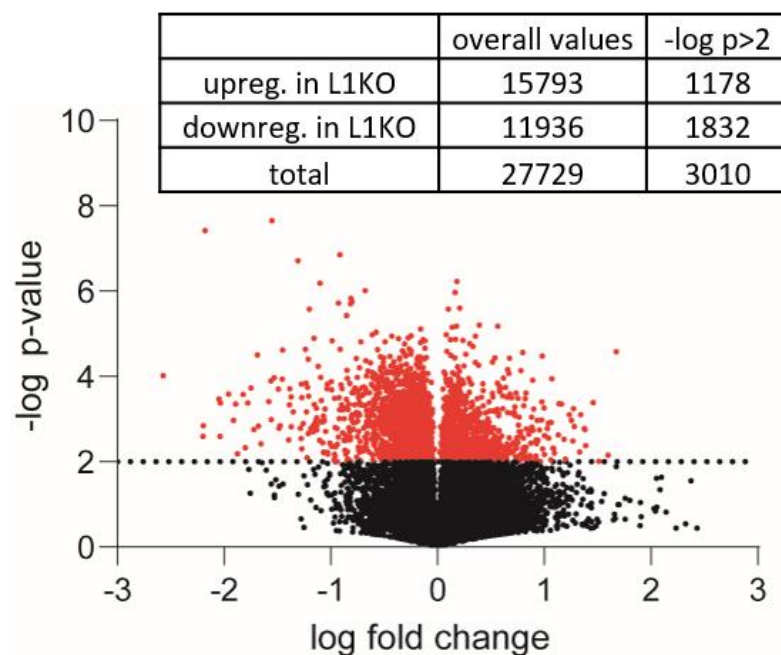


Fig. 38 Imbalanced ratio of up- and downregulated genes in L1KO organoids. This volcano plot reveals the distribution of RNA sequencing data by showing the negative log p value (Y-axis) and the log fold change (X-axis) of each gene. A total of 27729 genes were integrated. 15793 genes are higher expressed and 11936 genes are lower expressed in L1KO organoids compared to controls. The Volcano plot was generated using GraphPad Prism.

3.23 Panther GO analysis revealed changes in “binding processes” and “WNT signaling” in L1KO organoids

As an attempt to reveal altered processes and pathways in L1KO organoids we subjected RNA-seq data of control and L1KO organoids to GO analysis similar to the analysis of adult L1KO mice. We tried to elucidate here whether RNA-seq of L1KO organoids and adult L1KO mutant mice show similar dysregulations evoked by the absence of L1CAM. The principle of the GO database is to offer a brief overview about the special features of genes and their products regarding three criteria: biological processes, molecular function and pathways. In the following 6769 gene IDs of DEG ($p < 0.05$) were subjected to GO analysis with Panther [75,89] from which 6437 genes could be linked to specific GO terms. In each section of Panther analysis the most prominent processes or pathways were described exemplarily as well as the GO-term and an example for the corresponding process or pathway. The calculated percentage in each analysis represents the percentage of DEG of the total number of annotations in the GO term since each annotation represents one specific gene product linked to a specific function.

3.23.1 DEG between L1KO and wildtype associated with “cellular processes”

In Panther's biological processes the integrated gene IDs were combined into specific groups according to their protein function and interaction with other proteins from integrated genes to conduct specific tasks that frame the GO term [75]. Panther then displays the number of genes that belong to the same GO term. Panther analysis showed that the 6769 integrated DEG were associated with 11098 biological processes (Fig. 39). According to Panther analysis, among the 6437 DEG 3347 were related to “cellular process” (GO:0009987, e.g. cellular metabolic process) which is 1.13 % of all annotations (296698 annotations) in this GO term. Additionally, 2087 genes were allied to “metabolic process” (GO:0008152, e.g. organic substance metabolic process) which is 1.29 % of all annotations (161664 annotations) in this GO term. 1874 genes were known to be involved in “biological regulation” (GO:0065007, e.g. regulation of biological process) which is 1.04 % of all annotations (180796 annotations) in this GO term and 869 genes were connected to “response to stimulus” (GO:0050896, e.g. cellular response to stimulus) which is 0.76 % of all annotations (114263 annotations) in this GO term. Taken together, most differentially expressed genes were found in “cellular processes” with 3347 of 6437 DEG while the highest percentage of regulated genes in the specific GO term was found in “metabolic process” with 1.29 %.

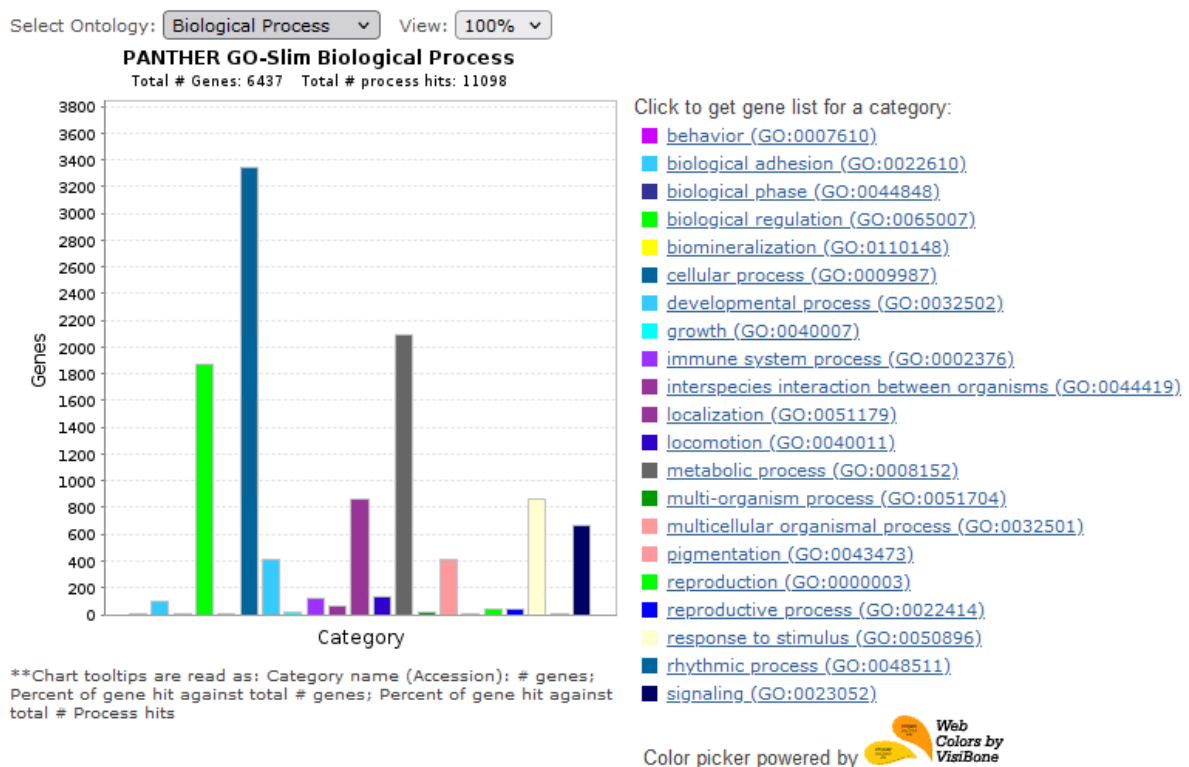


Fig. 39 Altered cellular processes in L1KO organoids. Biological process is one part of the RNA-seq data analysis with the online tool Panther. 3347 of 6437 DEG were related to “cellular process”, 2087 to “metabolic process”, 1874 to “biological regulation” and 869 gene IDs were connected to “response to stimulus. The graph shows the number of genes, that were matched to a specific GO term in biological processes.

3.23.2 DEG between L1KO and wildtype organoids associated with "binding"

In Panther's "molecular function", the online tool points to the specific protein function of the integrated genes or their immediate interaction partners "on a biochemical level" [75]. Panther GO analysis revealed that out of 6437 integrated DEG 4707 genes were involved in "molecular function" processes (Fig. 40). More precisely, 1940 genes were associated to "binding" (GO:0005488, e.g. protein binding) which is 0.5 % of all annotations (384197 annotations) in this GO term. 1397 genes were linked to "catalytic activity" (GO:0003824, e.g. hydrolase activity) which is 1.01 % of all annotations (138805 annotations) in this GO term. 755 genes were related to "molecular function regulator" (GO:0098772, e.g. transcription regulator activity) which is 6.96 % of all annotations (10854 annotations) in this GO term and 318 genes were connected to "transporter activity" (GO:0005215, e.g. transmembrane transporter activity) which is 0.8 % of all annotations (155491 annotations) in this GO term. Taken together, most DEG were found in "protein binding" with 1940 of 6437 DEG while the highest percentage of regulated genes in the specific GO term was found in "molecular function regulator" with 6.96 %.

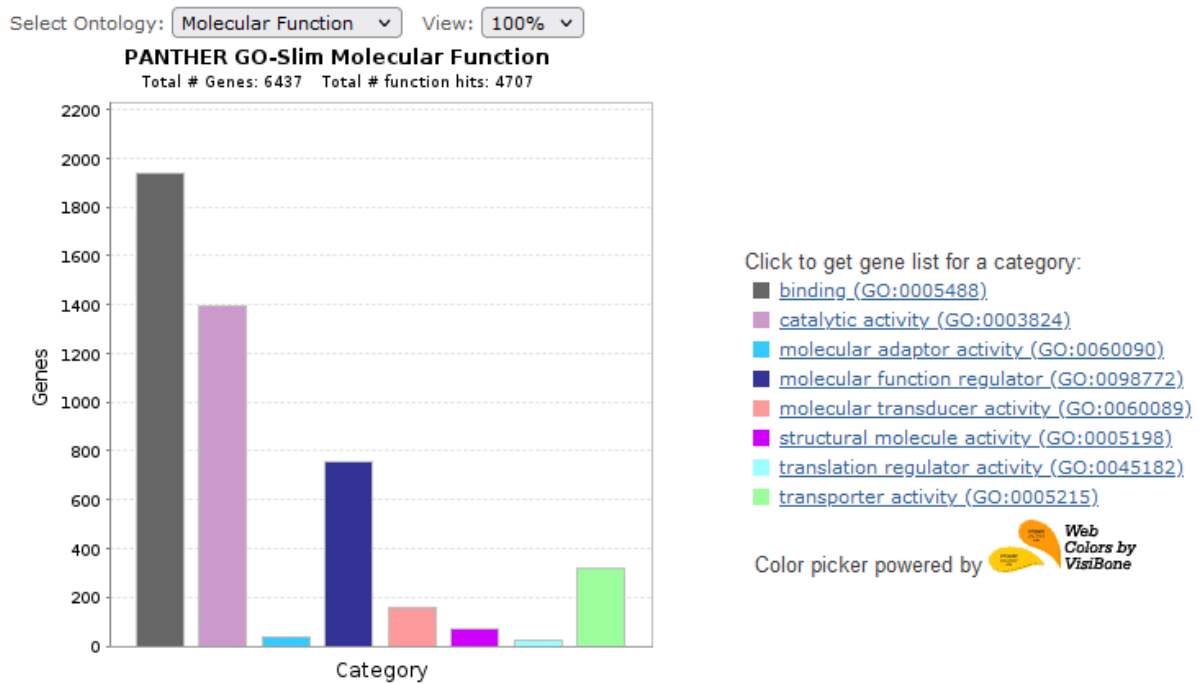


Fig. 40 Binding processes altered in L1KO organoids. Molecular function is one part of the RNA-seq data analysis with the online tool Panther. 1940 of 6437 DEG were related to "binding", 1397 to "catalytic activity", 755 to "molecular function regulator" and 318 gene IDs were connected to "transporter activity". The graph shows the number of genes, that were matched to a specific GO term in molecular function.

3.23.3 DEG between L1KO and wildtype organoids associated with “WNT signaling”

Panthers pathway analysis is based on the information generated in biological processes and additionally considers the “relationships between the interacting molecules” and displays the number of genes where its corresponding proteins are functionally connected [75]. Panther GO analysis of pathways illustrated that the 6437 integrated DEG were involved in 2357 pathways based on the gene ontology database (Fig. 41). Further, 112 genes were related to “WNT signaling” (P00057, e.g. Cadherin) which is 5.04 % of all annotations (2224 annotations) in this pathway. 109 genes were linked to “Gonadotropin-releasing hormone receptor pathway” (P06664 e.g. MAP3Ks) which is 46.19 % of all annotations (236 annotations) in this pathway. 78 genes were connected to “Inflammation mediated by chemokine and cytokine signaling pathway” (P00031 e.g. Myosin) which is 4.83 % of all annotations (1615 annotations) in this pathway and 71 genes were related to “Angiogenesis” (P00005 e.g. Wingless-type MMTV integration site family member) which is 5.85 % of all annotations (1213 annotations) in this pathway. Taken together, most differentially expressed genes were found in “WNT signaling” with 112 of 6437 DEG while the highest percentage of regulated genes in the specific pathway was found in “Gonadotropin-releasing hormone receptor pathway” with 46.19 %.

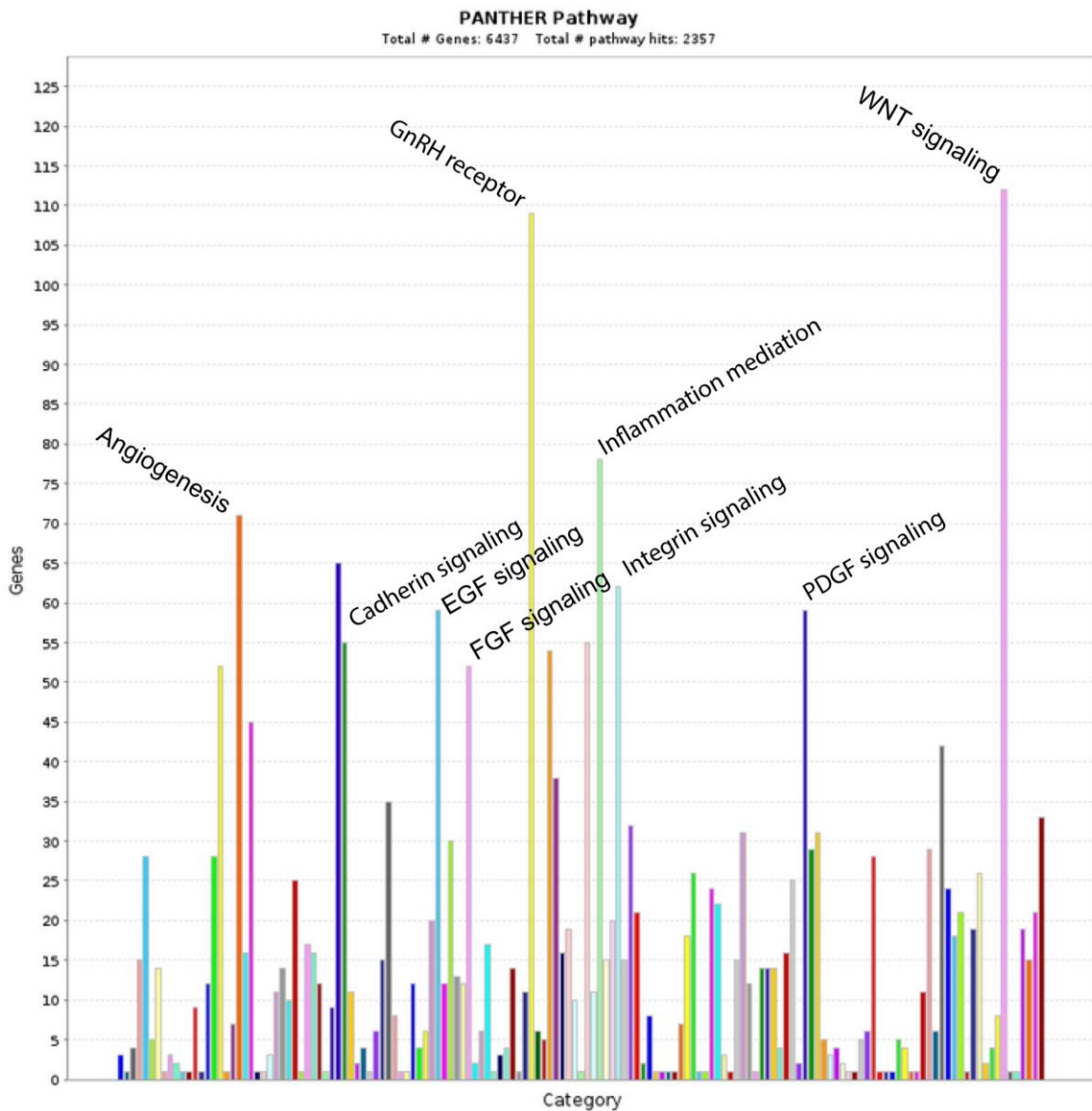


Fig. 41 Altered WNT signaling pathway in L1KO organoids. Panther's pathway is one part of the RNA-seq data analysis with the online tool Panther. 6437 IDs of DEG were integrated to Panther. 112 genes were linked to "WNT signaling pathway", 109 to "Gonadotropin-releasing hormone receptor pathway", 78 to "Inflammation mediated by chemokine and cytokine signaling pathway" and 71 genes were related to "Angiogenesis". The graph shows the number of genes that were matched to a specific pathway.

3.24 GOrilla/REVIGO analysis revealed DEG between L1KO and wildtype organoids are associated with proliferation, adhesion and development

Gene IDs of DEG ($p < 0.05$) were integrated to the free online tool GOrilla which matched the gene IDs to GO terms and calculated a p value for these GO terms. This data was then further integrated to another online tool called REVIGO (**R**educe & **V**isualize **G**ene **O**ntology) whose task was to visualize the data generated in GOrilla [39]. REVIGO sorts these integrated GO terms into different groups. The GOrilla-derived p values were visualized as a log₁₀ graph by REVIGO. The higher the number of genes matched to a specific GO term the lower the calculated log₁₀ p value for this GO term and the more likely it is that this process is actually affected by L1CAM deficiency. REVIGO analysis revealed that most DEG are involved in development, differentiation, proliferation and adhesion (Fig. 42).

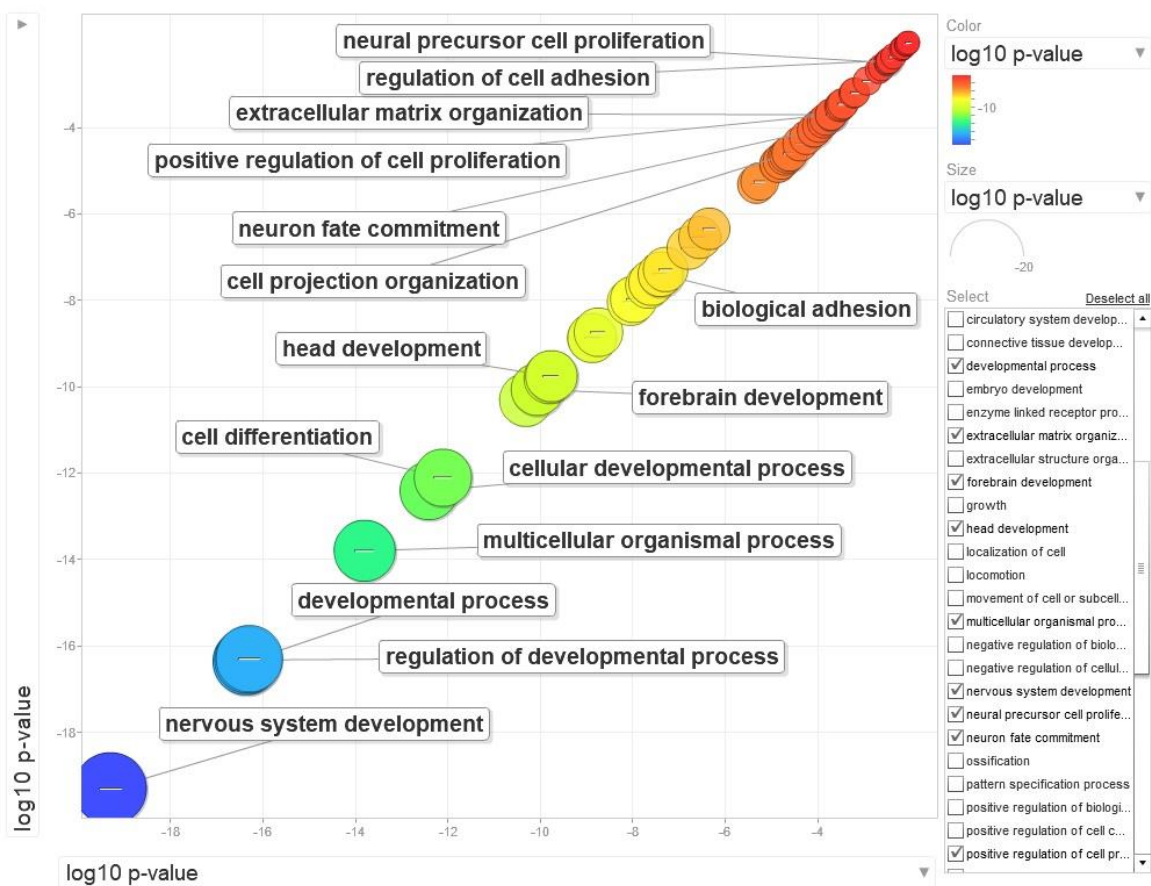


Fig. 42 REVIGO analysis showed changes in proliferation, adhesion and development. Gene IDs of DEG were subjected to GOrilla and further visualized with Princeton REVIGO. The graph shows log₁₀ p values of GO terms derived from GOrilla from low p values in blue to high p values in red.

3.25 IPA revealed DEG between L1KO and wildtype organoids are associated with axonal guidance, WNT signaling and hESC pluripotency

Another common pathway analysis was performed with the commercially available IPA software (Ingenuity Pathway Analysis, Qiagen). In contrast to previously conducted pathways analyses IPA software is able to assess gene expressions using a build-in scientific literature-based database (ingenuity.com). Only RNA-seq data from organoids were suitable for analysis with IPA, in contrast to RNA-seq data of adult L1KO mice. Gene IDs and expression values with a difference of mean group values higher than 3 and a fold change higher than 1.5 were subjected to IPA. IPA analysis revealed that the analyzed DEG matched with several processes (Fig. 43). The most relevant ones for this work were axonal guidance signaling, PCP pathway, WNT/ β -Catenin-signaling and hESC pluripotency.

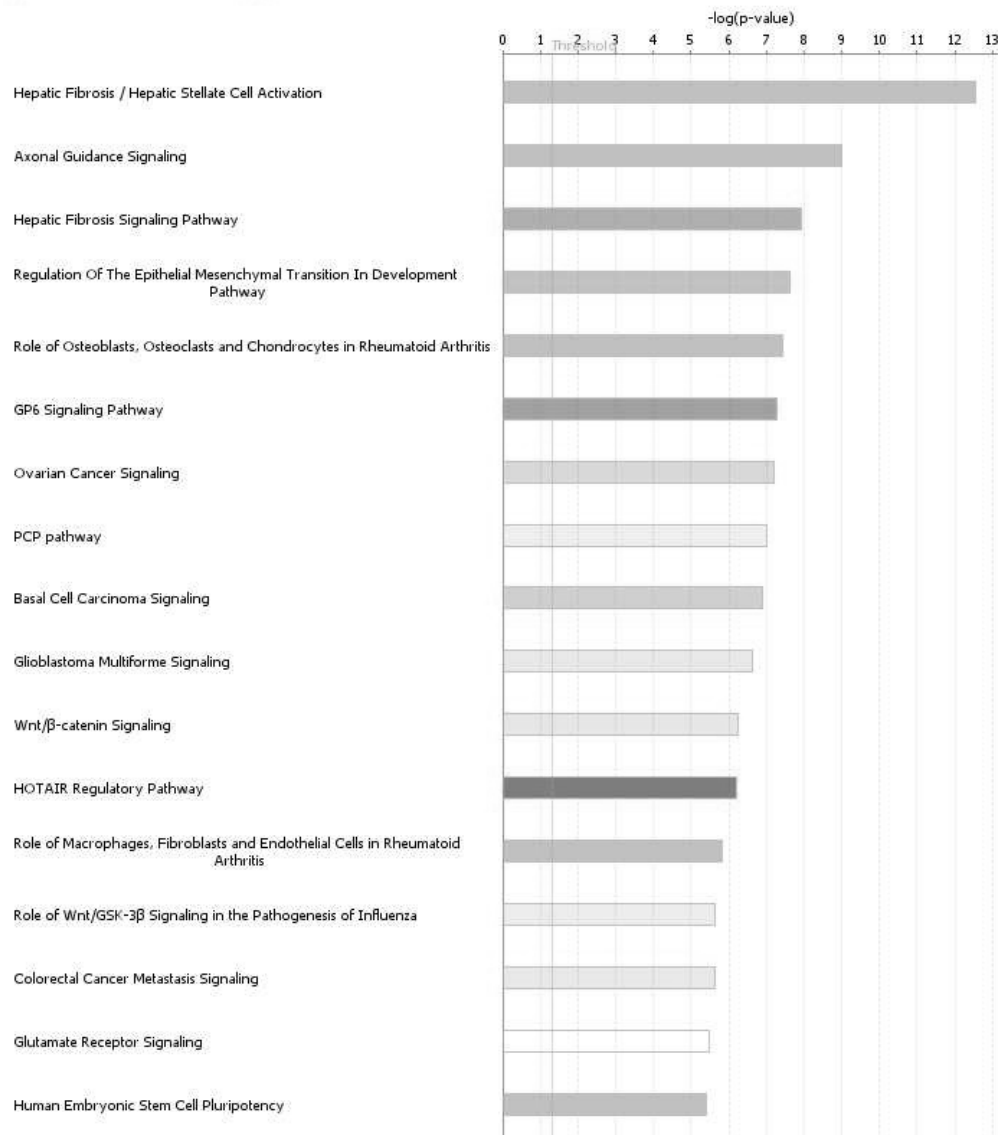


Fig. 43 Axonal guidance, WNT signaling and hESC pluripotency changed in L1KO organoids. The graph shows the result of Qiagens Ingenuity Pathway Analysis of RNA sequencing data as an addition to other pathway analyses which did not include expression values. Rankings of affected pathways are shown by negative log(p values).

3.26 Increased WNT signaling in L1KO organoids

Since IPA as well as GO analysis revealed altered WNT signaling in L1KO organoids, selected genes involved in WNT signaling were combined into a hierarchical cluster-heatmap using Morpheus [132]. This heatmap transferred expression values into a color scale that shows whether the value is above (red) or below (blue) the mean expression value of each gene. In our case, it indicates the comparative gene expression of 16 WNT genes between L1KO and control organoids (Fig. 44). Among these 16 selected genes 13 reached statistical significance (*WNT3* $p=0.00029$, *LEF1* $p=0.0003$, *LRP6* $p=0.002$, *HAND2* $p=0.0027$, *CTNNB1* $p=0.0038$, *CACNA1G* $p=0.001$, *HOXA11* $p=0.016$, *GSK2B* $p=0.034$, *POSTN* $p=0.035$, *ASCL1* $p=0.037$, *DLX2* $p=0.0016$, *NKX2-2* $p=0.0047$, *CDH3* $p=0.0027$, *DVL1* $p=0.0008$), while one gene shows altered regulation by tendency (*WNT3A* $p=0.089$). Within 16 analyzed gene expressions, 12 mean gene expression values were higher and 4 were lower in L1KO organoids than in control organoids.

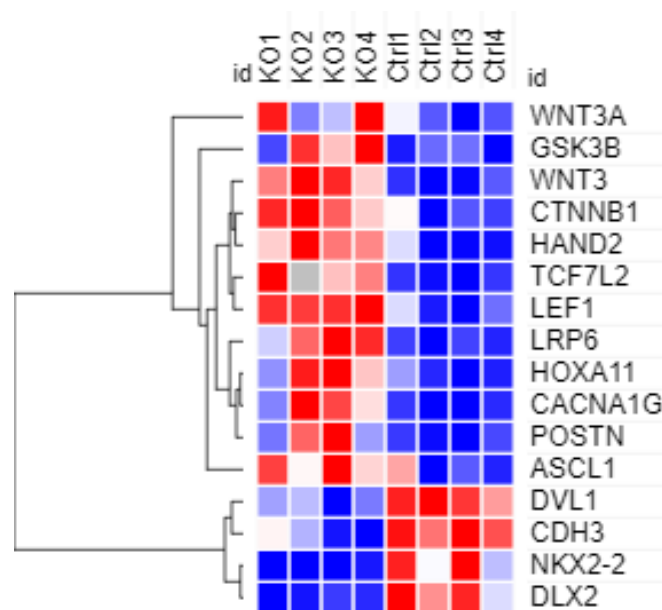


Fig. 44 Increased expression of WNT related genes in L1KO organoids. Hierarchical cluster-heatmap of gene expression values derived from 16 genes related to WNT signaling generated with Morpheus. Colorization: red = higher expression value than the mean gene expression value, blue = lower expression value than the mean gene expression value of the data set.

3.27 Similarities between L1KO adult mouse brains and L1KO cerebral organoids

As a final evaluation of RNA-seq data of L1KO brain tissue and human cerebral organoids all DEG ($p < 0.05$) were integrated into a Venn diagram [133] with the aim to find the number of identical DEG in both models. Mouse gene IDs had to be properly converted first with the online tool DAVID (david.ncifcrf.gov) to be able to compare mouse and human genes because of the different nomenclature. 3367 DEG were integrated from RNA-seq data of L1KO adult mice as well as 6769 DEG from organoid RNA-seq data (Fig. 45). 1084 DEG were found to be identical in both models which is 32.2 % of all integrated L1KO mouse genes and 16.01 % of all DEG in human cerebral organoids.

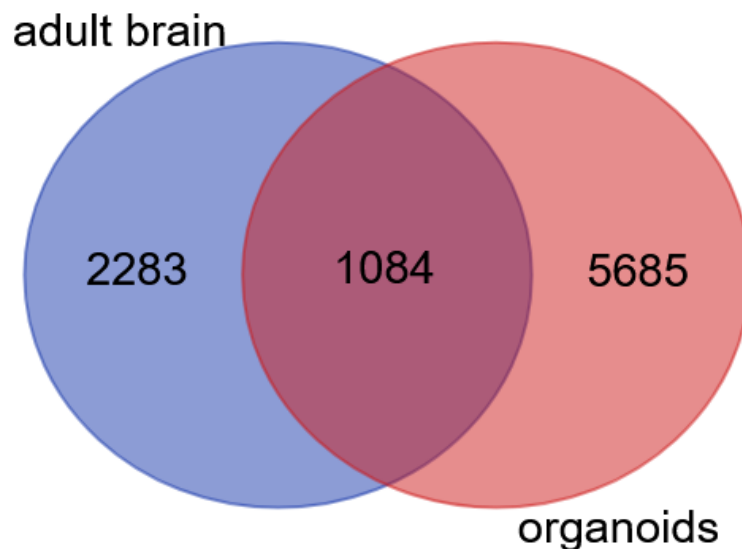


Fig. 45 High number of identically expressed genes in L1KO mice and L1KO organoids. 3367 differentially expressed genes of adult L1KO mice and 6769 genes of organoids were integrated in a Venn diagram, revealing 1084 identically expressed genes in both models.

3.28 L1OE diminishes induction of WNT signaling by LiCl

The RNA-seq data analyses indicated increased WNT signaling in L1KO organoids. To directly confirm or reject this hypothesis, a β -Catenin nuclear translocation assay was performed using easy transfectable HEK cells. For this reason, we addressed this issue by overexpression of L1CAM (L1OE) in HEK cells. L1OE should lower the nuclear translocation of β -Catenin-GFP in case our hypothesis is true.

In order to test whether L1OE has an effect on canonical WNT signaling HEK cells were transfected with either ER-RFP and β -Catenin-GFP (control) or L1CAM and β -Catenin expressing plasmids. 24 h after transfection the cultures were treated with 25 mM lithiumchloride (LiCl) for another 24 h to induce WNT signaling [134,135]. Afterwards, the cells were collected and a subcellular fractionation protocol was performed to separate nuclear from cytoplasmic proteins. If WNT proteins or agonists are present to activate the signaling pathway the β -Catenin/Gsk3b complex is terminated and β -Catenin translocates to the nucleus, where it acts as a transcription factor (Fig. 48). LiCl can activate WNT signaling by preventing the formation of the β -Catenin/Gsk3b complex. The extent of β -Catenin translocation was then analyzed via western blot. The fluorescence image of HEK cells transfected with β -Catenin shows the effect of the 24 h treatment with 25 mM LiCl (Fig. 46). LiCl increases the intensity of β -Catenin-GFP in the nucleus as seen by the bright green areas inside the HEK cells in the 25 mM LiCl condition.

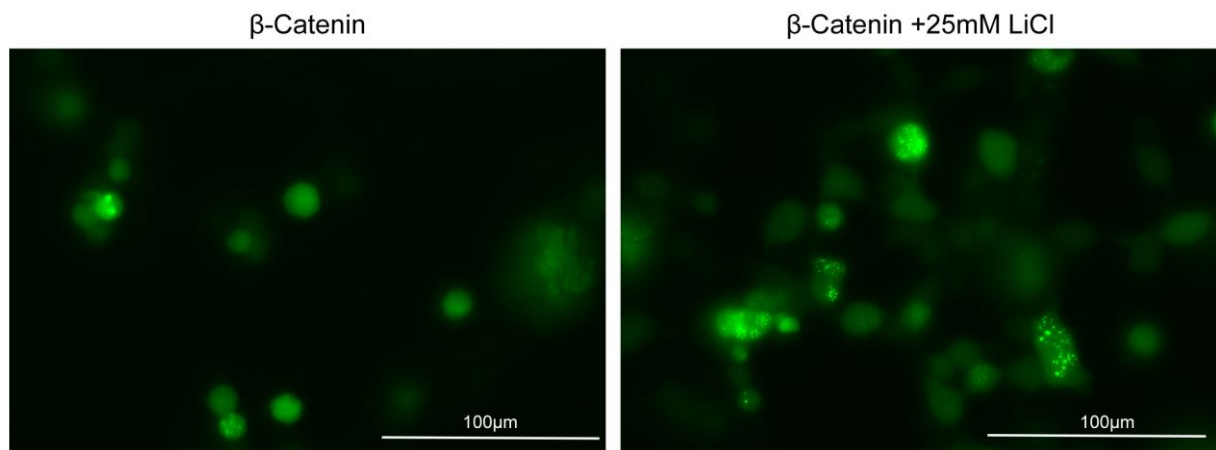


Fig. 46 Effect of 24 h incubation with 25 mM LiCl. The left image shows a HEK cell culture transfected with β -Catenin-GFP. The right image shows a HEK cell culture transfected with β -Catenin-GFP after a 24 h treatment with 25 mM LiCl. Images were taken using a fluorescence microscope. Scale=100 μ m.

Western blot analysis revealed the different signals of β -Catenin-GFP, L1CAM, GAPDH and H3 histone in the cytoplasmic and nucleic fraction of \pm L1OE and \pm 25 mM LiCl conditions (Fig. 47A). The β -Catenin-GFP signal was normalized to the nuclear housekeeping protein H3 histone while GAPDH was detected as a cytoplasmic housekeeping protein to confirm

adequate subcellular fractionation. The normalized values were expressed relative to the values from corresponding controls (RFP + β -Catenin-GFP -LiCl).

Western blot analysis resulted in significant 4.8-fold increase of nuclear β -Catenin-GFP signal after 24 h treatment with LiCl (Fig. 47B). There was no significant change of β -Catenin-GFP signal between L1OE cultures and the controls after LiCl treatment ($p=0.1625$). Here, the increase of β -Catenin-GFP signal after LiCl treatment was only 4.1-fold.

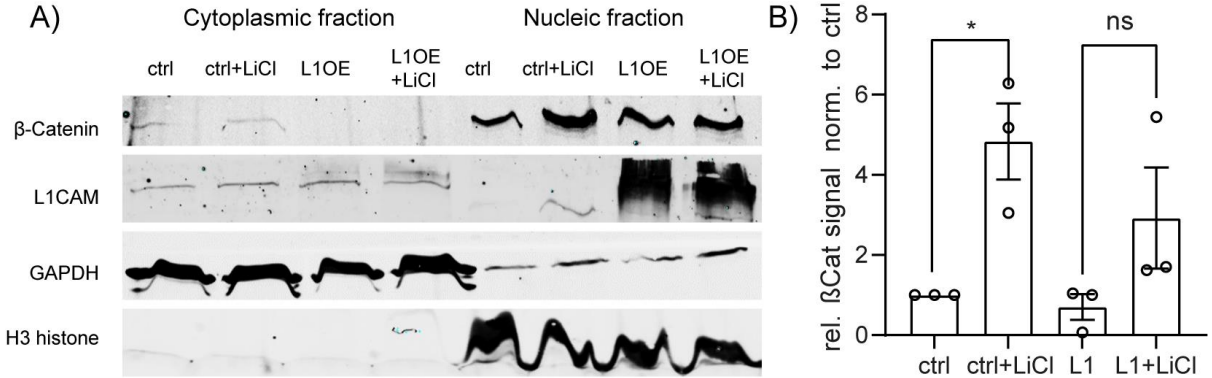


Fig. 47 L1OE diminishes induction of WNT signaling by LiCl. (A) Western Blot analysis of β -Catenin-assay to analyze nuclear translocation of β -Catenin in canonical WNT signaling. HEK cells were transfected with \pm L1CAM and treated with \pm 25 mM LiCl for 24 h. HEK cells were then subjected to SCF and analyzed by western blot. H3 histone signals were used for normalization of nucleic β -Catenin signals. GAPDH was used as a positive control for SCF. (B) The Graph shows individual signals of β -Catenin that were normalized to H3 and to the control condition of each trial (n=3). Values are displayed as mean \pm SEM. *P* values were calculated by t test (* $p<0.05$).

4. Discussion

This work comprised the histopathological and behavioral characterization of two L1 syndrome mouse models, a previously generated L1CAM-deficient mouse termed L1KO [81] and a novel mouse mutant carrying a human pathological missense mutation termed L1D201N [36]. Subsequently, L1KO mutant mice were studied in more detail along with the establishment of a human *in vitro* model of L1 syndrome using human cerebral organoids. RNA-seq analyses suggested a pathogenic role of the WNT signaling pathway, among others, in L1 syndrome which was supported by *in vitro* evidence suggesting that L1 inhibits canonical WNT signaling via β -Catenin.

There is no cure for L1 syndrome and treatments are restricted to symptomatic relief like a ventriculo-peritoneal shunt for patients with hydrocephalus or a splint for patients with adducted thumbs. Therefore, further investigations are required to enable novel therapeutic approaches. Since the pathological onset of L1 syndrome is during embryogenesis therapeutic genetic interventions would need to be performed at early embryonic stages. Our initial plan in this work was to establish an *in utero* therapy by intrathecal administration of viral vectors carrying wildtype L1CAM to compensate malfunction of mutant L1CAM. Unfortunately, due to breeding issues of our L1 mutant mice and the pandemic which did not allow practical courses to learn the technique for *in utero* intrathecal administrations we could not accomplish this idea. This is still a good concept and should be approached in future experiments.

In the present thesis, the mouse lines L1D201N and L1KO (with this genetic background) were investigated for the first time. Also, to the best of our knowledge L1KO human cerebral organoids have not been generated yet and we do not know about any investigations concerning L1CAM-related WNT signaling in neural tissue. The collected findings provide novel insights into the pathological phenotype of L1CAM mutant mice as well as transcriptional changes in human cerebral organoids caused by L1CAM deficiency. Our results revealed altered WNT signaling due to L1CAM deficiency which was further assessed and confirmed *in vitro*.

4.1 L1CAM mutant males show features of human L1 syndrome

The essential role of L1CAM in neural development has been described extensively in several publications that showed its involvement in proliferation, migration and differentiation of neurons as well as its importance in axon growth, arborization and pathfinding [41,136]. For these reasons, mutations in the *L1CAM* gene or changes of L1CAM expression levels can cause a variety of pathologies including cancer and L1 syndrome [137].

In the beginning of this work 8-9 week-old L1D201N and L1KO mice were investigated that are thought to resemble phenotypic features of the L1 syndrome of human patients. The L1D201N mouse line is a novel mouse model for L1 syndrome and was therefore not characterized before. Parts of the present thesis contributed to the first published description of this novel mouse model [36]. Indeed, the L1KO line was already partially analyzed by the laboratory that originally generated this mouse line [65,81] but our L1KO mice were backcrossed to a different genetic background which can also have an effect on the pathological outcome (past: C57BL/6J, today: 129SvJ). Also, investigations by Bartsch *et al.* were restricted to neuroanatomical analysis and did not include motor function or behavioral tests [81]. For these reasons L1D201N as well as L1KO mice were characterized from scratch.

Since L1D201N and L1KO mice are used as a murine model of L1 syndrome both lines were tested for known features seen in the human L1 syndrome namely motor and behavioral dysfunctions, ventriculomegaly and dysgenesis of the corpus callosum [36].

Increased locomotor activity was observed in L1D201N male and female mice whereas L1KO males showed a tendency towards increased locomotion. There was no difference between female L1KO mutants and controls concerning locomotor activity. Early investigations of another L1KO mutant mouse line already stated that their mutant mice displayed increased exploratory behavior which may explain increased locomotor activity in our mice [82]. Increased locomotor activity is also a behavioral feature in a mouse model of hyperactivity [135,138]. It was also shown that spastic paraplegia which is one feature of the human L1 syndrome can be connected to hyperactivity disorder which potentially elucidates why L1 mutant mice walked a greater distance [139]. In addition, dysmyelination is expected to occur in our L1 syndrome mice since reduced myelination is known to cause a volumetric reduction of the corpus callosum [140]. In that respect, investigations of acallosal mice also revealed increased locomotor activity [141,142]. Moreover, altered myelination in general was also suggested to contribute to a lifelong persistence of ADHD [143]. There were no genotype-dependent abnormalities in RR and Rearing counts in both mouse lines besides a decreased rearing activity in L1KO males which did not reach statistical significance. Taken together, literature indicates a link between myelination and hyperactivity and supports our finding of hyperactivity in L1 mutant mice.

In addition to a hyperactivity-like phenotype, L1D201N and L1KO mutant males displayed neurological deficits as evaluated with a scoring system adapted from previous publications to assess neurological outcome after brain injury [80,144,145]. Here, the mice collected most deficit score points in the walking beam test where they had to walk over 3 wooden sticks of decreasing width and therefore increasing difficulty.

We observed neurological deficits in L1D201N and L1KO mutant males revealed by evaluation of the NDS while female mice did not show significant motor dysfunctions. The neurological deficits observed in L1D201N and L1KO mutant males provide evidence for a proper modeling of the human L1 syndrome since human patients also show motor deficits. Earlier investigations of another L1KO mouse line already showed guidance errors of axons in the corticospinal tract which provides a potential cause for motor dysfunctions in our mice [64]. Looking at the individual values among the different tests e.g. NDS and locomotor activity of L1KO mutant males it can be seen that the level of severities strikingly differ from mouse to mouse. This is similar to the human syndrome where severities can also range from mild to severe, even in patients carrying the same L1CAM mutation [5,86]. Heatmaps of OFT data indicated altered walking paths of L1D201N and L1KO mutant male mice compared to wildtype controls. The increased residence in the middle of the cage seen in hemizygous males indicates decreased anxiety behavior. Native mice prefer to stay close to corners of a cage because it is seen as safer than the open area in the middle [146]. Published data already stated that L1^{DCX} knockout mice displayed decreased anxiety-related behavior [52]. Although representative mice were chosen for the heatmaps (regarding mean locomotor activity) the low number of included mice here only allowed preliminary conclusions. The fact that the L1CAM mutant males showed a more severe phenotype than females is consistent with the X-linked etiology of the L1 syndrome [5,147], although some publications also stated a pathological phenotype in heterozygous female L1 mutant mice [148,149]. However, although the pathologies we found in hemizygous males were relatively mild they were indispensable for further investigations. In case the mutant male mice would not have shown any pathological abnormalities, further animal assessments would not have been performed. The X-linked susceptibility of males is a reasonable explanation for the lowered yield of hemizygous males in the litters. Most likely, the pups with the predispositions for a severe pathological phenotype like an increased NDS and enlarged ventricles die before we determined the genotypes of 3-4 weeks-old mice. This again, would explain the relatively mild NDS observed in motor function tests of L1D201N/L1KO mutant males. However, our behavioral tests revealed neurological deficits and signs of hyperactivity in L1D201N and L1KO male mice indicating that these models enable more detailed behavioral analyses and pathomechanisms related to L1 syndrome in the future. Taken together, L1D201N mice showed a more severe phenotype than L1KOs as indicated by the high mortality of hemizygous males and a higher NDS. This observation can probably be attributed to the genetic background differences between the mouse lines. L1KO mice were generated on a 129SvJ background whereas L1D201N mice were backcrossed on a C57Bl/6 background. The C57Bl/6 background is known to be more vulnerable to pathologies and is said to cause more severe phenotypes than the 129SvJ background [81,150]. Another

suggestion is that a knockout is more likely to provoke compensatory mechanisms than a mutated protein which is normally presented on the cell surface [36].

Histological investigation of Nissl stained cryosections and assessment of ventricle sizes revealed enlarged ventricles in L1D201N mutant males but not in L1KO mutant males. On the one hand, ventriculomegaly in L1D201N males was somehow expected because the same mutation can also be found in human L1 syndrome patients where the emergence of hydrocephalus is common. On the other hand, normal ventricle sizes in adult L1KO males were surprising since previous assessments of these mice showed hydrocephalic brains [81]. Nevertheless, the absence of enlarged ventricles in our adult L1KO mutant males and the difference to first investigations of this line can be accredited to the deviating genetic background of both L1KO lines. Further, LFB stainings of cryosections allowed the analysis of the corpus callosum by staining the myelin sheath formed by oligodendrocytes. LFB analysis showed that L1D201N and L1KO mutant males exhibited a thinning of the medial and lateral corpus callosum. The essential role of L1CAM in axon myelination, growth and guidance was extensively described in multiple publications [100,136,151,152]. These functions of L1CAM provide explanations for the altered corpus callosum when L1CAM is not expressed correctly or not expressed at all. Further, reduced myelination was shown in primary cultures of L1D201N mice by Schachner *et al.* who also performed experiments with the L1D201N mutation [36]. Moreover, previous publications already confirmed a reduced callosal volume due to reduced axon myelination in L1CAM-deficient mice and rats which support our findings [63,153]. Since agenesis or dysgenesis of the corpus callosum is one characteristic feature of L1 syndrome in humans this indicates once more that these two mouse lines can be valid models for L1 syndrome. The neuroanatomical features revealed by histological assessments may not be the only initiators of the motor and behavioral dysfunctions displayed by NDS and OFT but they most likely play a major role.

4.2 Elevated WNT signaling in L1KO mutant males

For the purpose of getting deeper insights in mechanisms underlying pathological features of the murine L1 syndrome RNA samples of L1KO brain tissue were subjected to RNA-seq. Gene IDs of DEG were integrated in the online tool Panther for GO analysis. Panther analysis gave information about the mechanisms and pathways the integrated gene IDs are possibly involved in (without evaluation of expression values). In L1KO mutant males the most prominent altered GO term in biological process was “cellular process” with “cellular metabolic process” being the top-regulated biological process. This involves gene transcription which is consistent with findings that the cytoplasmic portion of L1CAM modulates transcription [154]. For example, L1CAM can activate NFκB signaling by binding to integrins and nuclear translocation of the intracellular L1CAM domain which can increase

the motility and invasiveness of cells [155,156]. Panther's molecular function analysis showed that the DEG were mostly involved in "binding" with "protein binding" being the most prominent molecular function here. One main function of L1CAM is to generate transmembrane signalings and regulate cell adhesion processes where homo- and heterophilic bindings of L1CAM are essential [44,47,155]. The results of Panther's biological processes and molecular function did not provide strikingly new information about L1CAM but they indicate that our method of analysis is suitable. Moreover, Panther's pathway analysis revealed that the most relevant regulated pathways in L1KO mice were "Gonadotropine releasing hormone (GnRH) signaling", "inflammation mediation", "integrin signaling" and "WNT signaling". GnRH signaling is regulated by GnRH producing neurons in the pituitary gland which release the fertility controlling protein GnRH. GnRH signaling includes MAP3K [157] which was the most prominent protein in this GO term and the positive effect of L1CAM on MAP3K expression was already shown [158]. GnRH pathway also involves Sema3a [159]. Sema3a expression is known to be reduced in L1CAM deficient mice leading to axonal guidance errors [160]. The next altered pathway revealed by Panther analysis was "Inflammation mediation by chemokine/cytokine signaling" with Myosins being the top term. Publications already stated several times that Myosins are involved in retrograde actin flow which is essential in axon guidance in growth cones and their motility similar to L1CAM [130,161,162]. This indicates a mutual pathway or interaction of Myosins and L1CAM which was also suggested by Abe *et al.* [130]. The third regulated pathway here was "Integrin signaling" with Collagens being one of the top involved proteins here. Several publications stated that L1CAM interacts with integrins to induce nuclear signaling. For example, the soluble ectodomain of L1CAM as well as the membrane-bound ectodomain can bind to integrins via its RGD-motif in the sixth Ig-domain and induce the NF κ B pathway [49,156,163]. The last Panther pathway which became important for this work was "WNT signaling". Cadherins are the most prominent term here and are known to be related to L1CAM [164]. WNT signaling is essential for the regulation of proliferation and differentiation and therefore also involved in carcinogenesis and tumor progression [165] similar to L1CAM [41]. Further, the *L1cam* gene is known to be a downstream target of β -Catenin-dependent WNT signaling [137]. Nuclear translocation of β -Catenin is a key feature of activated canonical WNT signaling and was shown to elevate *L1cam* expression [166,167]. The reverse approach, i.e. the investigation of WNT signaling levels in combination with altered L1CAM expression has not yet been investigated to our best knowledge. Therefore, we further examined the effect of L1CAM deficiency on WNT signaling in the part human cerebral organoids and in the β -Catenin nuclear translocation assay.

Although we did not observe enlarged ventricles in L1KO mutant males it is not precluded that pro-hydrocephalic processes don't take place. For this reason, RNA-seq gene

expression values of TJPs and related genes were investigated. *Cldn5*, *Tjp1* and *Lamb1* were found to be differentially expressed in L1KO mutant males. *Cldn5* mRNA levels were lowered in L1KO mutant males while *Tjp1* and *Lamb1* mRNA expression levels were elevated compared to their wildtype controls. To the best of our knowledge, these three genes have not yet been analyzed in any experiments directly related to L1CAM deficiency which is why explanations are suggestive. Altered gene expression of those genes are able to cause dysregulations in endo- and epithelial integrity and therefore also for the blood-brain-barrier and blood-CSF-barrier [97,168,169]. Although a hydrocephalus could not be detected in L1KO mutant males these altered expression levels indicate a dysregulation in blood-brain-barrier and blood-CSF-barrier. Up to now, there is no evidence yet that L1CAM and CLAUDIN-5 as well as *Tjp1*/ZO-1 share any direct pathways or immediate interactions. Little is also known about the relationship between L1CAM and Laminin which is why only suggestions can be made here. Anyhow, L1CAM is known to be related to Laminin (string-db.org) and is also known to get in complex with (reactome.org). Further, L1CAM was already proven to be essential for the binding of dissociated colorectal cancer cells to laminin [170] showing again that L1CAM is interacting with Laminin somehow. In general, TJPs are involved in the proper regulation of cell polarity which therefore might be altered in L1KO mutants. It has already been shown that a disrupted polarity of ependymal cilia can result in hydrocephalus [171]. Further, several markers involved in neural development were shown to be differentially expressed in RNA-seq data: *Sox2*, *Olig1*, *Olig2* and *Nkx6.2* by tendency. SOX2 is a transcription factor in neural progenitors and is indispensable for neurogenesis [172] and neural stem cell maintenance [173]. L1CAM is also known to promote proliferation and preventing premature differentiation [174] indicating a potential relationship between *Sox2* and *L1cam*. The finding of decreased *Sox2* expression was already shown in a previous publication where *L1cam* was knocked out in neural progenitor cells resulting in a decreased number of SOX2⁺ cells in the hippocampus [52]. The protein encoded by *Nkx6.2* is a transcription factor known to be involved in oligodendrogenesis [175]. Similar to human pathological mutations in *L1CAM*, mutations in *Nkx6.2* are involved in spastic ataxia and hypomyelination [175]. Early publications already stated that *Nkx6.2* is expressed in postmitotic differentiated oligodendrocytes [176]. This, the fact that L1CAM deficiency causes premature differentiation of progenitors and the slightly higher *Nkx6.2* expression found in L1KO mutant males indicate a trend towards premature oligodendrocytic differentiation happening in L1KO mutant males [52]. More recent work demonstrated that *Nkx6.2* is specifically expressed in mature APC⁺ oligodendrocytes which indicates a trend towards an increased number of these oligodendrocytes in L1KO mutant males. *Olig1* promotes the formation and maturation of oligodendrocytes predominantly in the brain (string-db) while *Olig2* is essential for the specification of oligodendrocytes and motor neurons mostly in the

spinal cord. They both interact in order to form the pMN domain of the neural tube (string-db). Previous data indicated that a reciprocal regulation of *Olig1* and *2* can occur due to a compensatory effect because *Olig1* is able to compensate a loss of *Olig2* via upregulation of its expression [177]. These findings indicate that L1KO mutant males may exhibit increased oligodendrocyte lineage specification [178] and premature differentiation of oligodendrocyte precursor cells [179].

4.3 Embryonic L1KO mice show L1CAM related pathologies

After completing the investigations of adult mice, we focussed on E16 L1KO embryonic mice. An analysis of L1 syndrome mouse embryos should be helpful since the pathological onset takes place at an early developmental stage [101,102]. Also, we had breeding issues with adult mice because the yield of hemizygous males was very low probably owed to hypermortality of said mice. In contrast to adult L1KO mutant males, the ratio of E16 L1KO mice was within the expected range which suggests that in this L1 syndrome model the mortality manifests between the late embryonic phase (E17-E21) and P21 the time-point of genotyping. In initial investigations of L1KO male embryos cryosections were subjected to histological analysis. Ventriculometry of Nissl stained cryosections revealed enlarged ventricles in L1KO E16 mutant males in contrast to adult L1KO mice. A possible explanation for the presence of hydrocephalus in L1KO embryos and absence in the adults is the composition of both brains. In mouse embryos, ventricles make up a larger proportion of the whole brain compared to the different ratio in adult mice [180]. The percentually increased size of ventricles in E16 L1KO male mutants may therefore vanish during embryo- and corticogenesis as the brain grows in size.

Immunohistochemical labelings for L1CAM demonstrated both the absence of L1CAM expression in L1KO hemizygous males as well as the distribution of L1CAM expression throughout the wildtype embryonic cortex. There was a high expression of L1CAM in the IZ, less expression in the CoP and almost no expression of L1CAM in the VZ/SVZ. These results are in agreement and extend earlier work showing the distribution of L1CAM expression in E14.5 mice [181].

It has already been shown that corticogenesis is affected in a L1 syndrome mouse model. Cortices of L1CAM-deficient male mice displayed altered migration of upper and deep layer neurons and malformed dendrites of pyramidal neurons. In severe cases of L1 syndrome, patients can display a thinned cerebral cortex due to enlarged ventricles that displace the neural tissue [182,183]. Itoh *et al.* demonstrated the importance of L1CAM for corticogenesis using a RNA silencing mediated knockdown of *L1cam* in E13.5 mice resulting in deficits of *Satb2*⁺, *Ctip2*⁺ and *Tbr1*⁺ neurons to correctly migrate to their destiny in the cortex [87]. Therefore, several cortical layers were investigated by IHC. α SOX2-labeling of L1KO cryosections showed a thinned dorsal VZ in L1KO mutant male mice compared to controls although there was no L1CAM expression in this cortical layer. However, this correlation of SOX2 and L1CAM expression was already shown in previous publications [184]. SOX2 is a marker for neural progenitors, proliferation, neural stem cell maintenance and also a marker for the cortical VZ [172,173]. Itoh *et al.* provided the initial idea to investigate the cortical layers including the VZ. The dorsal VZ is known to generate several classes of projection neurons at the age of E10.5 [14]. It is the L5 cortical projections neurons that form the

corticospinal tract which was already shown to be smaller in L1KO mutant mice [185]. Since the cells in the VZ are neural progenitors, the lack of L1CAM function in the regulation of proliferation and maturation may provide an explanation for the thinned SOX2 layer [174]. Therefore, the thinning of the VZ might be caused by alterations in the differentiation of SOX2⁺ neural progenitors. Comparing the ratios of neural progenitors, immature and mature neurons between L1KO males and wildtype littermates in more detail would be required to test this hypothesis. Altogether, this data indicates that a possible origin for malformations seen in the corticospinal tract in L1KO mutants might be an affected dorsal VZ.

In another set of IHC experiments the expression of KI67 and Claudin-5 was examined in the CP of E16 L1KO cryosections. The rationale of this experiment was to better understand relationships between TJPs, CP and hydrocephalus. For example, one type of murine hydrocephalus is known to be caused by altered levels of a tight junction associated protein that affects the CP integrity [62,186]. α KI67 labeling of proliferating cells exposed decreased proliferation of endothelial cells in the CP of L1KO mutant males compared to wildtype controls. In literature, there is no evidence that could clearly support or reject this finding in relation to the formation of hydrocephalus but increased proliferation of CP epithelium was found in an induced ventriculomegaly model [187] that would indicate an opposite regulation. Nevertheless, this model comprises a different type of hydrocephalus which is induced by intraventricular hemorrhage. Here, we also found a tendency towards a decreased signal of the TJP Claudin-5 in the E16 L1KO mutant CP compared to littermate wildtype controls. A lowered number of TJPs in the BBB destabilizes the BBB integrity and causes hyperpermeability [188] which is one factor that could contribute to the formation of hydrocephalus we detected in E16 L1KO mutant males.

In the next part of investigations in E16 L1KO mice a panel of marker genes was examined by qPCRs. The analysed genes are known to relate to glutamate signaling (*Vglut2*), axonogenesis (*Gap43*), apoptosis (*Trp53*, *Bax*, *Casp3*) and water homeostasis (*Aqp1/4*). *Vglut2* (*Slc17a6*) is encoding for a vesicular glutamatergic transporter located in growth cones and presynaptic terminals [121]. The expression levels of *Vglut2* were slightly increased in E16 L1KO mutant males compared to the controls. This result supports previous findings that glutamate signaling is elevated in patients with hydrocephalus [189]. No regulations were found for the axogenesis marker *Gap43* despite putatively shared roles with L1CAM in axonal guidance and pathfinding [190]. Analyses of pro-apoptotic markers were included here because apoptosis is indicated to be one of the main causes of neuronal injury in experimental hydrocephalus in mice [122,191]. However, expression levels of the main apoptotic gene markers *Trp53*, *Bax* and *Casp3* were unaltered suggesting that apoptosis did not play a major role in murine L1KO hydrocephalus. Further, gene expression levels of aquaporins 1 and 4 were investigated since they are both known to be altered in some types

of hydrocephalus. *Aqp1* was already shown to be downregulated and *Aqp4* upregulated in rats with experimental hydrocephalus [124]. In human non-obstructive hydrocephalus caused by hyperplasia of the CP and CSF overproduction, *Aqp1* expression is also decreased [192]. In our analysis, both aquaporins were not differentially expressed suggesting a different origin of the hydrocephalus we detected in E16 L1KO mutant males. RNA samples of L1KO E16 mice were subjected to RNA-seq analysis, too. However, the data was not included in the work because it was unsuitable for analysis due to a very low number of DEG. A reason for the low number of differentially expressed genes could be that the RNA used for RNA-seq was extracted not only from brain tissue but also included tissue like bone since the whole head was cryosectioned.

4.4 L1KO organoids share similar dysregulations as L1KO mice

In this part, human cerebral organoids were generated from L1CAM-deficient human embryonic stem cells (L1KO hESCs). The intention of this experiment was to establish an *in vitro* model for L1 syndrome since we were not able to get hands on samples of human L1 syndrome patients. Also, in regard to the 3R principle of scientific experiments we wanted to establish an *in vitro* model as an alternative for animal experiments in L1 syndrome research. Analysis of RNA levels of multiple neuronal markers by qPCR displayed lowered *PAX6* and increased *VGLUT2* levels in L1KO organoids compared to control organoids. *PAX6* is a transcription factor expressed by progenitor cells of the ventricular zone and a lowered *PAX6* expression indicates a lower number of specific progenitor cells. Similar to the thinned SOX2 layer in the L1KO adult mouse cortex this result may be explained by premature differentiation of progenitors due to the absence of *L1CAM* [174]. The finding of elevated *VGLUT2* expression in L1KO organoids is consistent with our results in L1KO E16 mice where a trend towards elevated *Vglut2* was observed in L1KO mutant males compared to controls. Increased expression of *Vglut2* was already shown in the cortex of a rat model for absence epilepsy and is also known to cause excitotoxic neurodegeneration in *Drosophila*. This indicates that excitotoxic events in L1KO organoids and mice [193,194]. *SOX2*, *GFAP* and *DCX* are expressed by neural progenitors and immature neurons. Since *L1CAM* is involved in regulating neural proliferation and differentiation we expected alterations here similar to the thinned SOX2 layer in adult L1KO mutant males but dysregulated gene expression levels could not be detected. *VGAT* and *GRIN2A* are important for the GABAergic and glutamatergic signaling pathways. *VGAT* is expressed in motoneurons and *GRIN2A* is expressed in excitatory glutamatergic neurons. *L1CAM* was shown to be enriched in corticospinal motoneurons in the developing brain [171] which makes *VGAT* a potentially altered target in L1KO organoids. However, *VGAT* and *GRIN2A* were unchanged in L1KO organoids indicating that *VGAT*- and *GRIN2A*-dependent signaling is not affected by L1CAM-

deficiency in the organoids. *GAP43* RNA levels did not show differences between L1KO organoids and controls although *GAP43* and *L1CAM* are both expressed in growth cones which are knowingly affected in L1 syndrome patients [195]. Taken together, the findings of decreased *PAX6* and increased *VGLUT2* expression in L1KO organoids both suggest that the L1KO organoid model shows similarities to E16 L1KO mice. Both models also displayed altered expression of VZ markers (*PAX6* and *SOX2*) and increased expression of *VGLUT2/Vglut2*.

In the following, RNA samples of human cerebral organoids were subjected to RNA-seq. The retrieved data was then analyzed in a similar manner to L1KO adult mice (Panther GO analysis, GOrilla analysis and illustration of selected genes). Gene IDs of DEG were again subjected to GO analysis using Panther. Panther's biological processes revealed alterations in "cellular process" with "cellular metabolic process" being the top process in this GO term. Technically speaking this result is quite unspecific but it can be supported by literature due to L1CAMs predicted involvement in several metabolic processes revealed by gene network prediction analysis [196]. In our adult L1KO mutant mice, "cellular process" was also the most altered GO term with the top term cellular metabolic process. Panther's molecular function showed that the most altered GO term was binding, with protein binding leading the list behind this GO term. This was also observed in molecular function analysis of adult L1KO mice. Panthers Pathways exposed that the top altered pathway was "WNT signaling" with Cadherin being the most prominent term here. The second pathway altered in L1KO organoids was "GnRH signaling" with MAP3Ks being the top term in this GO term. Both of these results were also observed and discussed in L1KO adult mutant mice. These almost identical GO analysis results of organoids and adult L1KO mice indicate that L1KO organoids show similar altered processes and pathways due to L1CAM-deficiency. Thus, the present thesis provides first evidence for the suitability of hESC-derived brain organoids as a valid alternative for L1 syndrome mice in future research.

Another way of GO analysis was performed with GOrilla [197] and visualized with REVIGO [198]. Here, the GO terms were presented in a log₁₀ graph showing the most strongly altered GO terms of the integrated data. Multiple GO terms in the graph can be associated with known functions of L1CAM such as several types of proliferation, adhesion and developmental processes [52,68] which support the organoid model and our way of analysis. IPA is another and quite common way to analyze RNA-seq data. In this pathway analysis not only Gene IDs but also their expression values were considered. IPA revealed an effect of L1CAM-deficiency on axonal guidance signaling, human embryonic stem cell pluripotency, PCP pathway and WNT/ β -Catenin-signaling. Several publications already proved the indispensability of L1CAM in axonal guidance [20,119,130,199]. Therefore, it is not a novelty but a confirmation of the model validity that axonal guidance was among the most regulated

pathways here. Further, IPA showed that human embryonic stem cell pluripotency is altered in L1KO organoids. Several research groups were able to show that a downregulation of L1CAM decreases self-renewal and proliferation of hESCs, neural stem and neural progenitor cells (NSC/NPC) [52,200]. They also suggest that a knockdown of *L1CAM* triggers spontaneous differentiation of hESCs since its expression is downregulated after differentiation under normal circumstances [52,63,201]. Lastly, IPA showed an effect of *L1CAM* deficiency on PCP and WNT/ β -Catenin signaling pathway which are also known as non-canonical and canonical WNT signaling. For this reason, we selected specific genes that are known to be involved in WNT signaling and merged their expression values to a hierarchical cluster-heatmap. Taken together, 11 differentially expressed genes indicated an upregulation of WNT signaling (*WNT3*, *LEF1*, *LRP6*, *HAND2*, *CTNNB1*, *HOXA11*, *POSTN*, *ASCL1*, *CDH3*, *TCF7L2*, *WNT3A*) while 5 genes indicated reduced WNT signaling in L1KO organoids compared to controls (*CACNA1G*, *GSK3B*, *DLX2*, *NKX2-2*, *DVL1*). We therefore hypothesized that *L1CAM* deficiency in human cerebral organoids results in increased WNT signaling. However, one publication stated that a knockdown of *L1CAM* by siRNA lowered WNT signaling which suggests the opposite effect [202]. Also, overexpression of *L1CAM* was shown to increase the expression of WNT related genes [203]. These deviating results may relate to the fact that they did not investigate neural tissue but tissue from lymph nodes and colon. We also suggest that the finding of elevated WNT signaling in L1KO organoids occurs as a compensatory effect due to a malfunctioning positive feedback loop. The reason for this assumption is that β -Catenin is supposed to increase *L1CAM* expression after nuclear translocation due to L1CAM being a downstream target of β -Catenin [166].

In E16 L1KO males we found decreased RNA and protein levels of *Claudin5*. Also, WNT signaling was seemingly elevated in L1KO organoids compared to controls. We assumed the same trend in adult L1KO mutant males where we also found altered WNT signaling. Previous publications stated an inverse regulation of WNT signaling activation and *Claudin-5* expression [204] which would explain the finding of decreased Claudin-5 levels in the CP of L1KO E16 mutant males and suggest a possible correlation of WNT signaling and BBB integrity. Associations of WNT signaling with neurodevelopmental syndromes were already reported in an *in vitro* model of Miller-Dieker-Syndrome which is a severe type of lissencephaly. Interestingly, they also used cerebral organoids as a model in this study [205]. Moreover, deficits of axons to cross the midline (as in L1KO mutant mice) due to abnormalities in WNT signaling were already shown in the posterior commissure in *Drosophila* [206].

We also analyzed the number of identical DEG in L1KO mice and L1KO organoids. 3367 DEG from L1KO adult mice RNA-seq data as well as 6769 genes of organoid RNA-seq data were integrated to a Venn-diagram. 1084 genes were found to be differentially expressed in

both models. Since no one ever generated L1KO human cerebral organoids to our best knowledge there are no references in literature to evaluate these numbers. 1084 at least seems to be a large proportion of each total number of DEG, pointing out similar effects of L1CAM-deficiency in both models.

4.5 L1-OE alleviates nuclear translocation of β -Catenin-GFP

The WNT signaling pathway is an essential pathway in embryonic development. Up to now, 2 branches of WNT signaling downstream from the frizzled receptor are known: the canonical and the non-canonical pathway (Fig. 48). Abnormal WNT signaling levels are known to be related to multiple types of cancers with colorectal, breast, lung and oral cancer being the most common ones [207].

In the non-activated canonical WNT signaling pathway (Fig. 48A) β -Catenin is bound in a complex with Gsk3b and others which label β -Catenin for degradation. If the WNT signaling pathway is activated (Fig. 48B) by WNT proteins binding to the frizzled receptor the β -Catenin/Gsk3b complex is terminated and β -Catenin accumulates in the cytoplasm which facilitates the translocation to the nucleus. Here, it binds to the transcriptional repressor complex TCF/LEF which causes a conformational change and release of TCF/LEF from the gene and makes the gene accessible to be transcribed [207].

The non-canonical pathway is independent from β -Catenin and TCF/LEF. This branch of WNT signaling includes the PCP/JNK-related pathway and the WNT/Ca²⁺ pathway (Fig. 48C). Activators for the human non-canonical pathway are Wnt5A, Wnt5B, and Wnt11 [207]. In order to induce WNT signaling *in vitro* several methods were already described in literature. Two possibilities are the overexpression of WNT3a or the application of recombinant WNT3a into the cell culture medium. Another possibility is to activate WNT signaling by inhibiting a WNT signaling repressor, e.g. by LiCl. LiCl induces WNT signaling because it prevents the formation of the Gsk3b complex, causes β -Catenin to accumulate in the cytoplasm and therefore promotes the nuclear translocation of β -Catenin. Published data shows that a concentration of 10-25mM is sufficient to evoke an induction without affecting the cell viability significantly [208].

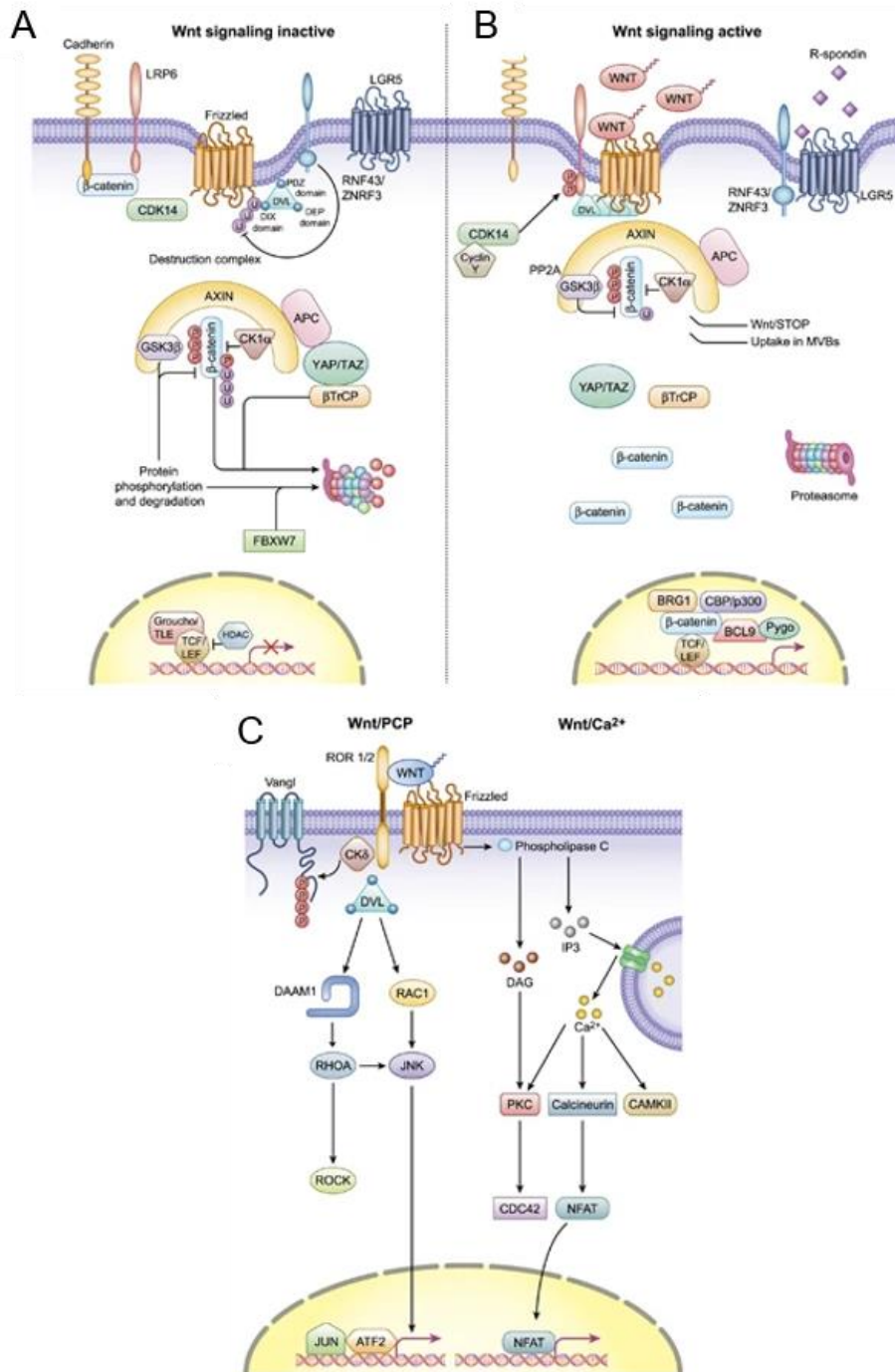


Fig. 48 Canonical and non-canonical WNT signaling. Schematic illustration of (A+B) canonical β -Catenin-dependent WNT signaling pathway including the (A) inactive and (B) active canonical pathway. (C) Schematic illustration of the non-canonical β -Catenin-independent WNT signaling (PCP) pathway [209].

Based on the results in L1KO human cerebral organoids that indicated increased WNT signaling, we attempted to confirm this finding in an independent *in vitro* assay using HEK cells. For this reason, HEK cells were transfected with L1-shRNA plasmid (provided by Dr. Daria Guseva, Institut für Ernährungsmedizin, Universität Hohenheim) which was supposed to be specific for human and for mouse *L1cam*. We proposed that a normal expression of

L1CAM prevents overstimulation of WNT signaling and further that a knockdown of L1CAM increases canonical WNT signaling similar to L1KO organoids. Unfortunately, after multiple tests we realized that the used L1-shRNA was sufficient to reduce mouse but not human L1CAM and was therefore not suitable for HEK cells (data not shown).

In another approach we tested the hypothesis that overexpression of L1CAM inhibits canonical WNT signaling. Therefore, we overexpressed L1CAM and β -Catenin-GFP in HEK cells to analyze L1CAM-related effects on nuclear translocation of β -Catenin after LiCl treatment. The nucleic fraction of β -Catenin was normalized to the nuclear housekeeping protein Histone H3 while GAPDH was used as a positive control for a successful subcellular fractionation since GAPDH is located in the cytoplasm. Looking at the control conditions there was a significant increase of relative nuclear β -Catenin-GFP signal after LiCl treatment which was already described in literature [134,135,210] and the effect we aimed for. A difference in β -Catenin-GFP signals between the conditions “control” and “control+L1CAM without LiCl” could not be observed. A reason for that is probably the already low β -Catenin level in both conditions since we did not add LiCl for induction here. Comparing the “control+LiCl” condition with “L1-OE+LiCl” condition, the significant increase of β -Catenin-signal after LiCl treatment we observed before vanished when L1CAM is overexpressed. This indicates an inhibitory effect of L1CAM on the nuclear translocation of β -Catenin and therefore on canonical WNT signaling.

5. Abstract

This thesis investigated two mouse models of the human L1 syndrome caused by mutations in the L1CAM gene. The mouse lines L1KO, deficient for L1CAM expression, and L1D201N, carrying a loss-of-function missense mutation, showed behavioral and neuropathological abnormalities including motor dysfunctions, hyperactivity, enlarged ventricles and corpus callosum hypoplasia. Both L1KO and L1D201N mice showed poor reproduction due to early hypermortality of hemizygous males resulting in the discontinuation of the more severely affected L1D201N mouse line after initial characterization of behavioral and histological phenotypes. Gene ontology analysis of RNA-seq data from L1KO brain samples suggested altered adhesional processes and axonal guidance pathways in L1KO males. Further, E16 L1KO mutant mice displayed normal reproduction which suggests that mice with severe pathologies probably die between E17 and P21. qPCR analysis of E16 mouse brains indicated increased RNA levels of the vesicular glutamate transporter *Vglut2* in L1KO mutant males which could later be confirmed with significant results in L1KO brain organoids suggesting excitotoxic events in both models. VGLUT2 was analyzed since it is located in axonal growth cones similar to L1CAM. Several analyses indicated a reduced number of neural progenitors caused by L1CAM-deficiency suggested by a thinned dorsal SOX2⁺ ventricular zone in L1KO E16 mutants and lowered RNA levels of *PAX6* in L1KO brain organoids. SOX2 and PAX6 are both essential transcription factors in neural stem cells. We further proposed a direct connection between the altered dorsal ventricular zone and the malformed corticospinal tract described in L1KO mice. In addition, RNA-seq revealed altered WNT signaling in adult male L1KO brains and increased WNT signaling in L1KO brain organoids which is why a β -Catenin nuclear translocation assay was performed to confirm this finding. β -Catenin is an important mediator of the canonical WNT signaling pathway. The assay showed that the LiCl-induced increase of nuclear β -Catenin translocation is diminished after overexpression of L1CAM thereby supporting the hypothesis that L1CAM inhibits WNT signaling. Altogether, both mouse lines can be characterized as valid models for a heterogeneous L1 syndrome since they both show similar pathologies to human patients but animals with severe pathologies probably die between E17 and P21 and withdraw from investigations. Further, investigations of brain organoids implicate that they can be a valid alternative for mouse models since L1KO brain organoids and L1KO mice share similar alterations regarding some neurodevelopmental mechanisms. The presented data provided a clearer understanding of embryonic development and pathomechanisms of L1 syndrome. Especially the novel finding of altered WNT signaling in L1KO mice and organoids suggests a promising new target for future investigations in L1 syndrome research. Also, the inhibiting effect of L1CAM on WNT-signaling should be further assessed in future experiments.

6. Zusammenfassung

Diese Arbeit untersuchte zwei Mausmodelle des menschlichen L1-Syndroms, das durch Mutationen im L1CAM-Gen verursacht wird. Die Mauslinien L1KO, die defizient für L1CAM sind, und L1D201N, die eine *Loss-of-Function-Missense*-Mutation tragen, zeigten Verhaltens- und neuropathologische Anomalien, einschließlich motorischer Dysfunktionen, Hyperaktivität, vergrößerter Ventrikel und Hypoplasie des Corpus Callosum. Sowohl L1KO- als auch L1D201N-Mäuse zeigten aufgrund früher Hypermortalität hemizygoter Männchen eine schlechte Reproduktion, was dazu führte, dass Untersuchungen der stärker betroffenen L1D201N-Mauslinie nach anfänglicher Charakterisierung von Verhaltens- und histologischen Phänotypen eingestellt wurden. Die Gene Ontology Analyse von RNA-seq-Daten aus L1KO-Gehirnproben deutete auf veränderte Adhäsionsprozesse und axonale Signalwege bei L1KO-Männchen hin. Weiterhin zeigten E16 L1KO Mutanten eine normale Reproduktion, was darauf hindeutet, dass Mäuse mit schweren Pathologien wahrscheinlich zwischen E17 und P21 sterben. Die qPCR-Analyse von E16-Mausgehirnen deutete auf erhöhte RNA-Spiegel des vesikulären Glutamattransporters *Vglut2* bei männlichen L1KO-Mutanten hin, was später mit signifikanten Ergebnissen in L1KO-Gehirnorganoiden bestätigt werden konnte. Dies deutete auf exzitotoxische Ereignisse in beiden Modellen hin. Die Expression von VGLUT2 wurde analysiert, da es ähnlich wie L1CAM in axonalen Wachstumskegeln lokalisiert ist. Mehrere Analysen wiesen auf eine reduzierte Anzahl neuraler Vorläuferzellen hin, die durch einen L1CAM-Mangel verursacht wurden. Gründe für diese Annahme sind eine ausgedünnte dorsale SOX2⁺-Ventrikulärzone in L1KO-E16-Mutanten und verringerte RNA-Spiegel von *PAX6* in L1KO-Gehirnorganoiden. SOX2 und PAX6 sind beide essentielle Transkriptionsfaktoren in neuralen Stammzellen. Wir schlugen ferner eine direkte Verbindung zwischen der veränderten dorsalen ventrikulären Zone und dem missgebildeten kortikospinalen Trakt vor, der bei L1KO-Mäusen beobachtet wurde. Darüber hinaus zeigten die RNA-seq Daten veränderte WNT-Signalwege in erwachsenen männlichen L1KO-Gehirnen und aktivierte WNT-Signalwege in L1KO-Gehirnorganoiden, weshalb ein β -Catenin-Kerntranslokationsassay durchgeführt wurde, um diesen Befund zu bestätigen. β -Catenin ist ein wichtiger Mediator des kanonischen WNT-Signalwegs. Der Assay zeigte, dass der LiCl-induzierte Anstieg der nukleären β -Catenin-Translokation nach einer Überexpression von L1CAM verringert wird, wodurch die Hypothese gestützt wird, dass L1CAM die WNT-Signalgebung hemmt. Insgesamt können beide Mauslinien als gültige Modelle für ein heterogenes L1-Syndrom charakterisiert werden, da sie beide ähnliche Pathologien wie menschliche Patienten zeigen, aber Tiere mit schweren Pathologien sterben wahrscheinlich zwischen E17 und P21 und entziehen sich den Untersuchungen. Darüber hinaus implizieren Untersuchungen von Gehirnorganoiden, dass sie eine gültige Alternative für Mausmodelle sein können, da L1KO-Gehirnorganoiden und L1KO-Mäuse ähnliche

Veränderungen in Bezug auf einige neurologische Entwicklungsmechanismen aufweisen. Die präsentierten Daten lieferten ein klareres Verständnis der embryonalen Entwicklung und der Pathomechanismen des L1-Syndroms. Insbesondere die neue Erkenntnis eines veränderten WNT-Signalwegs in L1KO-Mäusen und Organoiden bietet einen vielversprechenden neuen Ansatz für zukünftige Untersuchungen in der L1-Syndrom-Forschung hin. Auch die hemmende Wirkung von L1CAM auf die WNT-Signalgebung sollte in zukünftigen Experimenten weiter untersucht werden.

7. References

1. Arnould-Taylor W, *A Textbook of Anatomy and Physiology*. Journal, 1998,
2. <https://qbi.uq.edu.au/brain/brain-anatomy/corpus-callosum>,
3. Lohia A and McKenzie J, *Neuroanatomy, Pyramidal Tract Lesions*. Journal, 2022,
4. Singh V, *Textbook of Anatomy: Head, Neck and Brain, Vol 3, 3rd Updated Edition, eBook*. Journal, 2020,
5. Stumpel C and Vos YJ, *L1 Syndrome*. Journal, 1993,
6. www.dasgehirn.info,
7. <https://hpo.jax.org/app/browse/term/HP:0011283>,
8. Trepel M, *Neuroanatomie: Struktur und Funktion ; mit 27 Tabellen*. Journal, 2003,
9. Brady S, Siegel GJ, Albers RW and Price DL, *Basic Neurochemistry: Principles of Molecular, Cellular, and Medical Neurobiology*. Journal, 2012,
10. Huttner WB and Kosodo Y, *Symmetric versus asymmetric cell division during neurogenesis in the developing vertebrate central nervous system*. *Curr Opin Cell Biol*, 2005, **17**, p.648-657.
11. Agirman G, Broix L and Nguyen L, *Cerebral cortex development: an outside-in perspective*. *FEBS Lett*, 2017, **591**, p.3978-3992.
12. Niklison-Chirou MV, Agostini M, Amelio I and Melino G, *Regulation of Adult Neurogenesis in Mammalian Brain*. *Int J Mol Sci*, 2020, **21**,
13. Hevner RF, *Intermediate progenitors and Tbr2 in cortical development*. *J Anat*, 2019, **235**, p.616-625.
14. Mukhtar T and Taylor V, *Untangling Cortical Complexity During Development*. *J Exp Neurosci*, 2018, **12**, p.1179069518759332.
15. Saillour Y, Carion N, Quelin C, Leger PL, Boddaert N, Elie C, Toutain A, Mercier S, Barthez MA, Milh M, Joriot S, des Portes V, Philip N, Broglin D, Roubertie A, Pitelet G, Moutard ML, Pinard JM, Cances C, Kaminska A, Chelly J, Beldjord C and Bahi-Buisson N, *LIS1-related isolated lissencephaly: spectrum of mutations and relationships with malformation severity*. *Arch Neurol*, 2009, **66**, p.1007-1015.
16. Lee WS, Baldassari S, Stephenson SEM, Lockhart PJ, Baulac S and Leventer RJ, *Cortical Dysplasia and the mTOR Pathway: How the Study of Human Brain Tissue Has Led to Insights into Epileptogenesis*. *Int J Mol Sci*, 2022, **23**,

17. Damdimopoulou P, Rodin S, Stenfelt S, Antonsson L, Tryggvason K and Hovatta O, *Human embryonic stem cells*. Best Pract Res Clin Obstet Gynaecol, 2016, **31**, p.2-12.
18. Thomson JA, Itskovitz-Eldor J, Shapiro SS, Waknitz MA, Swiergiel JJ, Marshall VS and Jones JM, *Embryonic stem cell lines derived from human blastocysts*. Science, 1998, **282**, p.1145-1147.
19. King NM and Perrin J, *Ethical issues in stem cell research and therapy*. Stem Cell Res Ther, 2014, **5**, p.85.
20. Patzke C, Acuna C, Giam LR, Wernig M and Sudhof TC, *Conditional deletion of L1CAM in human neurons impairs both axonal and dendritic arborization and action potential generation*. J Exp Med, 2016, **213**, p.499-515.
21. Jones I, Novikova LN, Wiberg M, Carlsson L and Novikov LN, *Human Embryonic Stem Cell-derived Neural Crest Cells Promote Sprouting and Motor Recovery Following Spinal Cord Injury in Adult Rats*. Cell Transplant, 2021, **30**, p.963689720988245.
22. <https://hsci.harvard.edu/news/restoring-vision-clinical-trial>,
23. www.mayo.edu/research/clinical-trials,
24. Lancaster MA and Knoblich JA, *Organogenesis in a dish: modeling development and disease using organoid technologies*. Science, 2014, **345**, p.1247125.
25. Watanabe K, Kamiya D, Nishiyama A, Katayama T, Nozaki S, Kawasaki H, Watanabe Y, Mizuseki K and Sasai Y, *Directed differentiation of telencephalic precursors from embryonic stem cells*. Nat Neurosci, 2005, **8**, p.288-296.
26. Lancaster MA, Renner M, Martin CA, Wenzel D, Bicknell LS, Hurles ME, Homfray T, Penninger JM, Jackson AP and Knoblich JA, *Cerebral organoids model human brain development and microcephaly*. Nature, 2013, **501**, p.373-379.
27. Corro C, Novellademunt L and Li VSW, *A brief history of organoids*. Am J Physiol Cell Physiol, 2020, **319**, p.C151-C165.
28. Sutcliffe M and Lancaster MA, *A Simple Method of Generating 3D Brain Organoids Using Standard Laboratory Equipment*. Methods Mol Biol, 2019, **1576**, p.1-12.
29. Kim J, Koo BK and Knoblich JA, *Human organoids: model systems for human biology and medicine*. Nat Rev Mol Cell Biol, 2020, **21**, p.571-584.
30. McCauley HA and Wells JM, *Pluripotent stem cell-derived organoids: using principles of developmental biology to grow human tissues in a dish*. Development, 2017, **144**, p.958-962.
31. <https://www2.mrc-lmb.cam.ac.uk/group-leaders/h-to-m/madeline-lancaster/>,

32. Harjunpaa H, Lloret Asens M, Guenther C and Fagerholm SC, *Cell Adhesion Molecules and Their Roles and Regulation in the Immune and Tumor Microenvironment*. Front Immunol, 2019, **10**, p.1078.
33. Gandawijaya J, Bamford RA, Burbach JPH and Oguro-Ando A, *Cell Adhesion Molecules Involved in Neurodevelopmental Pathways Implicated in 3p-Deletion Syndrome and Autism Spectrum Disorder*. Front Cell Neurosci, 2020, **14**, p.611379.
34. Korotkov A, Luinenburg MJ, Romagnolo A, Zimmer TS, van Scheppingen J, Bongaarts A, Broekaart DWM, Anink JJ, Mijnsbergen C, Jansen FE, van Hecke W, Spliet WG, van Rijen PC, Feucht M, Hainfellner JA, Krsek P, Zamecnik J, Crino PB, Kotulska K, Lagae L, Jansen AC, Kwiatkowski DJ, Jozwiak S, Curatolo P, Muhlebner A, van Vliet EA, Mills JD and Aronica E, *Down-regulation of the brain-specific cell-adhesion molecule contactin-3 in tuberous sclerosis complex during the early postnatal period*. J Neurodev Disord, 2022, **14**, p.8.
35. Kurolap A, Kreuder F, Gonzaga-Jauregui C, Duvdevani MP, Harel T, Tammer L, Xin B, Bakhtiari S, Rice J, van Eyk CL, Gecz J, Mah JK, Atkinson D, Cope H, Sullivan JA, Douek AM, Colquhoun D, Henry J, Wlodkowic D, Parman Y, Candayan A, Kocasoy-Orhan E, Ilivitzki A, Soudry S, Leibur R, Glaser F, Sency V, Undiagnosed Diseases N, Ast G, Shashi V, Fahey MC, Battaloglu E, Jordanova A, Meiner V, Innes AM, Wang H, Elpeleg O, Kruer MC, Kaslin J and Baris Feldman H, *Bi-allelic variants in neuronal cell adhesion molecule cause a neurodevelopmental disorder characterized by developmental delay, hypotonia, neuropathy/spasticity*. Am J Hum Genet, 2022, **109**, p.518-532.
36. Loers G, Appel D, Lutz D, Congiu L, Kleene R, Hermans-Borgmeyer I, Schafer MKE and Schachner M, *Amelioration of the abnormal phenotype of a new L1 syndrome mouse mutation with L1 mimetics*. FASEB J, 2021, **35**, p.e21329.
37. Sun Y, Li Y, Chen M, Luo Y, Qian Y, Yang Y, Lu H, Lou F and Dong M, *A Novel Silent Mutation in the L1CAM Gene Causing Fetal Hydrocephalus Detected by Whole-Exome Sequencing*. Front Genet, 2019, **10**, p.817.
38. Okamoto N, Del Maestro R, Valero R, Monros E, Poo P, Kanemura Y and Yamasaki M, *Hydrocephalus and Hirschsprung's disease with a mutation of L1CAM*. J Hum Genet, 2004, **49**, p.334-337.
39. Supek F, Bosnjak M, Skunca N and Smuc T, *REVIGO summarizes and visualizes long lists of gene ontology terms*. PLoS One, 2011, **6**, p.e21800.

40. Reid RA and Hemperly JJ, *Variants of human L1 cell adhesion molecule arise through alternate splicing of RNA*. J Mol Neurosci, 1992, **3**, p.127-135.
41. Schafer MK and Altevogt P, *L1CAM malfunction in the nervous system and human carcinomas*. Cell Mol Life Sci, 2010, **67**, p.2425-2437.
42. Schafer MK, Schmitz B and Diestel S, *L1CAM ubiquitination facilitates its lysosomal degradation*. FEBS Lett, 2010, **584**, p.4475-4480.
43. Wisco D, Anderson ED, Chang MC, Norden C, Boiko T, Folsch H and Winckler B, *Uncovering multiple axonal targeting pathways in hippocampal neurons*. J Cell Biol, 2003, **162**, p.1317-1328.
44. Haspel J and Grumet M, *The L1CAM extracellular region: a multi-domain protein with modular and cooperative binding modes*. Front Biosci, 2003, **8**, p.s1210-1225.
45. Kim H, Hwang H, Lee H and Hong HJ, *L1 Cell Adhesion Molecule Promotes Migration and Invasion via JNK Activation in Extrahepatic Cholangiocarcinoma Cells with Activating KRAS Mutation*. Mol Cells, 2017, **40**, p.363-370.
46. Accogli A, Goergen S, Izzo G, Mankad K, Kraiden Haratz K, Parazzini C, Fahey M, Menzies L, Baptista J, Carpineta L, Tortora D, Fulcheri E, Gaetano Vellone V, Paladini D, Spaccini L, Toto V, Trayers C, Ben Sira L, Reches A, Malinger G, Salpietro V, De Marco P, Srour M, Zara F, Capra V, Rossi A and Severino M, *L1CAM variants cause two distinct imaging phenotypes on fetal MRI*. Ann Clin Transl Neurol, 2021, **8**, p.2004-2012.
47. Schafer MK, Nam YC, Moumen A, Keglowich L, Bouche E, Kuffner M, Bock HH, Rathjen FG, Raoul C and Frotscher M, *L1 syndrome mutations impair neuronal L1 function at different levels by divergent mechanisms*. Neurobiol Dis, 2010, **40**, p.222-237.
48. Riedle S, Kiefel H, Gast D, Bondong S, Wolterink S, Gutwein P and Altevogt P, *Nuclear translocation and signalling of L1-CAM in human carcinoma cells requires ADAM10 and presenilin/gamma-secretase activity*. Biochem J, 2009, **420**, p.391-402.
49. Gast D, Riedle S, Kiefel H, Muerkoster SS, Schafer H, Schafer MK and Altevogt P, *The RGD integrin binding site in human L1-CAM is important for nuclear signaling*. Exp Cell Res, 2008, **314**, p.2411-2418.
50. Loers G, Kleene R, Girbes Minguez M and Schachner M, *The Cell Adhesion Molecule L1 Interacts with Methyl CpG Binding Protein 2 via Its Intracellular Domain*. Int J Mol Sci, 2022, **23**,
51. Girbes Minguez M, Wolters-Eisfeld G, Lutz D, Buck F, Schachner M and Kleene R, *The cell adhesion molecule L1 interacts with*

- nuclear proteins via its intracellular domain*. FASEB J, 2020, **34**, p.9869-9883.
52. Gronska-Peski M, Schachner M and Hebert JM, *L1cam curbs the differentiation of adult-born hippocampal neurons*. Stem Cell Res, 2020, **48**, p.101999.
 53. Marx M, Diestel S, Bozon M, Keglowich L, Drouot N, Bouche E, Frebourg T, Minz M, Saugier-veber P, Castellani V and Schafer MK, *Pathomechanistic characterization of two exonic L1CAM variants located in trans in an obligate carrier of X-linked hydrocephalus*. Neurogenetics, 2012, **13**, p.49-59.
 54. Christaller WA, Vos Y, Gebre-Medhin S, Hofstra RM and Schafer MK, *L1 syndrome diagnosis complemented with functional analysis of L1CAM variants located to the two N-terminal Ig-like domains*. Clin Genet, 2017, **91**, p.115-120.
 55. Sztrihai L, Frossard P, Hofstra RM, Verlind E and Nork M, *Novel missense mutation in the L1 gene in a child with corpus callosum agenesis, retardation, adducted thumbs, spastic paraparesis, and hydrocephalus*. J Child Neurol, 2000, **15**, p.239-243.
 56. Shaw M, Yap TY, Henden L, Bahlo M, Gardner A, Kalscheuer VM, Haan E, Christie L, Hackett A and Gecz J, *Identical by descent L1CAM mutation in two apparently unrelated families with intellectual disability without L1 syndrome*. Eur J Med Genet, 2015, **58**, p.364-368.
 57. Zhang S, Ye X, Bai G, Fu Y, Mao C, Wu A, Liu X and Yan Z, *Alterations in Cortical Thickness and White Matter Integrity in Mild-to-Moderate Communicating Hydrocephalic School-Aged Children Measured by Whole-Brain Cortical Thickness Mapping and DTI*. Neural Plast, 2017, **2017**, p.5167973.
 58. Eskandari R, Abdullah O, Mason C, Lloyd KE, Oeschle AN and McAllister JP, 2nd, *Differential vulnerability of white matter structures to experimental infantile hydrocephalus detected by diffusion tensor imaging*. Childs Nerv Syst, 2014, **30**, p.1651-1661.
 59. Yang X, Li H, He W, Lv M, Zhang H, Zhou X, Wei H, Xu B, Chen J, Ma H, Xia J and Yang G, *Quantification of changes in white matter tract fibers in idiopathic normal pressure hydrocephalus based on diffusion spectrum imaging*. Eur J Radiol, 2022, **149**, p.110194.
 60. Schrandt-Stumpel C and Fryns JP, *Congenital hydrocephalus: nosology and guidelines for clinical approach and genetic counselling*. Eur J Pediatr, 1998, **157**, p.355-362.
 61. Hirano H, Hirahara K, Asakura T, Shimozuru T, Kadota K, Kasamo S, Shimohonji M, Kimotsuki K and Goto M, *Hydrocephalus due to*

- villous hypertrophy of the choroid plexus in the lateral ventricles. Case report. J Neurosurg, 1994, 80, p.321-323.*
62. Yang J, Simonneau C, Kilker R, Oakley L, Byrne MD, Nichtova Z, Stefanescu I, Pardeep-Kumar F, Tripathi S, Londin E, Saugier-
Veber P, Willard B, Thakur M, Pickup S, Ishikawa H, Schrotten H, Smeyne R and Horowitz A, *Murine MPDZ-linked hydrocephalus is caused by hyperpermeability of the choroid plexus. EMBO Mol Med, 2019, 11,*
 63. Demyanenko GP, Tsai AY and Maness PF, *Abnormalities in neuronal process extension, hippocampal development, and the ventricular system of L1 knockout mice. J Neurosci, 1999, 19, p.4907-4920.*
 64. Cohen NR, Taylor JS, Scott LB, Guillery RW, Soriano P and Furley AJ, *Errors in corticospinal axon guidance in mice lacking the neural cell adhesion molecule L1. Curr Biol, 1998, 8, p.26-33.*
 65. Rolf B, Kutsche M and Bartsch U, *Severe hydrocephalus in L1-deficient mice. Brain Res, 2001, 891, p.247-252.*
 66. Chen L and Zhou S, *"CRASH"ing with the worm: insights into L1CAM functions and mechanisms. Dev Dyn, 2010, 239, p.1490-1501.*
 67. Martin V, Mrkusich E, Steinel MC, Rice J, Merritt DJ and Whittington PM, *The L1-type cell adhesion molecule Neuroglian is necessary for maintenance of sensory axon advance in the Drosophila embryo. Neural Dev, 2008, 3, p.10.*
 68. Linneberg C, Toft CLF, Kjaer-Sorensen K and Laursen LS, *L1cam-mediated developmental processes of the nervous system are differentially regulated by proteolytic processing. Sci Rep, 2019, 9, p.3716.*
 69. Hong M, Tao S, Zhang L, Diao LT, Huang X, Huang S, Xie SJ, Xiao ZD and Zhang H, *RNA sequencing: new technologies and applications in cancer research. J Hematol Oncol, 2020, 13, p.166.*
 70. <https://www.nature.com/immersive/d42859-020-00099-0/index.html>,
 71. Ley TJ, Mardis ER, Ding L, Fulton B, McLellan MD, Chen K, Dooling D, Dunford-Shore BH, McGrath S, Hickenbotham M, Cook L, Abbott R, Larson DE, Koboldt DC, Pohl C, Smith S, Hawkins A, Abbott S, Locke D, Hillier LW, Miner T, Fulton L, Magrini V, Wylie T, Glasscock J, Conyers J, Sander N, Shi X, Osborne JR, Minx P, Gordon D, Chinwalla A, Zhao Y, Ries RE, Payton JE, Westervelt P, Tomasson MH, Watson M, Baty J, Ivanovich J, Heath S, Shannon WD, Nagarajan R, Walter MJ, Link DC, Graubert TA, DiPersio JF

- and Wilson RK, *DNA sequencing of a cytogenetically normal acute myeloid leukaemia genome*. *Nature*, 2008, **456**, p.66-72.
72. www.thesequencingcenter.com,
73. Gene Ontology C, *The Gene Ontology project in 2008*. *Nucleic Acids Res*, 2008, **36**, p.D440-444.
74. <http://geneontology.org>,
75. Mi H, Ebert D, Muruganujan A, Mills C, Albu LP, Mushayamaha T and Thomas PD, *PANTHER version 16: a revised family classification, tree-based classification tool, enhancer regions and extensive API*. *Nucleic Acids Res*, 2021, **49**, p.D394-D403.
76. Eden E, Navon R, Steinfeld I, Lipson D and Yakhini Z, *GOrilla: a tool for discovery and visualization of enriched GO terms in ranked gene lists*. *BMC Bioinformatics*, 2009, **10**, p.48.
77. Eden E, Lipson D, Yogev S and Yakhini Z, *Discovering motifs in ranked lists of DNA sequences*. *PLoS Comput Biol*, 2007, **3**, p.e39.
78. Tsenter J, Beni-Adani L, Assaf Y, Alexandrovich AG, Trembovler V and Shohami E, *Dynamic changes in the recovery after traumatic brain injury in mice: effect of injury severity on T2-weighted MRI abnormalities, and motor and cognitive functions*. *J Neurotrauma*, 2008, **25**, p.324-333.
79. Findley DL, Berquist MD and Hambuchen MD, *Methamphetamine-Induced Open Field Behavior and LD50 in Periplaneta americana Cockroaches (Blattodea: Blattidae)*. *J Econ Entomol*, 2021, **114**, p.476-480.
80. Appel D, Hummel R, Weidemeier M, Endres K, Golz C and Schafer MKE, *Pharmacologic Inhibition of ADAM10 Attenuates Brain Tissue Loss, Axonal Injury and Pro-inflammatory Gene Expression Following Traumatic Brain Injury in Mice*. *Front Cell Dev Biol*, 2021, **9**, p.661462.
81. Dahme M, Bartsch U, Martini R, Anliker B, Schachner M and Mantei N, *Disruption of the mouse L1 gene leads to malformations of the nervous system*. *Nat Genet*, 1997, **17**, p.346-349.
82. Fransen E, D'Hooge R, Van Camp G, Verhoye M, Sijbers J, Reyniers E, Soriano P, Kamiguchi H, Willemsen R, Koekkoek SK, De Zeeuw CI, De Deyn PP, Van der Linden A, Lemmon V, Kooy RF and Willems PJ, *L1 knockout mice show dilated ventricles, vermis hypoplasia and impaired exploration patterns*. *Hum Mol Genet*, 1998, **7**, p.999-1009.
83. Law JW, Lee AY, Sun M, Nikonenko AG, Chung SK, Dityatev A, Schachner M and Morellini F, *Decreased anxiety, altered place learning, and increased CA1 basal excitatory synaptic transmission*

- in mice with conditional ablation of the neural cell adhesion molecule L1*. J Neurosci, 2003, **23**, p.10419-10432.
84. Choleric E, Thomas AW, Kavaliers M and Prato FS, *A detailed ethological analysis of the mouse open field test: effects of diazepam, chlordiazepoxide and an extremely low frequency pulsed magnetic field*. Neurosci Biobehav Rev, 2001, **25**, p.235-260.
 85. Wiencken-Barger AE, Mavity-Hudson J, Bartsch U, Schachner M and Casagrande VA, *The role of L1 in axon pathfinding and fasciculation*. Cereb Cortex, 2004, **14**, p.121-131.
 86. Basel-Vanagaite L, Straussberg R, Friez MJ, Inbar D, Korenreich L, Shohat M and Schwartz CE, *Expanding the phenotypic spectrum of L1CAM-associated disease*. Clin Genet, 2006, **69**, p.414-419.
 87. Itoh K and Fushiki S, *The role of L1cam in murine corticogenesis, and the pathogenesis of hydrocephalus*. Pathol Int, 2015, **65**, p.58-66.
 88. www.genomatix.de,
 89. Mi H and Thomas P, *PANTHER pathway: an ontology-based pathway database coupled with data analysis tools*. Methods Mol Biol, 2009, **563**, p.123-140.
 90. Balakrishnan R, Harris MA, Huntley R, Van Auken K and Cherry JM, *A guide to best practices for Gene Ontology (GO) manual annotation*. Database (Oxford), 2013, **2013**, p.bat054.
 91. Cox JT, Gaglani SM, Jusue-Torres I, Elder BD, Goodwin CR, Haynes MR, Blitz AM and Rigamonti D, *Choroid plexus hyperplasia: A possible cause of hydrocephalus in adults*. Neurology, 2016, **87**, p.2058-2060.
 92. Dohrmann GJ, *The choroid plexus in experimental hydrocephalus. A light and electron microscopic study in normal, hydrocephalic, and shunted hydrocephalic dogs*. J Neurosurg, 1971, **34**, p.56-69.
 93. Cipolla MJ, Journal, 2009,
 94. Zihni C, Mills C, Matter K and Balda MS, *Tight junctions: from simple barriers to multifunctional molecular gates*. Nat Rev Mol Cell Biol, 2016, **17**, p.564-580.
 95. Suzuki T, *Regulation of intestinal epithelial permeability by tight junctions*. Cell Mol Life Sci, 2013, **70**, p.631-659.
 96. Imafuku K, Kamaguchi M, Natsuga K, Nakamura H, Shimizu H and Iwata H, *Zonula occludens-1 demonstrates a unique appearance in buccal mucosa over several layers*. Cell Tissue Res, 2021, **384**, p.691-702.

97. Greene C, Hanley N and Campbell M, *Claudin-5: gatekeeper of neurological function*. *Fluids Barriers CNS*, 2019, **16**, p.3.
98. Odenwald MA, Choi W, Kuo WT, Singh G, Sailer A, Wang Y, Shen L, Fanning AS and Turner JR, *The scaffolding protein ZO-1 coordinates actomyosin and epithelial apical specializations in vitro and in vivo*. *J Biol Chem*, 2018, **293**, p.17317-17335.
99. Loughner CL, Tiwari A, Kenchegowda D, Swamynathan S and Swamynathan SK, *Spatiotemporally Controlled Ablation of Klf5 Results in Dysregulated Epithelial Homeostasis in Adult Mouse Corneas*. *Invest Ophthalmol Vis Sci*, 2017, **58**, p.4683-4693.
100. Barbin G, Aigrot MS, Charles P, Foucher A, Grumet M, Schachner M, Zalc B and Lubetzki C, *Axonal cell-adhesion molecule L1 in CNS myelination*. *Neuron Glia Biol*, 2004, **1**, p.65-72.
101. Dwyer ND, Chen B, Chou SJ, Hippenmeyer S, Nguyen L and Ghashghaei HT, *Neural Stem Cells to Cerebral Cortex: Emerging Mechanisms Regulating Progenitor Behavior and Productivity*. *J Neurosci*, 2016, **36**, p.11394-11401.
102. Lavado A, Ware M, Pare J and Cao X, *The tumor suppressor Nf2 regulates corpus callosum development by inhibiting the transcriptional coactivator Yap*. *Development*, 2014, **141**, p.4182-4193.
103. Rodriguez EM and Guerra MM, *Neural Stem Cells and Fetal-Onset Hydrocephalus*. *Pediatr Neurosurg*, 2017, **52**, p.446-461.
104. Hutton SR and Pevny LH, *SOX2 expression levels distinguish between neural progenitor populations of the developing dorsal telencephalon*. *Dev Biol*, 2011, **352**, p.40-47.
105. Sansom SN, Griffiths DS, Faedo A, Kleinjan DJ, Ruan Y, Smith J, van Heyningen V, Rubenstein JL and Livesey FJ, *The level of the transcription factor Pax6 is essential for controlling the balance between neural stem cell self-renewal and neurogenesis*. *PLoS Genet*, 2009, **5**, p.e1000511.
106. Lv X, Ren SQ, Zhang XJ, Shen Z, Ghosh T, Xianyu A, Gao P, Li Z, Lin S, Yu Y, Zhang Q, Groszer M and Shi SH, *TBR2 coordinates neurogenesis expansion and precise microcircuit organization via Protocadherin 19 in the mammalian cortex*. *Nat Commun*, 2019, **10**, p.3946.
107. Kia'i N and Bajaj T, *Histology, Respiratory Epithelium*. *Journal*, 2022,
108. Rajendran P, Rengarajan T, Thangavel J, Nishigaki Y, Sakthisekaran D, Sethi G and Nishigaki I, *The vascular endothelium and human diseases*. *Int J Biol Sci*, 2013, **9**, p.1057-1069.

109. Bhat AA, Uppada S, Achkar IW, Hashem S, Yadav SK, Shanmugakonar M, Al-Naemi HA, Haris M and Uddin S, *Tight Junction Proteins and Signaling Pathways in Cancer and Inflammation: A Functional Crosstalk*. Front Physiol, 2018, **9**, p.1942.
110. Brunner J, Ragupathy S and Borchard G, *Target specific tight junction modulators*. Adv Drug Deliv Rev, 2021, **171**, p.266-288.
111. Abbott NJ, Patabendige AA, Dolman DE, Yusof SR and Begley DJ, *Structure and function of the blood-brain barrier*. Neurobiol Dis, 2010, **37**, p.13-25.
112. Citi S, *The mechanobiology of tight junctions*. Biophys Rev, 2019, **11**, p.783-793.
113. Sladojevic N, Stamatovic SM, Johnson AM, Choi J, Hu A, Dithmer S, Blasig IE, Keep RF and Andjelkovic AV, *Claudin-1-Dependent Destabilization of the Blood-Brain Barrier in Chronic Stroke*. J Neurosci, 2019, **39**, p.743-757.
114. Liddel SA, *Development of the choroid plexus and blood-CSF barrier*. Front Neurosci, 2015, **9**, p.32.
115. Rodewald M, Herr D, Fraser HM, Hack G, Kreienberg R and Wulff C, *Regulation of tight junction proteins occludin and claudin 5 in the primate ovary during the ovulatory cycle and after inhibition of vascular endothelial growth factor*. Mol Hum Reprod, 2007, **13**, p.781-789.
116. Owler BK, Pitham T and Wang D, *Aquaporins: relevance to cerebrospinal fluid physiology and therapeutic potential in hydrocephalus*. Cerebrospinal Fluid Res, 2010, **7**, p.15.
117. Verkman AS, *Aquaporins in clinical medicine*. Annu Rev Med, 2012, **63**, p.303-316.
118. Kudumala S, Freund J, Hortsch M and Godenschwege TA, *Differential effects of human L1CAM mutations on complementing guidance and synaptic defects in Drosophila melanogaster*. PLoS One, 2013, **8**, p.e76974.
119. Sherry T, Handley A, Nicholas HR and Pocock R, *Harmonization of L1CAM expression facilitates axon outgrowth and guidance of a motor neuron*. Development, 2020, **147**,
120. Shen Y, Mani S, Donovan SL, Schwob JE and Meiri KF, *Growth-associated protein-43 is required for commissural axon guidance in the developing vertebrate nervous system*. J Neurosci, 2002, **22**, p.239-247.
121. Berry CT, Sceniak MP, Zhou L and Sabo SL, *Developmental up-regulation of vesicular glutamate transporter-1 promotes*

- neocortical presynaptic terminal development*. PLoS One, 2012, **7**, p.e50911.
122. Felderhoff-Mueser U, Herold R, Hochhaus F, Koehne P, Ring-Mrozik E, Obladen M and Buhner C, *Increased cerebrospinal fluid concentrations of soluble Fas (CD95/Apo-1) in hydrocephalus*. Arch Dis Child, 2001, **84**, p.369-372.
 123. Kalani MY, Filippidis AS and Rekate HL, *Hydrocephalus and aquaporins: the role of aquaporin-1*. Acta Neurochir Suppl, 2012, **113**, p.51-54.
 124. Paul L, Madan M, Rammling M, Chigurupati S, Chan SL and Pattisapu JV, *Expression of aquaporin 1 and 4 in a congenital hydrocephalus rat model*. Neurosurgery, 2011, **68**, p.462-473.
 125. Janssens S, Schotsaert M, Karnik R, Balasubramaniam V, Dejoze M, Meissner A, Garcia-Sastre A and Zwaka TP, *Zika Virus Alters DNA Methylation of Neural Genes in an Organoid Model of the Developing Human Brain*. mSystems, 2018, **3**,
 126. Di Lullo E and Kriegstein AR, *The use of brain organoids to investigate neural development and disease*. Nat Rev Neurosci, 2017, **18**, p.573-584.
 127. Renner M, Lancaster MA, Bian S, Choi H, Ku T, Peer A, Chung K and Knoblich JA, *Self-organized developmental patterning and differentiation in cerebral organoids*. EMBO J, 2017, **36**, p.1316-1329.
 128. Pushchina EV, Zharikova EI and Varaksin AA, *Expression of Doublecortin, Glial Fibrillar Acidic Protein, and Vimentin in the Intact Subpallium and after Traumatic Injury to the Pallium in Juvenile Salmon, Oncorhynchus masou*. Int J Mol Sci, 2022, **23**,
 129. Jarvie BC and Hentges ST, *Expression of GABAergic and glutamatergic phenotypic markers in hypothalamic proopiomelanocortin neurons*. J Comp Neurol, 2012, **520**, p.3863-3876.
 130. Abe K, Katsuno H, Toriyama M, Baba K, Mori T, Hakoshima T, Kanemura Y, Watanabe R and Inagaki N, *Grip and slip of L1-CAM on adhesive substrates direct growth cone haptotaxis*. Proc Natl Acad Sci U S A, 2018, **115**, p.2764-2769.
 131. Burry RW, Lah JJ and Hayes DM, *Redistribution of GAP-43 during growth cone development in vitro; immunocytochemical studies*. J Neurocytol, 1991, **20**, p.133-144.
 132. <https://software.broadinstitute.org/morpheus>,
 133. <https://bioinformatics.psb.ugent.be/webtools/Venn/>,
 134. Zhang J, He L, Yang Z, Li L and Cai W, *Lithium chloride promotes proliferation of neural stem cells in vitro, possibly by triggering the*

- Wnt signaling pathway*. Anim Cells Syst (Seoul), 2019, **23**, p.32-41.
135. Xia MY, Zhao XY, Huang QL, Sun HY, Sun C, Yuan J, He C, Sun Y, Huang X, Kong W and Kong WJ, *Activation of Wnt/beta-catenin signaling by lithium chloride attenuates d-galactose-induced neurodegeneration in the auditory cortex of a rat model of aging*. FEBS Open Bio, 2017, **7**, p.759-776.
 136. Maness PF and Schachner M, *Neural recognition molecules of the immunoglobulin superfamily: signaling transducers of axon guidance and neuronal migration*. Nat Neurosci, 2007, **10**, p.19-26.
 137. Altevogt P, Doberstein K and Fogel M, *L1CAM in human cancer*. Int J Cancer, 2016, **138**, p.1565-1576.
 138. Zhu J, Lee KP, Spencer TJ, Biederman J and Bhide PG, *Transgenerational transmission of hyperactivity in a mouse model of ADHD*. J Neurosci, 2014, **34**, p.2768-2773.
 139. Aguilera-Albesa S, de la Hoz AB, Ibarluzea N, Ordonez-Castillo AR, Busto-Crespo O, Villate O, Ibiricu-Yanguas MA, Yoldi-Petri ME, Garcia de Gurtubay I, Perez de Nanclares G, Pereda A and Tejada MI, *Hereditary Spastic Paraplegia and Intellectual Disability: Clinicogenetic Lessons From a Family Suggesting a Dual Genetics Diagnosis*. Front Neurol, 2020, **11**, p.41.
 140. Yuan Z, Chen P, Zhang T, Shen B and Chen L, *Agenesis and Hypomyelination of Corpus Callosum in Mice Lacking Nsun5, an RNA Methyltransferase*. Cells, 2019, **8**,
 141. Yoo SW, Motari MG and Schnaar RL, *Agenesis of the corpus callosum in Nogo receptor deficient mice*. J Comp Neurol, 2017, **525**, p.291-301.
 142. Magara F, Ricceri L, Wolfer DP and Lipp HP, *The acallosal mouse strain l/LnJ: a putative model of ADHD?* Neurosci Biobehav Rev, 2000, **24**, p.45-50.
 143. Lesch KP, *Editorial: Can dysregulated myelination be linked to ADHD pathogenesis and persistence?* J Child Psychol Psychiatry, 2019, **60**, p.229-231.
 144. Hummel R, Lang M, Walderbach S, Wang Y, Tegeder I, Golz C and Schafer MKE, *Single intracerebroventricular progranulin injection adversely affects the blood-brain barrier in experimental traumatic brain injury*. J Neurochem, 2021, **158**, p.342-357.
 145. Hummel R, Ulbrich S, Appel D, Li S, Hirnet T, Zander S, Bobkiewicz W, Golz C and Schafer MKE, *Administration of all-trans retinoic acid after experimental traumatic brain injury is brain protective*. Br J Pharmacol, 2020, **177**, p.5208-5223.

146. Seibenhener ML and Wooten MC, *Use of the Open Field Maze to measure locomotor and anxiety-like behavior in mice*. J Vis Exp, 2015, p.e52434.
147. Yamasaki M, Nonaka M, Suzumori N, Nakamura H, Fujita H, Namba A, Kamei Y, Yamada T, Pooh RK, Tanemura M, Sudo N, Nagasaka M, Yoshioka E, Shofuda T and Kanemura Y, *Prenatal molecular diagnosis of a severe type of L1 syndrome (X-linked hydrocephalus)*. J Neurosurg Pediatr, 2011, **8**, p.411-416.
148. Sauce B, Wass C, Netrakanti M, Saylor J, Schachner M and Matzel LD, *Heterozygous L1-deficient mice express an autism-like phenotype*. Behav Brain Res, 2015, **292**, p.432-442.
149. Schmid JS, Bernreuther C, Nikonenko AG, Ling Z, Mies G, Hossmann KA, Jakovcevski I and Schachner M, *Heterozygosity for the mutated X-chromosome-linked L1 cell adhesion molecule gene leads to increased numbers of neurons and enhanced metabolism in the forebrain of female carrier mice*. Brain Struct Funct, 2013, **218**, p.1375-1390.
150. Tapanes-Castillo A, Weaver EJ, Smith RP, Kamei Y, Caspary T, Hamilton-Nelson KL, Slifer SH, Martin ER, Bixby JL and Lemmon VP, *A modifier locus on chromosome 5 contributes to L1 cell adhesion molecule X-linked hydrocephalus in mice*. Neurogenetics, 2010, **11**, p.53-71.
151. Brummendorf T, Kenwrick S and Rathjen FG, *Neural cell recognition molecule L1: from cell biology to human hereditary brain malformations*. Curr Opin Neurobiol, 1998, **8**, p.87-97.
152. Lemmon V, Farr KL and Lagenaur C, *L1-mediated axon outgrowth occurs via a homophilic binding mechanism*. Neuron, 1989, **2**, p.1597-1603.
153. Emmert AS, Vuong SM, Shula C, Lindquist D, Yuan W, Hu YC, Mangano FT and Goto J, *Characterization of a novel rat model of X-linked hydrocephalus by CRISPR-mediated mutation in L1cam*. J Neurosurg, 2019, **132**, p.945-958.
154. Gast D, Riedle S, Issa Y, Pfeifer M, Beckhove P, Sanderson MP, Arlt M, Moldenhauer G, Fogel M, Kruger A and Altevogt P, *The cytoplasmic part of L1-CAM controls growth and gene expression in human tumors that is reversed by therapeutic antibodies*. Oncogene, 2008, **27**, p.1281-1289.
155. Kiefel H, Bondong S, Hazin J, Ridinger J, Schirmer U, Riedle S and Altevogt P, *L1CAM: a major driver for tumor cell invasion and motility*. Cell Adh Migr, 2012, **6**, p.374-384.
156. Kiefel H, Bondong S, Erbe-Hoffmann N, Hazin J, Riedle S, Wolf J, Pfeifer M, Arlt A, Schafer H, Muerkoster SS and Altevogt P, *L1CAM-integrin interaction induces constitutive NF-kappaB*

- activation in pancreatic adenocarcinoma cells by enhancing IL-1beta expression. Oncogene, 2010, 29, p.4766-4778.*
157. Harris D, Bonfil D, Chuderland D, Kraus S, Seger R and Naor Z, *Activation of MAPK cascades by GnRH: ERK and Jun N-terminal kinase are involved in basal and GnRH-stimulated activity of the glycoprotein hormone LHbeta-subunit promoter. Endocrinology, 2002, 143, p.1018-1025.*
 158. Yi YS, Baek KS and Cho JY, *L1 cell adhesion molecule induces melanoma cell motility by activation of mitogen-activated protein kinase pathways. Pharmazie, 2014, 69, p.461-467.*
 159. Oleari R, Lettieri A, Paganoni A, Zanieri L and Cariboni A, *Semaphorin Signaling in GnRH Neurons: From Development to Disease. Neuroendocrinology, 2019, 109, p.193-199.*
 160. Castellani V, Chedotal A, Schachner M, Faivre-Sarrailh C and Rougon G, *Analysis of the L1-deficient mouse phenotype reveals cross-talk between Sema3A and L1 signaling pathways in axonal guidance. Neuron, 2000, 27, p.237-249.*
 161. Bridgman PC, Dave S, Asnes CF, Tullio AN and Adelstein RS, *Myosin IIB is required for growth cone motility. J Neurosci, 2001, 21, p.6159-6169.*
 162. Medeiros NA, Burnette DT and Forscher P, *Myosin II functions in actin-bundle turnover in neuronal growth cones. Nat Cell Biol, 2006, 8, p.215-226.*
 163. Kiefel H, Bondong S, Pfeifer M, Schirmer U, Erbe-Hoffmann N, Schafer H, Sebens S and Altevogt P, *EMT-associated up-regulation of L1CAM provides insights into L1CAM-mediated integrin signalling and NF-kappaB activation. Carcinogenesis, 2012, 33, p.1919-1929.*
 164. Shtutman M, Levina E, Ohouo P, Baig M and Roninson IB, *Cell adhesion molecule L1 disrupts E-cadherin-containing adherens junctions and increases scattering and motility of MCF7 breast carcinoma cells. Cancer Res, 2006, 66, p.11370-11380.*
 165. Liu J, Fukunaga-Kalabis M, Li L and Herlyn M, *Developmental pathways activated in melanocytes and melanoma. Arch Biochem Biophys, 2014, 563, p.13-21.*
 166. Cheriyaundath S and Ben-Ze'ev A, *Wnt/beta-Catenin Target Genes in Colon Cancer Metastasis: The Special Case of L1CAM. Cancers (Basel), 2020, 12,*
 167. Gavert N, Conacci-Sorrell M, Gast D, Schneider A, Altevogt P, Brabletz T and Ben-Ze'ev A, *L1, a novel target of beta-catenin signaling, transforms cells and is expressed at the invasive front of colon cancers. J Cell Biol, 2005, 168, p.633-642.*

168. Gautam J, Cao Y and Yao Y, *Pericytic Laminin Maintains Blood-Brain Barrier Integrity in an Age-Dependent Manner*. *Transl Stroke Res*, 2020, **11**, p.228-242.
169. Wang Y, Peng F, Xie G, Chen ZQ, Li HG, Tang T and Luo JK, *Rhubarb attenuates blood-brain barrier disruption via increased zonula occludens-1 expression in a rat model of intracerebral hemorrhage*. *Exp Ther Med*, 2016, **12**, p.250-256.
170. Ganesh K, Basnet H, Kaygusuz Y, Laughney AM, He L, Sharma R, O'Rourke KP, Reuter VP, Huang YH, Turkecul M, Emrah E, Masilionis I, Manova-Todorova K, Weiser MR, Saltz LB, Garcia-Aguilar J, Koche R, Lowe SW, Pe'er D, Shia J and Massague J, *L1CAM defines the regenerative origin of metastasis-initiating cells in colorectal cancer*. *Nat Cancer*, 2020, **1**, p.28-45.
171. Ohata S, Nakatani J, Herranz-Perez V, Cheng J, Belinson H, Inubushi T, Snider WD, Garcia-Verdugo JM, Wynshaw-Boris A and Alvarez-Buylla A, *Loss of Dishevelleds disrupts planar polarity in ependymal motile cilia and results in hydrocephalus*. *Neuron*, 2014, **83**, p.558-571.
172. Ferri AL, Cavallaro M, Braidà D, Di Cristofano A, Canta A, Vezzani A, Ottolenghi S, Pandolfi PP, Sala M, DeBiasi S and Nicolis SK, *Sox2 deficiency causes neurodegeneration and impaired neurogenesis in the adult mouse brain*. *Development*, 2004, **131**, p.3805-3819.
173. Favaro R, Valotta M, Ferri AL, Latorre E, Mariani J, Giachino C, Lancini C, Tosetti V, Ottolenghi S, Taylor V and Nicolis SK, *Hippocampal development and neural stem cell maintenance require Sox2-dependent regulation of Shh*. *Nat Neurosci*, 2009, **12**, p.1248-1256.
174. Ben Q, An W, Fei J, Xu M, Li G, Li Z and Yuan Y, *Downregulation of L1CAM inhibits proliferation, invasion and arrests cell cycle progression in pancreatic cancer cells in vitro*. *Exp Ther Med*, 2014, **7**, p.785-790.
175. Chelban V, Patel N, Vandrovcova J, Zanetti MN, Lynch DS, Ryten M, Botia JA, Bello O, Tribollet E, Efthymiou S, Davagnanam I, Group SS, Bashiri FA, Wood NW, Rothman JE, Alkuraya FS and Houlden H, *Mutations in NKX6-2 Cause Progressive Spastic Ataxia and Hypomyelination*. *Am J Hum Genet*, 2017, **100**, p.969-977.
176. Awatramani R, Scherer S, Grinspan J, Collarini E, Skoff R, O'Hagan D, Garbern J and Kamholz J, *Evidence that the homeodomain protein Gtx is involved in the regulation of oligodendrocyte myelination*. *J Neurosci*, 1997, **17**, p.6657-6668.

177. Takebayashi H, Nabeshima Y, Yoshida S, Chisaka O, Ikenaka K and Nabeshima Y, *The basic helix-loop-helix factor olig2 is essential for the development of motoneuron and oligodendrocyte lineages*. *Curr Biol*, 2002, **12**, p.1157-1163.
178. Wang CY, Sun YT, Fang KM, Ho CH, Yang CS and Tzeng SF, *Function of B-Cell CLL/Lymphoma 11B in Glial Progenitor Proliferation and Oligodendrocyte Maturation*. *Front Mol Neurosci*, 2018, **11**, p.4.
179. Hauser S, Bickel L, Weinspach D, Gerg M, Schafer MK, Pfeifer M, Hazin J, Schelter F, Weidle UH, Ramser J, Volkmann J, Meindl A, Schmitt M, Schrotzlmair F, Altevogt P and Kruger A, *Full-length L1CAM and not its Delta2Delta27 splice variant promotes metastasis through induction of gelatinase expression*. *PLoS One*, 2011, **6**, p.e18989.
180. Haddad MR, Donsante A, Zervas P and Kaler SG, *Fetal Brain-directed AAV Gene Therapy Results in Rapid, Robust, and Persistent Transduction of Mouse Choroid Plexus Epithelia*. *Mol Ther Nucleic Acids*, 2013, **2**, p.e101.
181. Samata B, Takaichi R, Ishii Y, Fukushima K, Nakagawa H, Ono Y and Takahashi J, *L1CAM Is a Marker for Enriching Corticospinal Motor Neurons in the Developing Brain*. *Front Cell Neurosci*, 2020, **14**, p.31.
182. Isik E, Onay H, Atik T, Akgun B, Cogulu O and Ozkinay F, *Clinical and genetic features of L1 syndrome patients: Definition of two novel mutations*. *Clin Neurol Neurosurg*, 2018, **172**, p.20-23.
183. Lutz D, Sharaf A, Drexler D, Kataria H, Wolters-Eisfeld G, Brunne B, Kleene R, Loers G, Frotscher M and Schachner M, *Proteolytic cleavage of transmembrane cell adhesion molecule L1 by extracellular matrix molecule Reelin is important for mouse brain development*. *Sci Rep*, 2017, **7**, p.15268.
184. Giordano M and Cavallaro U, *Different Shades of L1CAM in the Pathophysiology of Cancer Stem Cells*. *J Clin Med*, 2020, **9**,
185. Olivares-Moreno R, Lopez-Hidalgo M, Altamirano-Espinoza A, Gonzalez-Gallardo A, Antaramian A, Lopez-Virgen V and Rojas-Piloni G, *Mouse corticospinal system comprises different functional neuronal ensembles depending on their hodology*. *BMC Neurosci*, 2019, **20**, p.50.
186. Feldner A, Adam MG, Tetzlaff F, Moll I, Komljenovic D, Sahn F, Bauerle T, Ishikawa H, Schroten H, Korff T, Hofmann I, Wolburg H, von Deimling A and Fischer A, *Loss of Mpdz impairs ependymal cell integrity leading to perinatal-onset hydrocephalus in mice*. *EMBO Mol Med*, 2017, **9**, p.890-905.

187. Asami A, Kurganov E and Miyata S, *Proliferation of endothelial cells in the choroid plexus of normal and hydrocephalic mice*. J Chem Neuroanat, 2020, **106**, p.101796.
188. Jia W, Lu R, Martin TA and Jiang WG, *The role of claudin-5 in blood-brain barrier (BBB) and brain metastases (review)*. Mol Med Rep, 2014, **9**, p.779-785.
189. Madeira C, Vargas-Lopes C, Brandao CO, Reis T, Laks J, Panizzutti R and Ferreira ST, *Elevated Glutamate and Glutamine Levels in the Cerebrospinal Fluid of Patients With Probable Alzheimer's Disease and Depression*. Front Psychiatry, 2018, **9**, p.561.
190. Zhang Y, Bo X, Schoepfer R, Holtmaat AJ, Verhaagen J, Emson PC, Lieberman AR and Anderson PN, *Growth-associated protein GAP-43 and L1 act synergistically to promote regenerative growth of Purkinje cell axons in vivo*. Proc Natl Acad Sci U S A, 2005, **102**, p.14883-14888.
191. Del Bigio MR and Zhang YW, *Cell death, axonal damage, and cell birth in the immature rat brain following induction of hydrocephalus*. Exp Neurol, 1998, **154**, p.157-169.
192. Smith ZA, Moftakhar P, Malkasian D, Xiong Z, Vinters HV and Lazareff JA, *Choroid plexus hyperplasia: surgical treatment and immunohistochemical results. Case report*. J Neurosurg, 2007, **107**, p.255-262.
193. Daniels RW, Miller BR and DiAntonio A, *Increased vesicular glutamate transporter expression causes excitotoxic neurodegeneration*. Neurobiol Dis, 2011, **41**, p.415-420.
194. Touret M, Parrot S, Denoroy L, Belin MF and Didier-Bazes M, *Glutamatergic alterations in the cortex of genetic absence epilepsy rats*. BMC Neurosci, 2007, **8**, p.69.
195. Engle EC, *Human genetic disorders of axon guidance*. Cold Spring Harb Perspect Biol, 2010, **2**, p.a001784.
196. <http://imp.princeton.edu>,
197. <http://cbl-gorilla.cs.technion.ac.il/>),
198. <http://revigo.irb.hr/>,
199. Bye CR, Rytova V, Alsanie WF, Parish CL and Thompson LH, *Axonal Growth of Midbrain Dopamine Neurons is Modulated by the Cell Adhesion Molecule ALCAM Through Trans-Heterophilic Interactions with L1cam, Chl1, and Semaphorins*. J Neurosci, 2019, **39**, p.6656-6667.
200. Terraneo N, Jacob F, Peitzsch C, Dubrovskaja A, Krudewig C, Huang YL, Heinzelmann-Schwarz V, Schibli R, Behe M and Grunberg J, *L1 Cell Adhesion Molecule Confers Radioresistance to*

- Ovarian Cancer and Defines a New Cancer Stem Cell Population.* Cancers (Basel), 2020, **12**,
201. Son YS, *Brief report: L1 cell adhesion molecule, a novel surface molecule of human embryonic stem cells, is essential for self-renewal and pluripotency.* Stem Cells, 2011, **29**, p.2094-2099.
 202. Shkurnikov MY, Knyazev EN, Wicklein D, Schumacher U, Samatov TR and Tonevitskii AG, *Role of L1CAM in the Regulation of the Canonical Wnt Pathway and Class I MAGE Genes.* Bull Exp Biol Med, 2016, **160**, p.807-810.
 203. Basu S, Gavert N, Brabletz T and Ben-Ze'ev A, *The intestinal stem cell regulating gene ASCL2 is required for L1-mediated colon cancer progression.* Cancer Lett, 2018, **424**, p.9-18.
 204. Laksitorini MD, Yathindranath V, Xiong W, Hombach-Klonisch S and Miller DW, *Modulation of Wnt/beta-catenin signaling promotes blood-brain barrier phenotype in cultured brain endothelial cells.* Sci Rep, 2019, **9**, p.19718.
 205. Iefremova V, Manikakis G, Krefft O, Jabali A, Weynans K, Wilkens R, Marsoner F, Brandl B, Muller FJ, Koch P and Ladewig J, *An Organoid-Based Model of Cortical Development Identifies Non-Cell-Autonomous Defects in Wnt Signaling Contributing to Miller-Dieker Syndrome.* Cell Rep, 2017, **19**, p.50-59.
 206. Yoshikawa S, McKinnon RD, Kokel M and Thomas JB, *Wnt-mediated axon guidance via the Drosophila Derailed receptor.* Nature, 2003, **422**, p.583-588.
 207. Patel S, Alam A, Pant R and Chattopadhyay S, *Wnt Signaling and Its Significance Within the Tumor Microenvironment: Novel Therapeutic Insights.* Front Immunol, 2019, **10**, p.2872.
 208. Yang Y, Yang J, Liu R, Li H, Luo X and Yang G, *Accumulation of beta-catenin by lithium chloride in porcine myoblast cultures accelerates cell differentiation.* Mol Biol Rep, 2011, **38**, p.2043-2049.
 209. Zhan T, Rindtorff N and Boutros M, *Wnt signaling in cancer.* Oncogene, 2017, **36**, p.1461-1473.
 210. Abu-Baker A, Laganriere J, Gaudet R, Rochefort D, Brais B, Neri C, Dion PA and Rouleau GA, *Lithium chloride attenuates cell death in oculopharyngeal muscular dystrophy by perturbing Wnt/beta-catenin pathway.* Cell Death Dis, 2013, **4**, p.e821.

8. Appendix

8.1 List of figures

Fig. 1 Schematic illustration of corticogenesis in mice.	2
Fig. 2 Cerebral organoids can show structures similar to the embryonic mouse cortex.	4
Fig. 3 Schematic structure of L1CAM.	5
Fig. 4 Mutation site of L1D202N.	7
Fig. 5 Pathological phenotype of L1 syndrome.	8
Fig. 6 Axonal guidance deficits in L1KO mice.	9
Fig. 7 Genotyping of L1CAM-mutant mice.	22
Fig. 8 RotaRod device for motor function test.	25
Fig. 9 Ethovision XT Open field test setup for behavioral investigation.	26
Fig. 10 Trial layout in EthovisionXT software.	27
Fig. 11: Mendelian distribution of L1 adult mice.	35
Fig. 12 Increased NDS and locomotor activity in L1D201N mutant males.	37
Fig. 13 Increased NDS in L1KO male mice.	38
Fig. 14 Altered travel paths in mutant male mice.	39
Fig. 15 L1D201N male mice show enlarged ventricles.	41
Fig. 16 Unaltered ventricle sizes in L1KO mice.	42
Fig. 17 Measurement of callosal thickness.	43
Fig. 18 Thinned corpus callosum in L1D201N and L1KO mutant males.	44
Fig. 19 Principal component analysis.	46
Fig. 20 Imbalanced ratio of up- and downregulated genes in L1KO mutant males.	47
Fig. 21 Cellular processes altered in L1KO mutant males.	49
Fig. 22 Binding processes altered in L1KO mutant mice.	50

Fig. 23 WNT signaling pathway altered in L1KO mutant mice.	51
Fig. 24 Altered expression of TJP genes and Lamb1.....	52
Fig. 25 Changed expression of genes involved in oligodendrogenesis.	53
Fig. 26 Normal yield of hemizygous L1KO E16 males.	54
Fig. 27 Increased ventricle sizes in E16 L1KOs.....	55
Fig. 28 Dorsal and medial cortical areas for analysis.....	56
Fig. 29 No L1CAM expression in VZ/SVZ.....	56
Fig. 30 Thinned SOX2-layer in L1KO mutant dorsal cortex.	58
Fig. 31 Junctions and desmosomes.	59
Fig. 32 Less KI67 ⁺ cells in L1KO choroid plexus.....	60
Fig. 33 Gene expression analyses of E16 L1WT and L1KO mice.....	62
Fig. 34 Almost no expression of L1CAM in L1KO hESCs.	63
Fig. 35 Size of cerebral organoids peaked after 42DIV.....	65
Fig. 36 PAX6 and VGLUT2 expression altered in L1KO organoids.....	67
Fig. 37 Principal component analysis detects 2 outliers.....	68
Fig. 38 Imbalanced ratio of up- and downregulated genes in L1KO organoids	69
Fig. 39 Altered cellular processes in L1KO organoids.....	71
Fig. 40 Binding processes altered in L1KO organoids.	72
Fig. 41 Altered WNT signaling pathway in L1KO organoids.....	74
Fig. 42 REVIGO analysis showed changes in proliferation, adhesion and development.....	75
Fig. 43 Axonal guidance, WNT signaling and hESC pluripotency changed in L1KO organoids.	76
Fig. 44 Increased expression of WNT related genes in L1KO organoids.	77
Fig. 45 High number of identically expressed genes in L1KO mice and L1KO organoids.	78
Fig. 46 Effect of 24 h incubation with 25 mM LiCl.	79

Fig. 47 L1OE diminishes induction of WNT signaling by LiCl.....	80
Fig. 48 Canonical and non-canonical WNT signaling.....	94

8.2 List of tables

Table 1 L1CAM animal models.....	10
Table 2 Chemicals and substances.....	13
Table 3 Buffers and media	15
Table 4 Devices.....	16
Table 5 Consumables.....	17
Table 6 Primary Antibodies	17
Table 7 Anti IgG secondary antibodies	18
Table 8 Kits	18
Table 9 PCR primer.....	19
Table 10 Software	20
Table 11 Genotyping PCR program.....	21
Table 12 L1D201N restriction endonuclease mix.....	21
Table 13 NDS scoresheet	24

8.3 Publications

Appel D, Hummel R, Weidemeier M, Endres K, Gölz C, Schäfer MKE. Pharmacologic Inhibition of ADAM10 Attenuates Brain Tissue Loss, Axonal Injury and Pro-inflammatory Gene Expression Following Traumatic Brain Injury in Mice. *Front Cell Dev Biol.* 2021 Mar 15;9:661462. doi: 10.3389/fcell.2021.661462. PMID: 33791311; PMCID: PMC8005610.

Loers G, **Appel D**, Lutz D, Congiu L, Kleene R, Hermans-Borgmeyer I, Schäfer MKE, Schachner M. Amelioration of the abnormal phenotype of a new L1 syndrome mouse mutation with L1 mimetics. *FASEB J.* 2021 Feb;35(2):e21329. doi: 10.1096/fj.202002163R. PMID: 33484186.

Ritter K, Jung K, Dolderer C, **Appel D**, Oswald CC, Ritz U, Schäfer MKE. Early Reciprocal Effects in a Murine Model of Traumatic Brain Injury and Femoral Fracture. *Mediators Inflamm.* 2021 Jan 18;2021:8835730. doi: 10.1155/2021/8835730. PMID: 33531878; PMCID: PMC7834824.

Hummel R, Ulbrich S, **Appel D**, Li S, Hirnet T, Zander S, Bobkiewicz W, Gölz C, Schäfer MKE. Administration of all-trans retinoic acid after experimental traumatic brain injury is brain protective. *Br J Pharmacol.* 2020 Nov;177(22):5208-5223. doi: 10.1111/bph.15259. Epub 2020 Oct 23. PMID: 32964418; PMCID: PMC7588818.

Writing in progress: Yong Wang, Isa Wernersbach, Jenny Strehle, Shuailong Li, **Dominik Appel**, Matthias Klein², Katharina Ritter, Regina Hummel, Irmgard Tegeder, Michael K. E. Schäfer, Microglia/macrophage targeting via CSF1R inhibition during the early phase of TBI improves long-term neuronal maintenance and recovery

8.4. Acknowledgements

Firstly, I would like to thank the department for anesthesiology, namely [REDACTED] and [REDACTED]

Special thanks, of course, are directed to [REDACTED] for the opportunity to work in this excellent team, for planning the interesting projects of my master and doctoral thesis and for all the help and advices over the last years during my experiments and the writing of my theses.

I am very grateful that I was able to get to know the co-workers in this lab who were always there to help when help was needed, whether it was professional or private, namely [REDACTED] [REDACTED] Especially all their support concerning the animals is not take-for-granted and made work so much easier.

I also want to thank my PhD colleagues [REDACTED] and [REDACTED] not only for their helpful input for my experiments, but also for the fun talks we had during incubation times.

Also, many thanks to my friends for always cheering me up when experiments did not go as planned and when my mood wasn't at its peak.

Lastly, great thanks to [REDACTED] for their continuous support throughout my whole life and for giving me the opportunity to visit university and pursue my interests. I certainly wouldn't have made it to this point in my career without them.

8.5 Statutory declaration

I declare that I have authored this thesis independently, that I have not used other than the declared sources / resources and that I have explicitly marked all material which has been quoted either literally or by content from the used sources. I also declare, that this work has not been submitted in any form to any examination commission and that I am aware of the doctoral regulations of the department of biology at the Johannes Gutenberg-Universität Mainz from the 01.04.2018.

Mainz,

(Dominik Appel)